In compliance with the Canadian Privacy Legislation some supporting forms may have been removed from this dissertation.

While these forms may be included in the document page count, their removal does not represent any loss of content from the dissertation.

# Sensitivity of the hydrology and the energy budget of the Mackenzie River Basin to uncertainties in solar radiation

# Nathalie Voisin Atmospheric and Oceanic Sciences Department

McGill University, Montreal

November 2002

A thesis submitted to McGill University in partial fulfilment of the requirements of the degree of Master of Science.

Copyright © Nathalie Voisin 2002



National Library of Canada

Acquisitions and Bibliographic Services

395 Wellington Street Ottawa ON K1A 0N4 Canada Bibliothèque nationale du Canada

Acquisisitons et services bibliographiques

395, rue Wellington Ottawa ON K1A 0N4 Canada

> Your file Votre référence ISBN: 0-612-88324-8 Our file Notre référence ISBN: 0-612-88324-8

The author has granted a nonexclusive licence allowing the National Library of Canada to reproduce, loan, distribute or sell copies of this thesis in microform, paper or electronic formats.

The author retains ownership of the copyright in this thesis. Neither the thesis nor substantial extracts from it may be printed or otherwise reproduced without the author's permission.

L'auteur a accordé une licence non exclusive permettant à la Bibliothèque nationale du Canada de reproduire, prêter, distribuer ou vendre des copies de cette thèse sous la forme de microfiche/film, de reproduction sur papier ou sur format électronique.

L'auteur conserve la propriété du droit d'auteur qui protège cette thèse. Ni la thèse ni des extraits substantiels de celle-ci ne doivent être imprimés ou aturement reproduits sans son autorisation.

# Canadä

## Acknowledgements

I would like, first, to thank my supervisor, Prof. Henry Leighton, for his precious advices, day-to-day availability and patience. I also thank Prof. Eric Soulis, for his co-supervision on the hydrologic part, and receiving me for one week at the University of Waterloo for a 'WATCLASS briefing', at the beginning of the research.

Thanks to Jian Feng, who provided me the available satellite data derived at the surface and a figure from his Ph.D. thesis. He was very helpful for the satellite data processing and the radiation results interpretations.

I would like to thank the crew of the University of Waterloo for their close collaboration: Bruce Davison ran for me the seven-land-class WATCLASS simulations on the more performant computers of the University of Waterloo. Also, working together made the understanding of some obscur WATCLASS code pieces much faster (and more fun). Furthermore, Bruce came to McGill University for a few days: it enabled me to determine an inconsistency I had in my preliminary results and also to validate the code modifications I implemented for my thesis' use. Frank Seglenieks provided me the original WATCLASS code and also all GEM outputs required to drive WATCLASS.

Thanks also to Murray Mackay and Steve Fassnacht, whose papers were a good opportunity to validate, to a certain extent, my results. Thanks to the people from the department, graduates and undergraduates, for keeping a good atmosphere and professors for their broad and interesting lectures.

Finally, I would like to thank my family, and especially my mother, my grand mother and my fiancé, for their love and support.

## **Abstract**

One of the goals of the Mackenzie GEWEX Study (MAGS) is to model the critical components of the water and energy cycles that affect the climate of the Mackenzie Basin. The land surface - hydrological model WATCLASS is used to simulate the energy and water transports at and below the surface. Atmospheric input to WATCLASS is provided by the output from the atmospheric model GEM. There may be significant uncertainties in the GEM incoming solar radiation due largely to difficulties in simulating clouds and their radiative properties. The question that we address is how these uncertainties affect the simulation of the energy and water budgets of this northern river watershed.

To assess this sensitivity, two series of two WATCLASS model runs are compared. Both runs are driven by atmospheric data from GEM for the 1998-99 water-year, but in the second run shortwave radiation fluxes retrieved from satellite measurements replace the GEM fluxes. Land cover differs in the two series of runs and so provides an assessment of the sensitivity to vegetation variability. Results show that the atmospheric model overestimates the incoming solar radiation field by 36%. This results in an increase in the basin annual average surface temperature of about 1°C and an overestimation in net longwave radiation, and sensible and latent heat fluxes. Snowmelt starts earlier with a decreased first snowmelt peak in runoff and discharge hydrographs. The overall consequence is an annual discharge underestimation.

Keywords: WATCLASS

MAGS

solar radiation

hydrology sensitivity

## Résumé

Un des objectifs de l'étude GEWEX dans le basin de la rivière Mackenzie (MAGS) est de modéliser les principaux éléments du cycles de l'eau et de la conservation de l'énergie, qui sont impliquées dans sa climatologie. Le modèle WATCLASS simule les transports d'eau et d'énergie sous le sol et à la surface. Les sorties du modèle atmosphérique GEM constituent les entrées necéssaires à WATCLASS. Quelques imprécisions non négligeables, provenant des difficultés de GEM à simuler la couche nuageuse ainsi que ses propiétés radiatives, peuvent apparaître dans les simulations des flux de radiations solaires arrivant à la surface. Ainsi, dans quelle mesure la simulation de WATCLASS, des variables énergétiques et hydrologiques, est-elle affectée par ces incertitudes dans ces données en entrée?

Afin de quantifier cet impact, deux séries de deux simulations de WATCLASS sont analysées. Pour chaque simulation, WATCLASS est tourné pendant un an, de Octobre 1998 à Septembre 1999, avec en entrée les sorties atmosphériques de GEM. Cependant, dans la deuxième simulation de chaque série, le champ de radiations solaires arrivant à la surface, simulé par GEM, est remplacé par un champ équivalent mais issu d'observations satellite. Afin de quantifier la sensibilité de WATCLASS par rapport à la végétation, caractéristique essentielle de la surface, celle-ci diffère dans les deux séries de simulations. Les résultats montrent que le modèle atmospérique GEM surestime par 36% les flux de radiations solaires arrivant à la surface. Il en résulte une surévaluation d'environ 1°C de la température annuelle moyenne de surface, et de même une surestimation des flux nets de radiations terrestres et des flux de chaleurs sensible et latente. La fonte des neiges commence plus tôt avec, à cette période, un écoulement de surface ainsi que des débits sous-estimés. Finalement, le débit annuel des différents cours d'eau est aussi sous-estimé.

## Acronyms

AVHRR: Advanced Very High Resolution Radiometer

**CAGES**: Canadian GEWEX Enhanced Study

**CLASS**: Canadian Land Surface Scheme.

**E**: Evapotranspiration.

**G(T)**: heat conduction through the ground.

**GEM**: Global Environmental Multi-scale model, atmospheric model providing the atmospheric inputs to WATCLASS.

**GEM run**: WATCLASS simulation driven by incoming solar radiation simulated by GEM.

**GEM 1**: GEM run with a single land class for the land cover simulation.

**GEM 7**: GEM run with seven land classes for the land cover simulation.

**ISR**: Incoming Solar radiation.

NSR: Net Solar Radiation.

**P**: Precipitation.

QE: latent heat flux.

**QH**: sensible heat flux.

**SAT run**: WATCLASS simulation driven by incoming solar radiation based on field, retrieved from satellite observations at the top of atmosphere.

SAT 7: SAT run with seven land classes for the land cover simulation.

**SAT 1**: SAT run with a single land class for the land cover simulation.

**T**: surface temperature.

 $T_c$ : canopy Temperature.

**TOA**: Top Of Atmosphere

WATCLASS: coupling between the land-surface scheme CLASS and the

hydrologic model WATFLOOD.

**WATFLOOD**: distributed flood-forecasting model

# List of contents

Chapter I	Introduction.	1
Chapter I	I Methodology and theory	7
1. M	lethodology	7
2. G	EM-WATCLASS simulation: theory	Turney que
A.	Energy Fluxes	12
B.	Snowpack	16
C.	Water Balance	18
Chapter I	III Data Processing	20
1. G	EM simulated solar radiation	20
2. Sa	atellite observed solar radiation	21
A.	First procedure of interpolation/extrapolation	22
B.	Filling all missing data and transfer into incoming solar radiation	26
3. In	ncoming Solar radiation field	31
4. W	VATCLASS code modifications	33
A.	3-hour averages and albedo computation	33
B.	WATCLASS structure	35
C.	WATCLASS time	36
Chapter I	IV Results	38
1. E	nergy budget	40
A.	Net Solar Radiation and Albedo	40
B.	Surface and canopy temperatures	43
C.	Net Longwave radiation.	46
D.	Latent Heat flux	48
E.	Sensible Heat Flux	49
F.	Bowen Ratio QH/QE	51
G.	Evaporative Fraction OE / (OH+OE)	51

	H.	Ground heat conduction.	. 52
2.	. S	nowpack	. 54
	À.	Snow temperature	. 54
	B.	Energy used for Snowmelt	. 55
	C.	Precipitation	. 57
	D.	Snow Accumulation	. 58
	E.	Fractional snow cover	. 61
3	. V	Vater Balance	. 63
	A.	Evapotranspiration	. 63
	В.	Moisture Storage	. 64
	C.	Runoff	. 67
	D.	Stream flow	. 69
	E.	Discharge	. 75
Cha	pter	V Discussion – Conclusion	. 78
1	. S	ummary	. 78
2		Comparison with similar studies	. 81
	A.	WATCLASS sensitivity to incoming longwave radiation	. 82
	В.	CRCM/CLASS - WATFLOOD: ISR decrease	. 83

# List of figures

Figure 1: The Mackenzie River Basin
Figure 2: Location of the 7 GEWEX continental-scale experiments
Figure 3: The seven land-class distribution over the Basin for the second series of
WATCLASS runs. 8
Figure 4: The seven land classes are grouped into 'canopy' or 'bare ground' cover types.9
Figure 5: Vegetation distribution, as canopy or bare ground, over the Mackenzie River
Basin
Figure 6: Summary of GEM and WATCLASS process simulations. ISR stands for
incoming solar radiation, NSR for net solar radiation, ILR for incoming longwave
radiation, NLR for net longwave radiation, QH for sensible heat flux, QE for latent
heat flux, T for the surface temperature, G(T) for the heat conduction into the
ground and $\sigma$ is the Stefan-Boltzman constant and A the surface albedo
Figure 7: Timing of the satellites NOAA-12 and -14 overpasses over the Mackenzie
River Basin, in March 1999 (Courtesy of Jian Feng)
Figure 8: Available satellite NSR data for one particular day, on 1999, May 24 ( in W.m
<sup>2</sup> )
Figure 9: Available satellite NSR data, for 1999, May 24, after the first step of
extrapolation ( in W.m <sup>-2</sup> )
Figure 10: Comparison of the available basin monthly average net solar radiation satellite
with the GEM averages using the corresponding data
Figure 11: Second approach filled incoming satellite solar radiation retrieval using
WATCLASS albedo from the previous time step
Figure 12: Daily basin average incoming solar radiation field
Figure 13: Monthly incoming solar radiation difference between GEM and SAT 33

Figure 14: Albedo, 3-hour averaged and real hourly incoming solar radiation compared
with the hourly net solar radiation for a typical day. Overestimation of the computed
net solar radiation fluxes occurs at 3, 10 and 11 UTC
Figure 15: Water routing indices in WATFLOOD: a topographic index approach water
routing goes from low to higher grid-box indexes, up to 4668 at the delta (in red). 35
Figure 16: Incoming solar radiation (ISR) input with and without the time inconsistency,
and non-zero albedo during local daylight hours for a typical day
Figure 17: Non-zero albedo during daylight hours and net solar radiation (NSR) with and
without the time inconsistency for a typical day: NSR overestimation if the
inconsistency is not corrected
Figure 18: The sub-basins in the Mackenzie River Basin
Figure 19: Monthly basin average NSR for the single and the seven-land-class runs 41
Figure 20: Monthly basin average albedo for the seven-land-class runs
Figure 21: Monthly NSR absolute difference between GEM 7 and SAT 7 runs, in the
different sub-basins
Figure 22: Monthly albedo absolute difference between GEM 7 and SAT 7 runs, for the
different sub-basins. 43
Figure 23: Monthly basin average surface temperature for the single and seven-land-class
runs
Figure 24: Monthly average surface temperature difference between GEM 7 and SAT 7
runs, in the different sub-basins
Figure 25: Monthly basin average canopy temperature for the seven-land-class runs 45
Figure 26: Monthly average canopy temperature difference between GEM 7 and SAT 7,
for the different sub-basins
Figure 27: Monthly basin average NLR for the single and seven-land-class runs 47
Figure 28: Monthly average NLR difference between GEM 7 and SAT 7 runs, for the
different sub-basins. 47
Figure 29: Monthly basin average latent heat flux for the single and seven-land-class
runs
Figure 30: Monthly average QE difference between GEM 7 and SAT 7 runs, for the
different sub-basins. 49

Figure 31: Monthly basin average QH for the single and seven-land-class runs 50
Figure 32: Monthly average QH differences between GEM 7 and SAT 7 runs, for the
different sub-basins
Figure 33: Monthly basin average Bowen ratio in summer, for the seven-land-class runs.
Figure 34: Monthly basin average evaporative fraction for the seven-land-class runs 52
Figure 35: Monthly basin average heat flux into the ground, for the seven-land-class runs
Figure 36: Monthly average heat flux into the ground difference between GEM 7 and
SAT 7 runs, for the different sub-basins
Figure 37: Monthly basin average snowpack temperature for the seven-land-class runs. 54
Figure 38: Monthly average snow temperature difference between GEM 7 and SAT
runs, for the different sub-basins.
Figure 39: Monthly basin average snowmelt energy for the single and seven-land-class
runs
Figure 40: Monthly average snowmelt energy difference between GEM 7 and SAT
runs, for the different sub-basins.
Figure 41: Monthly average accumulated precipitation in the different sub-basins 58
Figure 42: Daily snow and precipitation accumulations over the Mackenzie River Basin.
Figure 43: Correlation between the GEM 7 and SAT 7 runs accumulated snov
accumulations, in the different sub-basins
Figure 44: Monthly average snow accumulation differences between GEM 7 and SAT
runs, for the different sub-basins
Figure 45: Daily fractional snow cover, averaged over bare ground or canopy areas, fo
GEM 7 and SAT 7 runs.
Figure 46: Daily fractional snow-cover differences between GEM 7 and SAT 7 runs, fo
the different sub-basins.
Figure 47: Monthly basin average evapotranspiration rate for the single and seven-land
class runs.
UIASS (IIIIS

Figure 48: Monthly average differences in the evapotranspiration and sublimation rate
between GEM 7 and SAT 7 runs, for the different sub-basins. 64
Figure 49: Monthly basin average frozen and liquid moisture contents of the 3 layers for
the seven-land-class runs
Figure 50: Daily basin average liquid moisture content change in the three soil layers for
GEM 7 and SAT 7 runs. 65
Figure 51: Daily basin average frozen moisture content in the three soil layers for the
seven-land-class runs. 66
Figure 52: Monthly average liquid and frozen moisture content differences between GEM
7 and SAT 7 runs, in the three soil layers and for the different sub-basins
Figure 53: Daily basin average runoff for the single and seven-land-class runs
Figure 54: Monthly average runoff differences between GEM 7 and SAT 7 runs for the
different sub-basins. 68
Figure 55: Daily basin average water balance for the seven-land-class runs
Figure 56: Location of gauge stations in the Mackenzie River Basin
Figure 57: GEM 7, SAT 7 and observed stream flows at Mackenzie River at Arctic Red
River
Figure 58: GEM 7, SAT 7 and observed stream flows at Mackenzie River at Norman
Wells
Figure 59: Athabasca River streamflows at Hinton (#1), Athabasca (#3) and below
McMurray (#5), obtained through GEM 7 and SAT 7 runs
Figure 60: Peace River streamflows at Dunvegan Bridge (#14), at Peace River (#18) and
at Peace Point (#21), obtained through GEM 7 and SAT 7 runs
Figure 61: Liard River stream flow at Fort Liard (#26) and South Nahanni River
streamflow above Virginia Falls (#25), as simulated by GEM 7 and SAT 7 runs74
Figure 62: Mackenzie River streamflows at Fort Simpson (#29), at Norman Wells (#31)
and at Arctic Red River (#34), obtained through GEM 7 and SAT 7 runs 75
Figure 63: Scheme presenting the relationships between components of the energy budget
and the water balance. ISR is incoming solar radiation, NSR net solar radiation,
NLW net long wave radiation, QE latent heat, QH sensible heat and G(T) the heat
conduction into the ground80

# List of tables

Table 1: Monthly basin average ratios NSR <sub>sat</sub> /NSR <sub>GEM</sub> at 10, 13, 16, 19 and 25 UTC 28
Table 2: Summary of possible input to WATCLASS and their analysis interest
Table 3: Fractional land cover for the seven land-class WATCLASS runs, distinguished
as canopy or bare ground
Table 4: Discharge relative errors between GEM and SAT runs for the single and the
seven-land-class simulations. Arrows indicates the flow direction, from the mos
upstream to the most downstream gauge station

# Chapter I

## Introduction

Canada has the largest amount of fresh water of any country in the world. This resource is, however, very sensitive to natural climatic variations and there are concerns about how anthropogenic forcing may alter the Canadian climate. Furthermore, climate observations suggest that substantial warming of about 1.5°C has occurred over the last few decades over northwestern Canada (Cao et al, 2001 for example). There is an international effort, through the World Climate Research Programme's (WCRP) Global Energy and Water Cycle Experiment (GEWEX), to better understand and simulate the moisture and energy transports. The Canadian involvement in GEWEX is focused on the Mackenzie River Basin, through the Mackenzie GEWEX Experiment (MAGS). The Mackenzie Basin is located in the northern latitudes of Canada (figure 1), spreads over 15° of longitude and is centered on the 60° North latitude. It has an area of 1.787 million km² and is 4,240 km long. In addition, it is the main North American source of fresh water into the Arctic Ocean (9,100 m³.s⁻¹), thereby influencing the thermohaline circulation (Woods 1994, Aagard and Carmack 1989), and hence, to a certain extent, the global climate.



Figure 1: The Mackenzie River Basin.

The MAGS project is one of 7 regional experiments being conducted in different regions of the world: the other regional studies are characterized by quite different climate and geographical conditions (figure 2). These include the Mississippi River (GAPP), the Amazon River (LBA), the Baltic Sea area (BALTEX), the Asian Monsoon region (GAME), the Murray-Darling Basin in Australia (MDB) and the African contribution (CATCH). MAGS is the northern climate watershed contribution, not affected by the monsoon and featuring cold-region phenomena such as snow and ice processes, permafrost, arctic clouds, radiation interactions. Therefore, experiments, results and simulations should be representative of any other high northern latitude watershed.

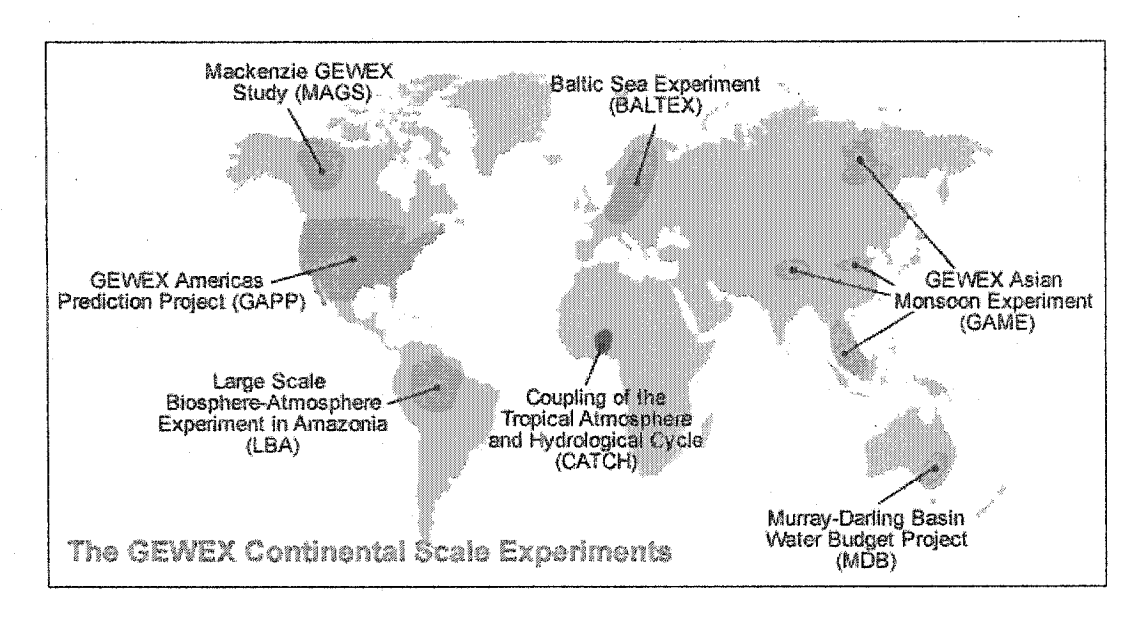


Figure 2: Location of the 7 GEWEX continental-scale experiments.

MAGS aims to better understand and predict changes to Canada's water resources arising from climatic change, to understand and model the high latitude water and energy cycles that play roles in the climate system, and to improve the ability to assess the changes to Canada's water resources that arise from climate variability and anthropogenic climate change (Stewart et al. 1998). A stated MAGS outcome is to couple an atmosphere - land surface - hydrology model and validate numerical simulations of moisture and energy transport through and into the Mackenzie Basin. Validation will be assessed with respect to observations measured during the Canadian GEWEX Enhanced Study (CAGES) period of 1998-99: this concerns water vapor, precipitation, snow cover, radiation, snowmelt, evaporation and stream discharges measurements.

To achieve MAGS's goals, the following models have been adopted and some are already coupled:

CLASS (Canadian Land Surface Scheme) has been developed at Environment Canada (Verseghy (1991) and Verseghy et al. (1993)) and is a second-generation land surface scheme: it includes treatment of bare ground and vegetation separately, with several thermal and soil layers. Basically this is a column model, which aims at improving the representation of soil water balance in order to

simulate exchanges with the atmosphere. Land surface schemes are implicit in atmospheric models and their accuracy is essential for accurate atmospheric – climate change studies. The version used in WATCLASS for this study was CLASS 2.6.

- GEM (Global Environmental Multi-scale model) is the operational Canadian Meteorological Centre Meteorological Research Branch (CMC-MRD) model developed by Cote et al. (1998), used for short and mid-term operational weather forecasting. Implicit in GEM is a first generation land surface scheme, the force-restore scheme (Deardoff 1978), to optimize the exchanges of energy and moisture between the atmosphere and the surface. GEM simulates physical, chemical and hydrological processes (cloud formation, rain, snow, etc.) and surface processes (evapotranspiration, sensible heat fluxes, etc.).
- WATFLOOD is a distributed flood-forecasting model designed at the University of Waterloo by Kouwen et al. (1993). WATFLOOD is driven mainly by precipitation and air temperature. WATFLOOD simulates infiltration, runoff, and then routes water masses to streamflows using topographic-based indices.

In order to provide better long-term forecasts, WATFLOOD and CLASS have been coupled into WATCLASS (Soulis and Kouwen 2001). The more complex and complete vertical water sub-routines in CLASS replace WATFLOOD sub-routines, and WATFLOOD is responsible for horizontal water routines and routes runoff generated by the system to open channels, which can be validated against stream flow gauge measurements. The coupling has increased the realism of the soil moisture budget representation in CLASS by introducing horizontal hydrological considerations. WATCLASS can be forced by either gridded meteorological station data or numerical weather prediction data.

Atmospheric input to WATCLASS is provided by the output from the atmospheric model GEM. Uncertainties in WATCLASS model simulations can arise

from limitations of WATCLASS itself, as well as from the data that are used to drive the model. All aspects of the simulations need to be studied in order to assess the reliability of the model results. Thus, one needs to evaluate the output of the atmospheric model and to assess how errors in the atmospheric model output may impact on the basin hydrology and the surface energy budget, as modeled by WATCLASS. One of the key fields that couples the atmospheric model GEM and WATCLASS is the incoming solar radiation flux.

Satellite measurements of solar radiation fluxes at the top of atmosphere have been used to derive net solar radiation at the surface for the CAGES year over the Mackenzie Basin (Feng 2001), showing good agreement with surface-based measurements. Furthermore, Feng (2002) analysed GEM-simulated net solar radiation fluxes with respect to these satellite retrievals for summer months (June to August 1999) at different sites spread over the Mackenzie basin: GEM was found to overestimate net surface short-wave radiation fluxes by 25% to 31% for all sky conditions, and more interestingly by only 3% for clear skies but 45% for overcast skies. Feng (2002) argued that this GEM net solar radiation overestimation, which is only significant for cloudy skies, was due to a cloud thickness simulation issue in GEM. The question that we are addressing is how sensitive are the modeled hydrology and the surface energy budget of this northern climate watershed, to these uncertainties in the solar radiative input.

To assess this sensitivity, two series of two WATCLASS model runs are compared. Both series of runs are driven offline by atmospheric data from GEM for the 1998-99 water-year (pressure, humidity, screen-level temperature, precipitation, wind speed, longwave and shortwave radiation), but in the second run of each series shortwave radiation fluxes retrieved from satellite measurements replace the GEM fluxes. Land cover type and distribution differ in the two series of runs, and so provide an assessment of the sensitivity to vegetation variability. Uncertainties in incoming solar radiation might have more or less impact depending on the surface albedo. In the first series the land is fully covered by evergreen needleleaf trees, while the second series of runs has a more

realistic land cover, with the insertion of seven land classes including different forest types, tundra, wetland and lakes.

Hereafter, chapter 2 gives some theoretical background on the model WATCLASS. Chapter 3 explains the preliminary input data processing. Chapter 4 presents the analysis of the energy budget, snowpack and the water balance between runs, having as input either GEM or satellite observed incoming solar radiation fields, and between the two series of WATCLASS runs with a different vegetation distribution. The analysis mainly focuses on the snowmelt period, since this is the time where variations in the energy balance induces important changes on the snowpack and the water balance. Chapter 6 summarizes, evaluates and discusses the previous results.

## **Chapter II**

# Methodology and theory

## 1. Methodology

In order to assess the sensitivity of the Mackenzie River watershed hydrology to incoming solar radiation, WATCLASS is run for an almost one water-year period, more precisely 343 days from October 1<sup>st</sup>, 1998 to September 7<sup>th</sup>, 1999 with two different sources for the incoming solar radiation fields, and two different land cover schemes, i.e. two series of two runs. The runs were not for a full year because of some technical issues.

The following atmospheric fields, which are generated by GEM, drive WATCLASS: specific humidity, wind speed, sea-level pressure, precipitation, screen-level temperature, downward longwave radiation and incoming shortwave radiation. The first series of runs is driven by incoming shortwave radiation simulated by GEM. However, in the second series of runs the incoming shortwave radiation fields are based on the field retrieved from satellite observations at the top of atmosphere. The difference

between the GEM and satellite-retrieved incoming solar radiation provides an estimate of the potential errors in the simulation of incoming solar radiation at the surface by GEM.

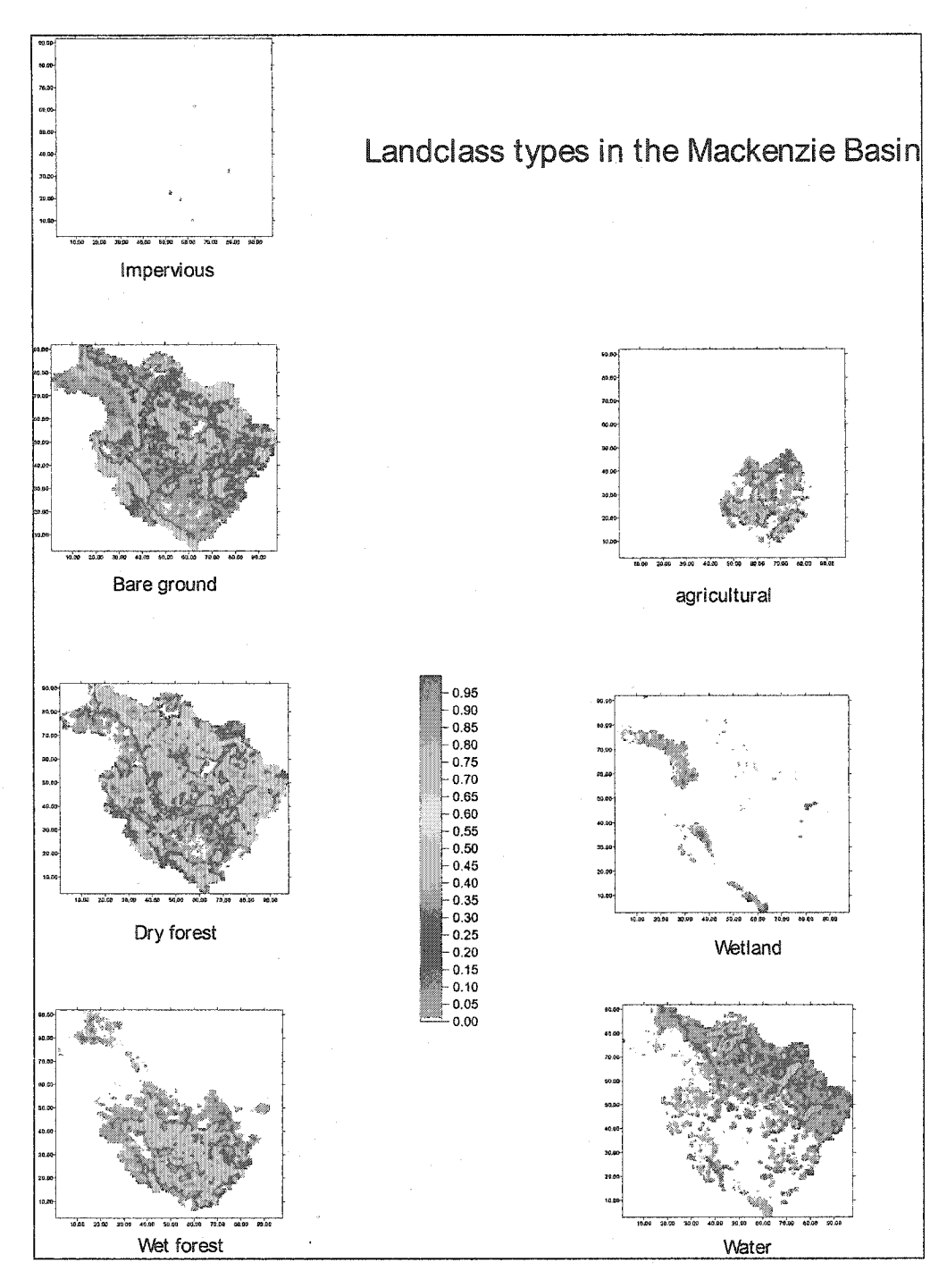


Figure 3: The seven land-class distribution over the Basin for the second series of WATCLASS runs.

Each series consists of two runs: one with a single land class (100% evergreen needle leaf, accounting for a 100% canopy basin average cover) and the other with seven land classes (figure 3) (wet forest, dry forest, wetland, agriculture, water, impervious, barren soils), accounting for a basin average cover of about 51% canopy and 49% bare ground meaning bare and short vegetation.

The seven land classes differ in their vegetation composition, and therefore in albedo as well as leaf area index, soil roughness and other vegetation parameters. Hereafter we will commonly distinguish canopy from bare ground/short vegetation distribution, as shown in figure 4, to compare vegetation types.

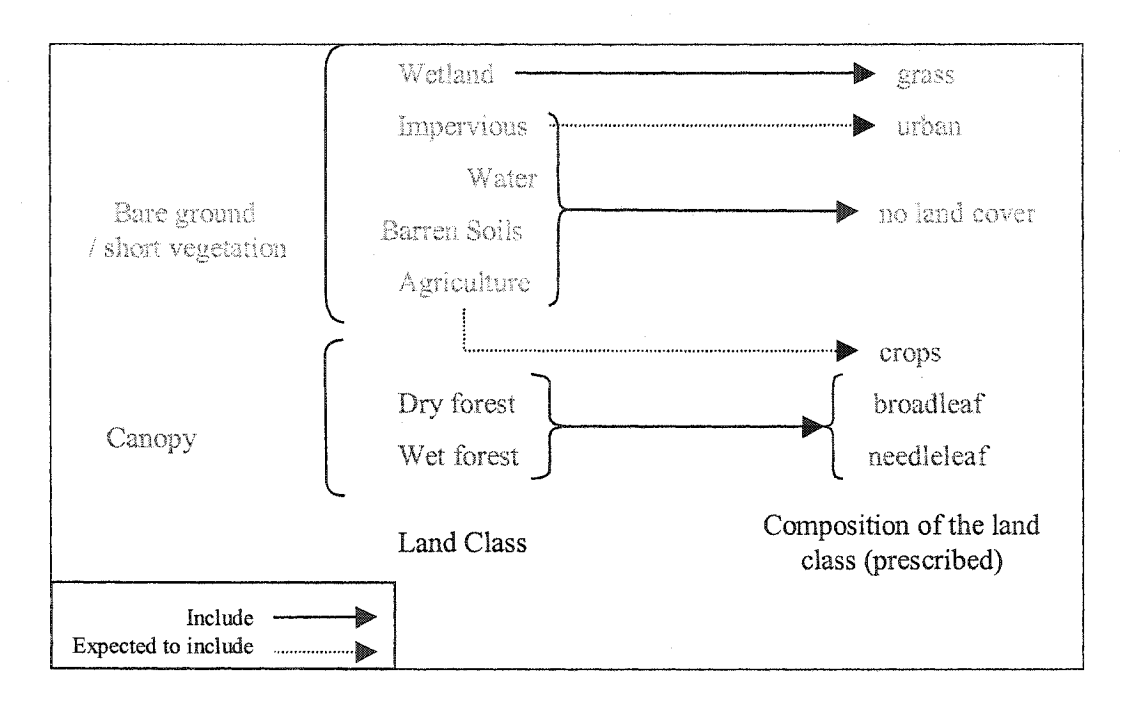


Figure 4: The seven land classes are grouped into 'canopy' or 'bare ground' cover types.

Canopy vegetation type includes two land classes, wet and dry forests, both consisting in 60% of needle leaf and 40% of broadleaf trees. Bare ground vegetation type includes the five remaining land classes: barren soils, wetland, agriculture, impervious and water. In the present runs, the impervious land class is set up to account for impervious soil with no vegetation (in general this land class also accounts for urban areas). The agriculture land class is also set up in these simulations with no crops and therefore is included in the bare ground land cover category. The distribution is the one

used for BOREAS study (Hall, 1999) and has not been changed as more modifications would have been required, such as the hydraulic parameters associated with each particular vegetation combination. We note that the vegetation composition in each land class is not necessarily realistic: for example there is no cropland in the agricultural land class and no urbanization in impervious areas. Hence it is interesting to test two different series of runs where the land class distributions differ, so as to be able to assess more critically the sensitivity of the model.

Figure 5 shows the distribution of the two vegetation categories, canopy or bare ground over the basin. Canopy is mainly present in the south and bare ground mainly in the north of the basin.

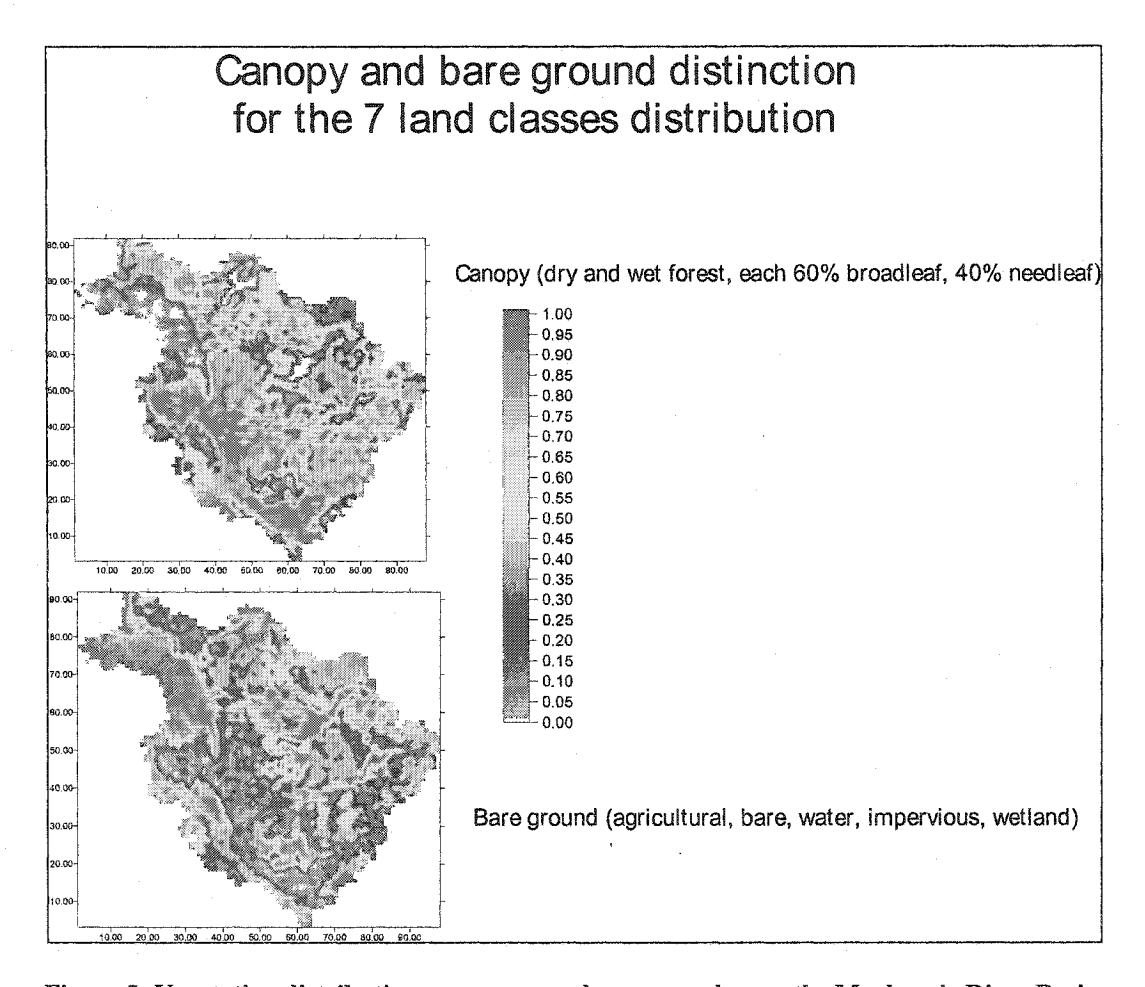


Figure 5: Vegetation distribution, as canopy or bare ground, over the Mackenzie River Basin.

I call 'GEM 1' the single land-class WATCLASS simulation driven by the GEM incoming solar radiation, similarly the 'GEM 7 run' refers to the seven land-class

WATCLASS simulation, 'SAT 1 run' the single-land class WATCLASS simulation driven by the satellite observed incoming solar radiation field, and 'SAT 7 run' the seven land-class WATCLASS run. The runs with different numbers of land classes allow us to test the sensitivity of WATCLASS to uncertainties in the vegetation cover. One knows that the sensitivity of the model to uncertainties in solar radiation will be more or less significant depending on how much solar radiation is absorbed at the surface, hence on the reality of the albedo simulation.

## 2. GEM-WATCLASS simulation: theory

The atmospheric model GEM drives the hydrological model WATCLASS offline and by providing to WATCLASS the following energy and moisture input: incoming longwave radiation (ILR), incoming shortwave radiation (ISR), precipitation and some other atmospheric parameters characterizing energy and moisture fluxes at the surface: wind speed, sea-level pressure, specific humidity, screen-level air temperature. WATCLASS provides the following energy and moisture flux output: net longwave and shortwave radiation, sensible and latent heat fluxes, radiative surface temperature, heat conduction into the ground, runoff, evapotranspiration, streamflows, moisture storage, snow accumulation, fractional snow cover and snowmelt energy. See figure 6 for a summary. One has also to note that since GEM and WATCLASS are not coupled, any induced changes in moisture transports or energy fluxes at the surface do not yield any feedback on the precipitation rate or screen-level temperature, which in reality they must do. Since precipitation type (rain or snow) is defined in WATCLASS in terms of screen-level temperature, the amount, distribution and type of precipitation is identical in each run, even though surface temperatures in the four simulations may differ.

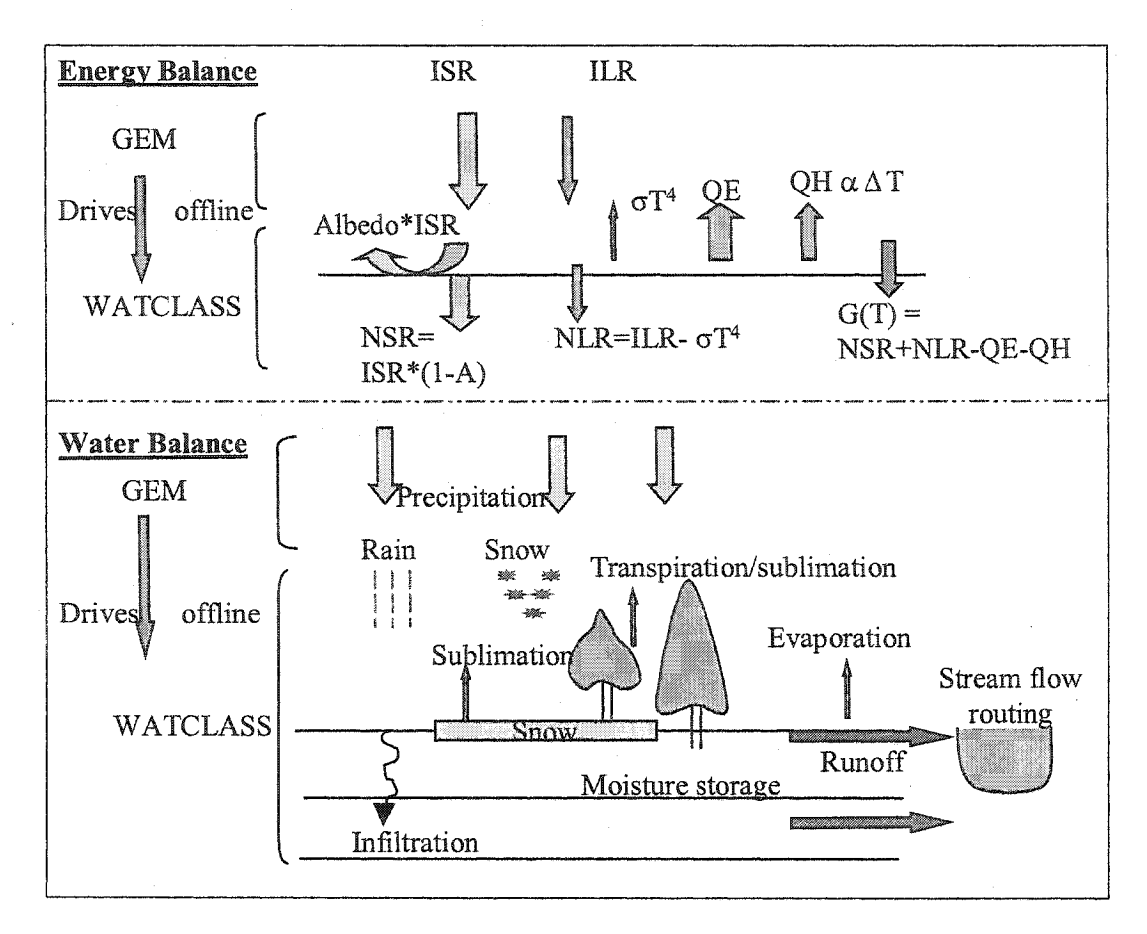


Figure 6: Summary of GEM and WATCLASS process simulations. ISR stands for incoming solar radiation, NSR for net solar radiation, ILR for incoming longwave radiation, NLR for net longwave radiation, QH for sensible heat flux, QE for latent heat flux, T for the surface temperature, G(T) for the heat conduction into the ground and  $\sigma$  is the Stefan-Boltzman constant and A the surface albedo.

This section, based on the description of CLASS described in Verseghy, (1991) and Verseghy et al. (1993), aims at explaining how different variables are simulated in WATCLASS, and therefore which ones, in theory, could be sensitive to uncertainties in incoming solar radiation, as simulated by the atmospheric model GEM. Energy fluxes will be presented first, followed by variables describing the snowpack and finally moisture transport variables.

### A. Energy Fluxes

WATCLASS simulates first the albedo and the different vegetation type transmissivities (broadleaf, needleleaf, crops or grass) taking into account the land cover

(snow, vegetation type and maturity), and then solves the energy balance equations iteratively so as to determine the surface temperature under the canopy (if present), T, and the canopy temperature, T<sub>c</sub>:

For the ground and ground overlaid by canopy, if present:

$$NSR + NLR(T) - QE(T) - QH(T) = G(T)$$

And for the canopy:

$$NSR_c + NLR_c(T_c) - QE_c(T_c) - (QH_c(T_c) - QH(T)) + S_c = \frac{C_c}{\Delta t} \times (T_c(t) - T_c(t-1))$$

where  $NSR_g$  and  $NSR_c$  are net solar radiation for the ground and the canopy respectively. Similarly  $NLR_g$  and  $NLR_c$  are net longwave radiation,  $QE_g$  and  $QE_c$  the latent heat fluxes,  $QH_g$  and  $QE_c$  the sensible heat fluxes, G(T) the heat flux into the ground,  $S_c$  the source/sink term for freezing or thawing of moisture stored on the canopy and  $C_c$  the heat capacity of the canopy. Once the effective radiative temperatures T and  $T_c$  are set up, the different fluxes are once again computed and stored for the water balance calculation and the next time step.

#### a) Net Solar Radiation

Net solar radiation is computed through the incoming solar radiation energy input ISR, the albedo and the vegetation transmissivities:

$$NSR = ISR (1-A_{ground})$$
 for ground  $NSR = \tau \cdot ISR (1-A_{ground})$  for ground overlaid by canopy  $NSR_c = ISR (1-A_{canopy})$  for canopy

where A is the albedo,  $\tau$  the canopy transmissivity and  $NSR_{g/c}$  the net solar radiation for the ground underlying canopy.

The uncertainty in net solar radiation (NSR) is due to uncertainties in incoming solar radiation, and also to induced uncertainties in albedo and vegetation transmissivities. For example, with a larger energy input, variations in albedo are induced by a different snowpack evolution: if snow melts earlier, then the albedo decreases earlier as well.

There is also a large albedo difference between the two different land class distribution runs: canopy has a smaller winter albedo (maximum of 0.2) than any other vegetation cover because fresh snow intercepted by the canopy falls from the canopy very quickly: hence more solar radiation is absorbed. Finally, uncertainties in vegetation transmissivities arise, as their computation takes into account the incoming solar radiation (see Verseghy et al. 1993 for more details).

Uncertainties in incoming solar radiation generate uncertainties in net solar radiation. In turn, the changes in net solar radiation fluxes drive the changes in the energy balance computations, which set the surface and canopy temperatures. Therefore, changes in these temperatures are expected.

#### b) Net Longwave radiation

Net longwave radiation is related to the surface and canopy temperatures:

$$NLR = \chi \left( ILR - \sigma T^4 \right)$$

$$NLR_c = (1 - \chi) \left( ILR - \sigma T_c^4 \right)$$

where  $\sigma$  is the Stefan-Boltzmann constant,  $\chi$  is the sky view factor which is a measure of the canopy closure and  $T_c$  the effective canopy temperature. The ground and the canopy are both considered to radiate as black bodies.

Thereby, a variation in the surface temperature  $T_c$ , or in the canopy temperature  $T_c$ , is expected to drive to a negatively correlated variation in NLR.

#### c) Latent Heat flux

Latent and sensible heat fluxes are computed in CLASS through the bulk aerodynamic approach for canopy, and the bulk transfer formulae for ground surfaces (Verseghy 1993). CLASS assumes that both fluxes from the ground, the sensible and latent heat, are negligible for ground overlaid by canopy because of small wind speed. Hence the latent heat flux corresponds to either the canopy latent heat flux, or the bare

ground latent heat flux. The latent heat flux (QE) represents evapotranspiration and sublimation.

For ground surfaces,

$$QE = \rho_a L_v V_a C_D (q_g - q_a)$$

where  $\rho_a$ ,  $V_a$ ,  $q_a$  are the air density, wind speed, specific humidity as input in WATCLASS,  $L_V$  the vaporization latent heat,  $C_D$  the surface roughness and  $q_g$  the surface specific humidity, which is function of and positively correlated to T (Verseghy 1991).

For the canopy, the latent heat flux differs depending on the occurrence of precipitation:

- If there is precipitation,

$$QE_{canopy, wet} = \rho_a L_v V_a C_D (q_{sat}(T_c) - q_a)$$

where q<sub>sat</sub> is the saturated specific humidity at T<sub>canopy</sub>.

- If there is not precipitation,

$$QE_{canopy, dry} = \rho_a L_v \frac{1}{\frac{1}{V_a C_D} + r_c} (q_{sat}(T_c) - q_a)$$

where a stomatal resistance  $r_c$  is added in the relation to prevent excessive transpiration. This bulk stomatal resistance to incoming solar radiation is represented by a proportionality factor of Max(1, 500/ISR-1.5). In practice this factor is most often set to one.

If snowpack is present on the ground, or if snow is falling, the sublimation latent heat is used, which is larger than the vaporization latent heat.

Hence, any induced increase in surface or canopy radiative temperature yields a positive change in the latent heat flux through a change in specific humidity. Changes in solar radiation also influence the latent heat flux through changes in stomatal resistance. If snow is falling, or if snowpack is present, the latent heat flux will be especially sensitive to temperature changes. In the case of incomplete snow cover, variations in fractional cover will influence the latent heat flux.

#### d) Sensible Heat Flux

The sensible heat flux (QH) is sensitive to the difference in temperature between air and the surface (canopy or ground), and represents free convection. Similarly to the latent heat flux, the sensible heat flux corresponds to either the canopy sensible heat flux, or the bare ground sensible heat flux:

$$QH = \rho_a C_p V_a C_D (T - Ta)$$

$$QH_c = \rho_a C_a V_a C_D (T_c - Ta)$$

where Ta is the screen-level temperature (input to WATCLASS),  $C_p$  the air specific heat for ground or canopy surfaces,  $C_D$  the surface drag coefficient and  $\rho_a$  the air density. Another relation for the sensible heat flux from snow overlying ground is used and is function of the surface specific humidity, which is dependant on the surface temperature (see Verseghy 1991 and Verseghy et al 1993).

Therefore a change in temperatures yields a direct change in the sensible heat fluxes.

#### e) Heat flux into the ground

The heat flux into the ground is computed through the energy balance computation at the ground:

$$G(T) = NSR + NLR - QH - QE$$

where G(T) is the heat flux into the ground.

When the G(T) turns positive in spring, this means that energy is available for snowmelt. Changes in G(T) would result from a change in the ground temperature.

## B. Snowpack

Snow is considered in CLASS as having complete coverage when the minimum depth is at least 10 cm everywhere. Snow temperature is computed through the same energy

balance equations as defined above, with Cs as the new heat capacity. Changes in snow temperature are expected to change the snowpack evolution.

Melting of the snowpack can occur in two different ways:

- If the surface energy balance generates a surface temperature above 0°C, energy is available for melting the surface of the snowpack. However, if the snowpack temperature is below zero, this melted water will percolate and refreeze, releasing latent heat and allowing for a snowpack temperature increase.
- Melting can also occur through heat conduction from the ground below the snowpack. When T<sub>ground</sub> goes above zero. This melted water, being at the bottom layer, is considered as 'rainfall' for the ground, and either infiltrates or ponds.

#### a) Snow Accumulation

GEM and SAT runs receive the same amount of precipitation, i.e. snow and rain. The snow accumulation is representative of the snowpack evolution: it increases when snow is falling, and decreases when snowmelt occurs or snow sublimates. Therefore, any change in NSR flux that results in changes in the temperatures and in the energy budget is expected to generate changes in snow accumulation.

#### b) Fractional snow cover

For full snow cover, the snowpack depth must be a minimum of 10 cm. During snowmelt, the fractional snow cover will start decreasing when the snowpack depth decreases below 10 cm. Therefore, although the beginning of the fractional snow cover depletion does *not* indicate when snowmelt starts, its delay between each run is a measure of the different snowpack evolution in the different runs, including different snowmelt timing and rate.

The criterion that we arbitrarily choose to quantify the beginning of the period, when snow starts to disappear significantly, is when the fractional snow cover has diminished by 10% of its maximal value reached in winter. This method is arbitrary, but nevertheless gives us a measure of the delay, if there is one, in the different runs.

#### C. Water Balance

#### a) Evapotranspiration

The evapotranspiration rate indicates the rate at which the water is lost to the atmosphere by sublimation, evaporation and transpiration. A change in latent heat flux is equivalent to a change in this moisture transport. And a change in evapotranspiration impacts directly on moisture storage and runoff.

#### b) Moisture storage

The moisture content depends on the moisture input and output, and soil and vegetation ability to retain the water. Hence a change in evapotranspiration directly impacts on the moisture storage, which influences runoff. The moisture content is computed as liquid or frozen, in the three different soil layers of the model.

#### c) Runoff

Runoff is the excess of water going out of the grid-box. Being quasi non-existent in wintertime as the snowpack stores all the water, a first peak in runoff in spring is interpreted as the snowmelt start.

The total runoff is the sum of the surface runoff from both pervious and impervious areas, as well as base flow and interflow. The water balance is given by:

$$P - E - R - \Delta S = residual$$

where P is precipitation, E the evapotranspiration, R the runoff and  $\Delta S$  the change in moisture storage from one time step to the other.

Since precipitation is identical in all runs, changes in runoff result from changes in evapotranspiration and in moisture storage, assuming a negligible residual.

#### d) Streamflow

WATFLOOD is responsible for the horizontal water balance in WATCLASS, and hence routes the runoff of each grid-box down to mainstream flow channels, and on to

the delta. In the output from WATCLASS, simulated stream flow can be compared with observed stream flow at different gauge stations. However, this being a sensitivity study, we will mainly focus on any changes in magnitude and timing of streamflows that could occur as a consequence of uncertainties in incoming solar radiation, and in particular on the first peak in spring, indicating snowmelt.

The next chapter explains the characteristics of the two different incoming solar radiation fields, one generated by GEM and the other retrieved from satellite observations, and assesses the uncertainties in the incoming solar radiation simulated by GEM.

## **Chapter III**

## **Data Processing**

The output variables from GEM, used to drive WATCLASS offline, are air specific humidity, sea-level pressure, screen-level air temperature, incoming solar radiation, incoming longwave radiation, wind speed and precipitation. To fulfill the WATCLASS input requirements, some initial hydrological variables such as streamflows and snow amount are added.

## 1. GEM simulated solar radiation

Available GEM archived fields for this study are incoming and net surface solar radiation accumulated over three hours for the period of interest (from October 1998 to September1999). GEM net solar radiation field is only used for processing the satellite solar radiation field, as explained in the section below, whereas GEM incoming solar radiation field is input to WATCLASS. The land surface scheme used in the GEM simulations is the force-restore method (Deardoff 1978).

The hourly values of incoming and net solar radiation fields ( $\underline{ISR_{GEM}}$  and  $\underline{NSR_{GEM}}$ ) are simply obtained from the three-hour average GEM fields by dividing the accumulated fields by three.  $\underline{ISR_{GEM}}$  is stored on a sub-polar stereographic grid, being true scale at 60°N, with a 20 km-resolution and  $\underline{NSR_{GEM}}$  is stored on a latitude-longitude grid, with the same resolution.

#### 2. Satellite observed solar radiation

The satellite-observed fields are Advanced Very High Resolution Radiometer (AVHRR) narrowband outgoing solar radiances at the top of atmosphere (TOA), from polar orbiting environmental satellites NOAA-12 and NOAA-14. As described in Feng (2001), these TOA instantaneous satellite data are interpolated and extrapolated, taking into account the solar zenith angle, to obtain hourly values. However one needs the complete solar radiation spectrum (broadband). Thus narrowband solar radiances are converted into broadband outgoing fluxes using narrowband to broadband conversion (Feng et al. 2002), and an angular distribution model (Suttles et al, 1988). Net solar radiation fluxes at the surface are derived from the Li et al. (1993a) algorithm, and verified against surface observations (Li et al., 1993b and Feng, 2001), showing good agreement.

Depending on the time of the year, there may be a total of as many as six daytime passes over the Mackenzie Basin by the two satellites (figure 7). We only generate radiation fields from the satellite data for times between 11 to 26 UTC (i.e. 2 UTC on the following day). This is not a limitation in winter, but we miss data for early and late hours of the day in summer when there is still light. Also, there are no satellite overpasses near noon (figure 7), and some parts of the basin, such as the northern portion, are not well observed at certain hours: one needs to fill these data fields and transform them into incoming solar radiation fields in order to drive WATCLASS.

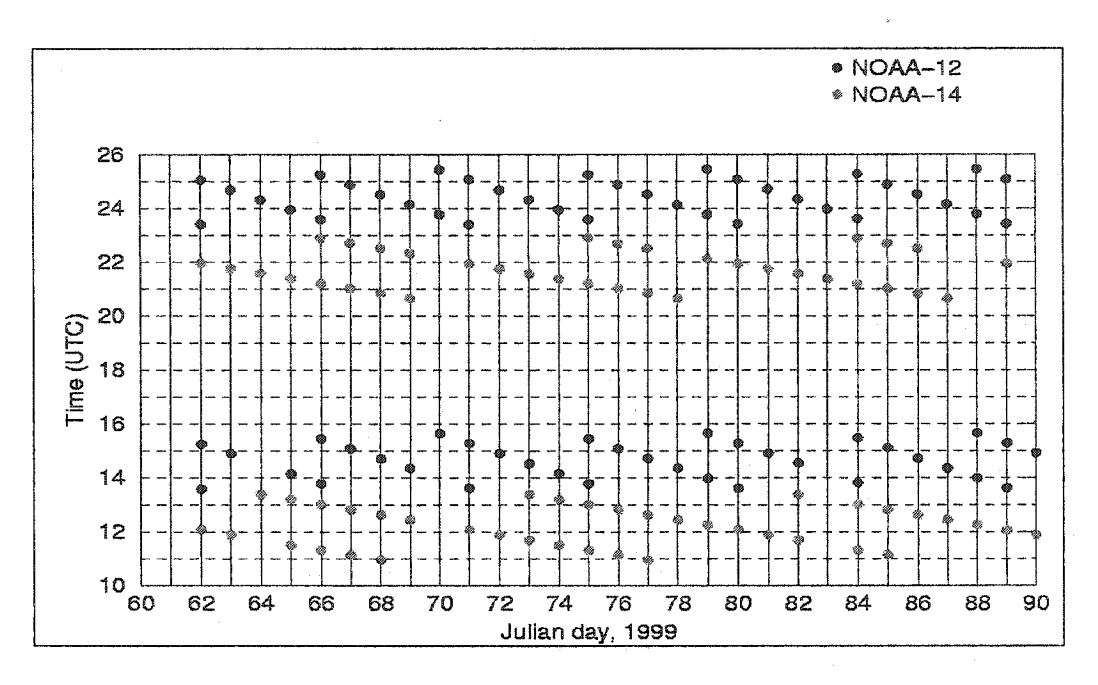


Figure 7: Timing of the satellites NOAA-12 and -14 overpasses over the Mackenzie River Basin, in March 1999 (Courtesy of Jian Feng).

#### A. First procedure of interpolation/extrapolation

We first put the available satellite net solar radiation into a latitude/longitude grid with a 20 km-resolution.

To fill temporal gaps in the net solar flux at the surface, we simply assume a cos (SZA) dependence of the flux, where SZA is the solar zenith angle. This is an oversimplified assumption, which does not bias the sensitivity runs afterwards, since we are only trying to obtain as many observational data as possible so as to be able to compare satellite net solar radiation field to GEM corresponding field in a first step. We use the following inverse temporal weighted equation, which limits the extrapolation/interpolation to two hours in order to limit the errors in what we still consider as being observational data:

- Interpolation case: if  $(h_{for}-h)$  and  $(h-h_{back}) \le 2$ 

$$\frac{NSR(x,y,h)}{SZA(y,h)} = \frac{(h_{for} - h)}{(h_{for} - h_{back})} \times \frac{NSR(x,y,h_{back})}{SZA(y,h_{back})} + \frac{(h - h_{back})}{(h_{for} - h_{back})} \times \frac{NSR(x,y,h_{for})}{SZA(y,h_{for})}$$

- Extrapolation case:

$$\frac{NSR(x,y,h)}{SZA(y,h)} = \frac{NSR(x,y,h_{back})}{SZA(y,h_{back})}$$
 if (h<sub>for</sub>-h)>2

$$\frac{NSR(x,y,h)}{SZA(y,h)} = \frac{NSR(x,y,h_{for})}{SZA(y,h_{for})}$$
 if (h-h<sub>back</sub>)>2

- Missing data: if (h<sub>for</sub>-h) and (h-h<sub>back</sub>) 
$$> 2$$
 
$$\frac{NSR(x,y,h)}{SZA(y,h)} = 0$$

where x is the longitude index, y is the latitude index, h is the current time step,  $h_{back}$  is the first available (meaning non-zero) backward satellite observation time, and  $h_{for}$  the first available forward satellite observation time, with  $(h_{for}-h)$  and  $(h-h_{back})$  not exceeding two hours.

Figure 8 shows the original satellite data for 1999, May 24 with ten missing hourly fields. Figure 9 shows the processed satellite data with the procedure described above: three time steps have been filled by extrapolation.

Therefore, this step increases the number of observations, but it does not fill missing data at every time step. This partially filled net solar radiation field then undergoes a second filling procedure as described below.

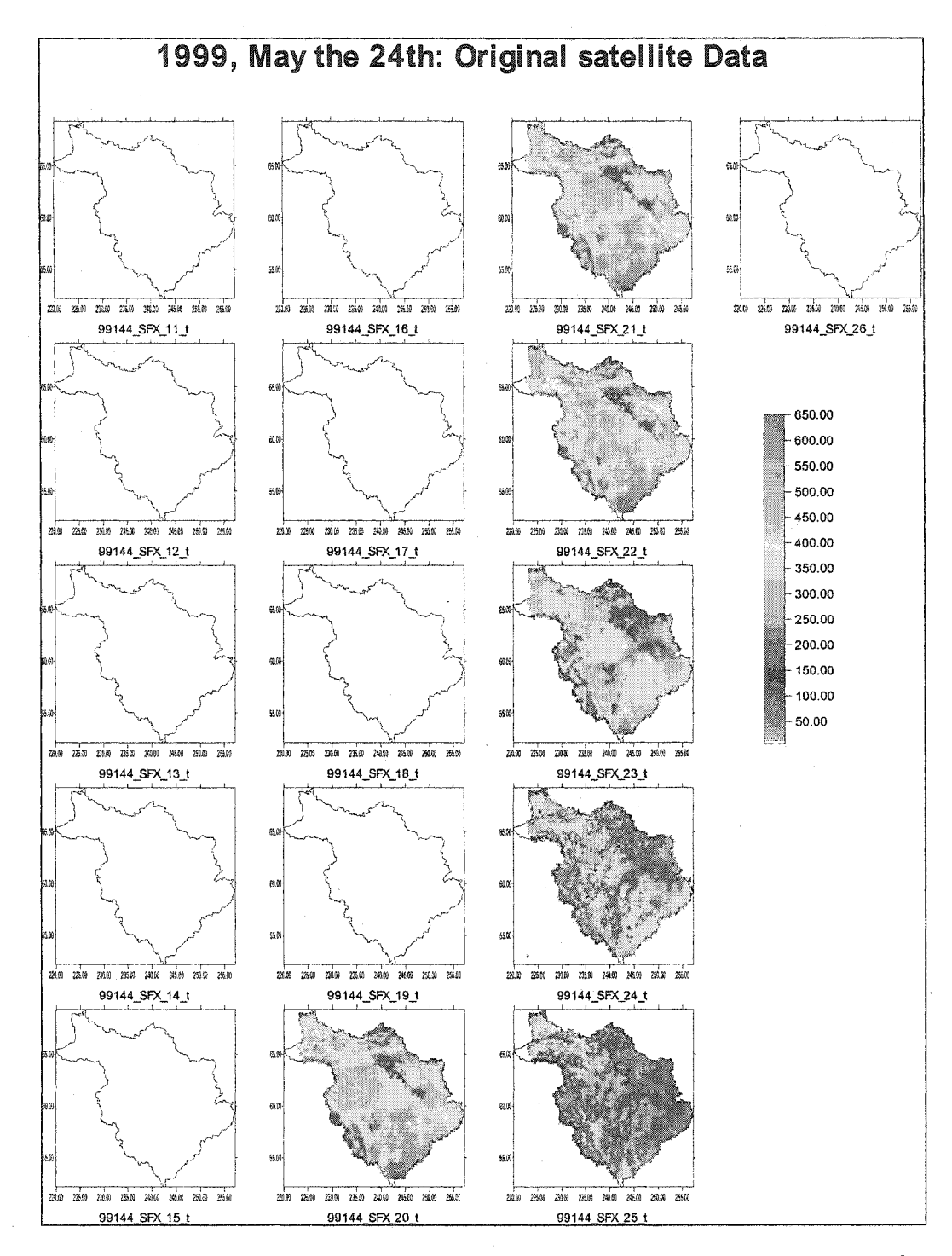


Figure 8: Available satellite NSR data for one particular day, on 1999, May 24 (in W.m<sup>-2</sup>).

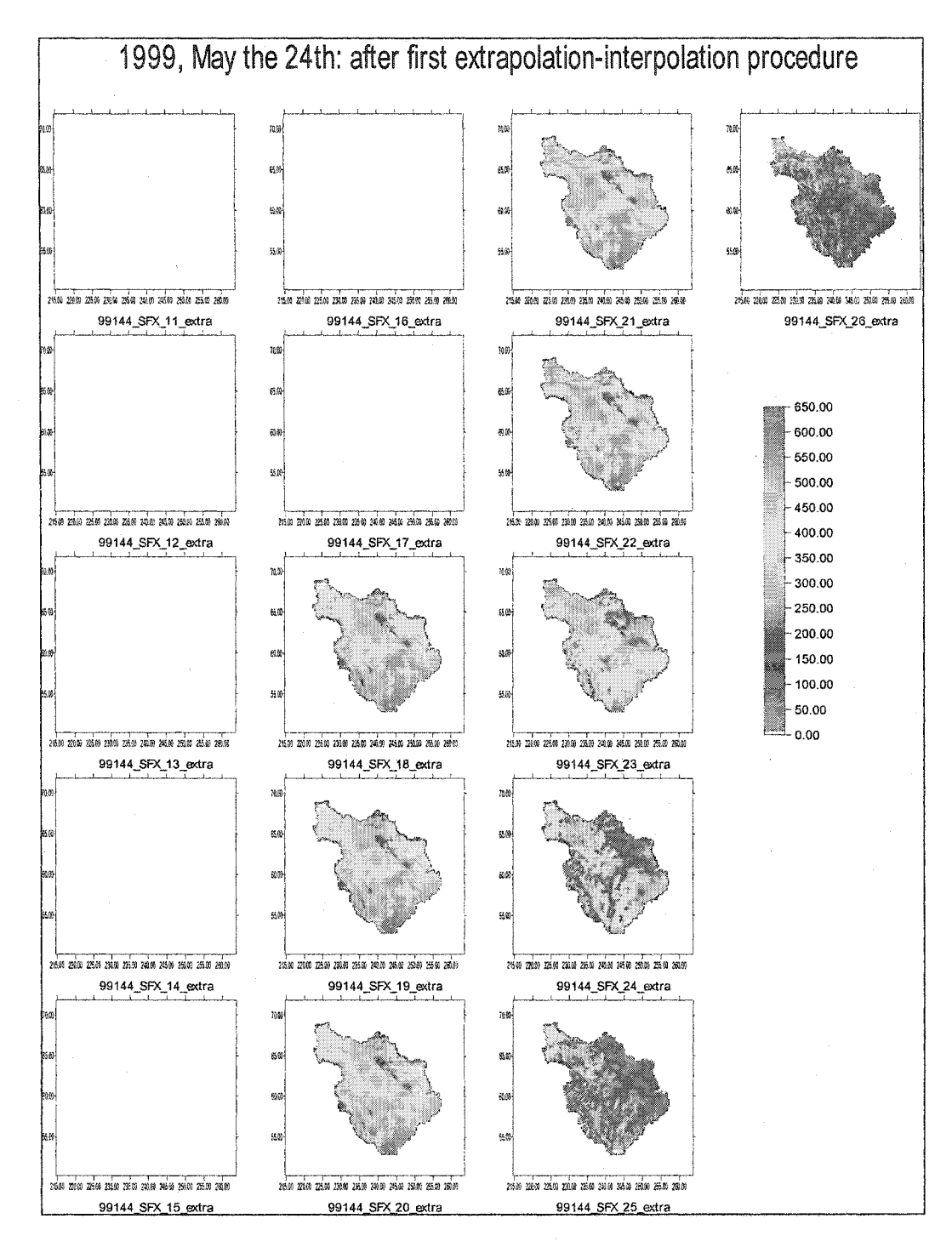


Figure 9: Available satellite NSR data, for 1999, May 24, after the first step of extrapolation ( in  $W.m^{-2}$ ).

# B. Filling all missing data and transfer into incoming solar radiation

Two approaches to fill the entire satellite observed net solar radiation field have been tested, and are presented below. However, only one will be used in this thesis because it was more appropriate for a test of sensitivity to a change in the net solar radiation field.

#### a) The 'normalization' method

The first approach fills and transforms the net solar radiation field into incoming solar radiation field at the same time. At all locations and times, where satellite observations, as obtained from the previous step, are available, we generate the three-hour average net satellite observed solar radiation flux *NSR<sub>sat</sub>*, from 10 to 12 UTC, 13 to 15 UTC, 16 to 18 UTC, 19 to 21 UTC, 22 to 24 UTC and 25 to 27 UTC. But since satellite observations were never available at 10 and 27 UTC, the average values from 10-12 and 25-27 UTC are taken to be the two-hour averages 11-12 and 25-26 UTC. Figure 10 shows the correlation between the basin monthly average net solar radiation fluxes *NSR<sub>SAT</sub>*(hour) and *NSR<sub>GEM</sub>*(hour): there is a significant GEM overestimation, largest in spring from February to June.

Next we compute a ratio of three-hour averaged net solar radiation fields <u>NSR<sub>sat</sub>/NSR<sub>GEM</sub></u>(x,y,hour), which is then averaged spatially over the basin, considering only non-zero ratio. Table 1 presents the basin 3-hour average ratio <u>NSR<sub>sat</sub>/NSR<sub>GEM</sub></u>(hour), at 10 UTC for example, which is applied from 10 to 12 UTC and similarly at 13, 16, 19, 22 and 25 UTC. The ratios are generally smaller than unity, implying a significant GEM net solar radiation overestimation.

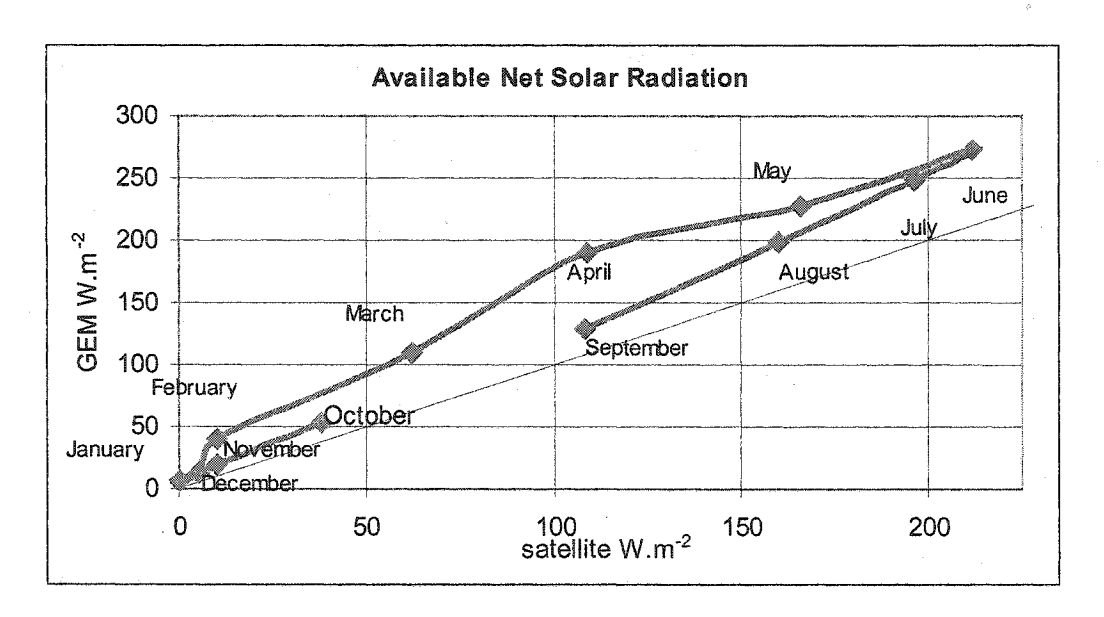


Figure 10: Comparison of the available basin monthly average net solar radiation satellite with the GEM averages using the corresponding data.

Because at 10 and 25 UTC ratios were computed from two-hour average satellite net solar radiation, and also because in winter GEM and satellite NSR values are very small (in the order of 1 W.m<sup>-2</sup>) early in the morning between 11 and 12 UTC, unrealistic ratios were generally set to one. Some unrealistic ratios at 13 and 22 UTC in winter were also set to one: they resulted from a lack of satellite data, thus also involving two-hour averages <u>NSR<sub>SAT</sub></u>. Actually, it would have been more objective to set all unrealistic ratios, those larger than 2 for example, to a unit value. Nevertheless, keeping large ratio values at 10 UTC has a limited impact afterwards, since incoming solar radiation values are still very low at that time.

The satellite data field,  $NSR_{sat}$ , is filled and transformed into incoming solar radiation  $ISR_{sat}$  with the value of incoming solar radiation from,  $ISR_{GEM}$ , normalized by the basin monthly average of the corresponding three-hour average **net fluxes** ratio  $NSR_{sat}/NSR_{GEM}$ , at 10, 13, 16, 19, 22 or 25 UTC:

 $\underline{ISR_{Sat}}(x', y', hour) = \underline{ISR_{GEM}}(x', y', hour) \cdot (\underline{NSR_{Sat}}/\underline{NSR_{GEM}})$  (hour) where x' and y' are the polar stereographic indices.

NSR <sub>sat</sub> /NSR <sub>GEM</sub>	10 UTC	13 UTC	16 UTC	19 UTC	22 UTC	25 UTC
98/10	1.00	1.25	1.14	0.67	0.72	1.06
98/11	1.00	1.00	1.11	0.59	0.29	1.00
98/12	1.00	1.00	0.19	0.07	0.08	1.00
99/01	1.00	1.54	0.52	0.71	1.00	1.00
99/02	1.00	1.00	1.34	0.47	0.52	0.43
99/03	1.00	1.30	0.76	0.53	0.50	0.60
99/04	11.66	0.79	0.62	0.54	0.53	0.55
99/05	4.28	0.79	0.72	0.78	0.72	0.67
99/06	2.64	0.82	0.78	0.81	0.74	0.68
99/07	3.43	0.86	0.77	0.82	0.77	0.71
99/08	16.86	1.22	0.90	0.82	0.71	0.65
99/09	1.12	1.45	0.94	0.83	0.76	0.91

Table 1: Monthly basin average ratios  $NSR_{Sal}/NSR_{GEM}$  at 10, 13, 16, 19 and 25 UTC

This procedure assigns to the satellite incoming solar radiation field the same spatial distribution of fluxes as GEM, but values are normalized. The differences in the net solar radiation at the surface from GEM and the application of the Li et al. algorithm to the satellite data are, apart from measurement errors, due to differences in the transmission of the atmosphere implicit in the GEM model and the algorithm, and due to implicit differences in surface albedo. Inherent in the renormalization by <u>NSR<sub>sat</sub>/NSR<sub>GEM</sub></u> is the assumption that the differences are in fact due to atmospheric transmission and not to albedo, which is consistent with the observation that the differences in *NSR<sub>sat</sub>* and *NSR<sub>GEM</sub>* are small for clear skies (Feng 2002):

$$\alpha_{Algorithm} = 1 - A_{GEM}$$

where  $\alpha_{Algorithm}$  is the surface absorptivity implicit in the Li et al algorithm, and  $A_{GEM}$  the albedo simulated by GEM.

#### b) The statistical filling method

The second approach, which has not been used hereafter in this study, was to compute a monthly average of the available retrievals of net solar radiation at each grid-box and every hour, from 11 to 26 UTC, ignoring the solar zenith angle dependence. Looking at the monthly averages at different hours, the basin was entirely filled, except at the extreme southern part for about 5 grid-boxes, and the extreme north-west, for about 15 grid-boxes. These few (compared to the 4668 grid-boxes in the basin) were filled by spatial extrapolation from adjacent regions. These monthly averages are then used to fill the missing hourly data at all of the grid-boxes. The incoming solar flux is deduced from this net field and the surface albedo from WATCLASS as calculated at the previous time step (figure 11). WATCLASS computes the albedo only during daytime. The above procedure required a small change in the code, so as to generate the albedo at all time steps.

The major biases of this method are that, although it might be quite acceptable on a monthly scale, the incoming solar radiation fields will be inaccurate on a daily scale, and even more so on the 30 minutes WATCLASS time step. Perhaps more importantly there is an albedo inconsistency. When comparing the outputs from WATCLASS, having input the incoming solar radiation field either from GEM or satellite retrievals, differences will not only be a result of differences in the incoming solar radiation fields between GEM simulation and satellite observations, but will also be due to the different WATCLASS and Li et al. algorithm surface transmission (table 2).

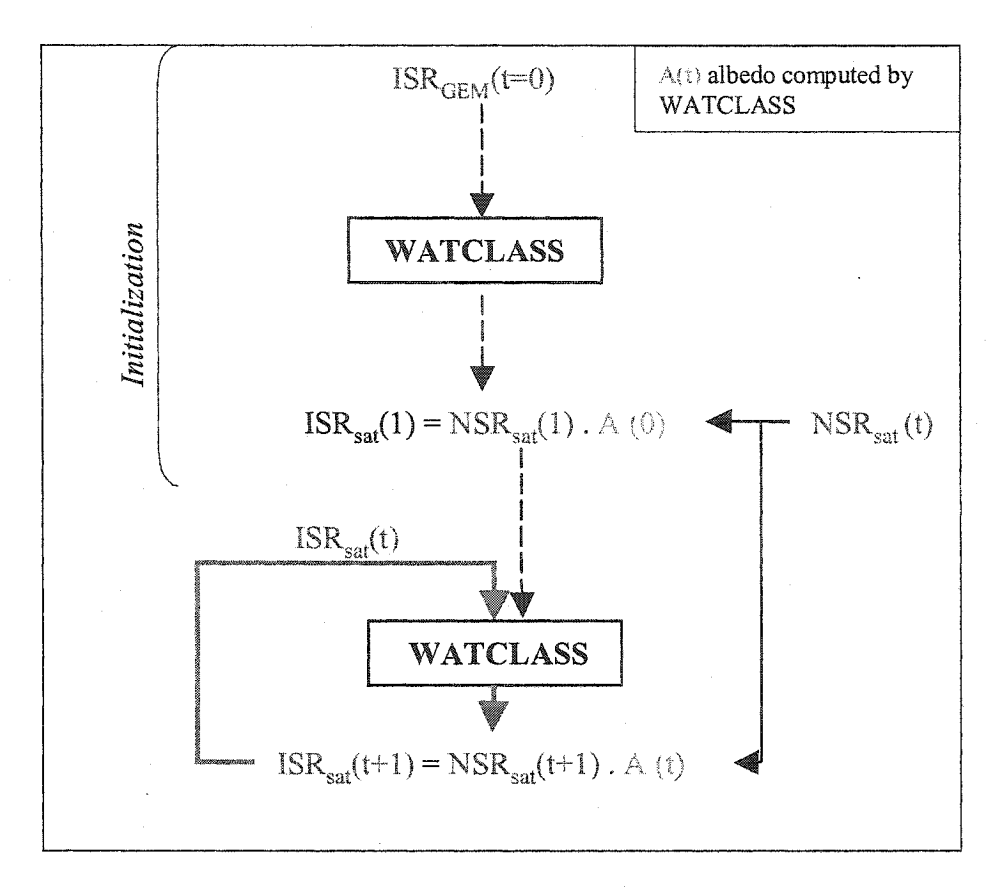


Figure 11: Second approach filled incoming satellite solar radiation retrieval using WATCLASS albedo from the previous time step.

Hence, we cannot deduce if WATCLASS is more sensitive to a change in the net solar radiation field, or in the albedo computation. Therefore, we decided not to go on with this second approach. However this approach could be compared in future work to the first method of filling data, so as to discern the sensitivity of WATCLASS to both incoming solar radiation and albedo/transmission changes (table 2).

WATCLASS	GEM runs	SAT runs: 1st Approach	SAT runs: 2nd Approach		
		'Normalization method'	'Statistical filling'		
ISR Input	<u>ISR<sub>GEM</sub></u>	ISR <sub>GEM</sub> . (NSR <sub>sat</sub> /NSR <sub>GEM</sub> )	NSR <sub>sat</sub> /(1-A <sub>CLASS</sub> )		
		$\sim NSR_{sat} / (1-A_{GEM})$	$= ISR_{sat.} \alpha_{Algorithm}/(1-A_{CLASS})$		
·		$\sim \underline{ISR_{sat}}$ . $\alpha_{Algorithm}/(1-A_{GEM})$			
		= <u>ISR<sub>sat</sub></u>			
		α is the surface absorptivity			
		implicit in the Li et al. algorithm			
NSR Output	ISR <sub>GEM</sub> .(1-A <sub>CLASS</sub> )	ISR <sub>SAT</sub> . (1-A <sub>CLASS</sub> )	$NSR_{sat} = ISR_{sat} \cdot \alpha_{Algorithm}$		
Interest for		Assuming that	Albedo inconsistency:		
comparison		$\alpha_{Algorithm} = (1-A_{GEM}),$	α <sub>Algorithm</sub> different from (1-		
with 'GEM		we compare the effect of	A <sub>CLASS</sub> ), and the filling		
runs'		changes in ISR only, due to	method is less accurate		
		different atmospheric			
		transmission (Feng 2002)			
Comparison			Would provide effect of		
between			changes in surface		
'SAT runs'			transmission Cl <sub>Algorithm</sub> and		
			(1-A <sub>CLASS</sub> )		

Table 2: Summary of possible input to WATCLASS and their analysis interest.

# 3. Incoming Solar radiation field

In each series of WATCLASS runs, we input either the GEM simulated ISR field or the 'satellite ISR', that is the field retrieved from satellite observations and obtained with the 'normalization method', as explained earlier.

Figure 12 shows the basin mean incoming solar radiation fluxes (ISR) from the satellite and from GEM on a day-to-day evolution: there is a 36% relative error (34 W m<sup>2</sup>) in the annual average ISR of GEM relative to the satellite ISR, and in absolute terms the differences are often more than 50 W m<sup>-2</sup> in spring and early summer.

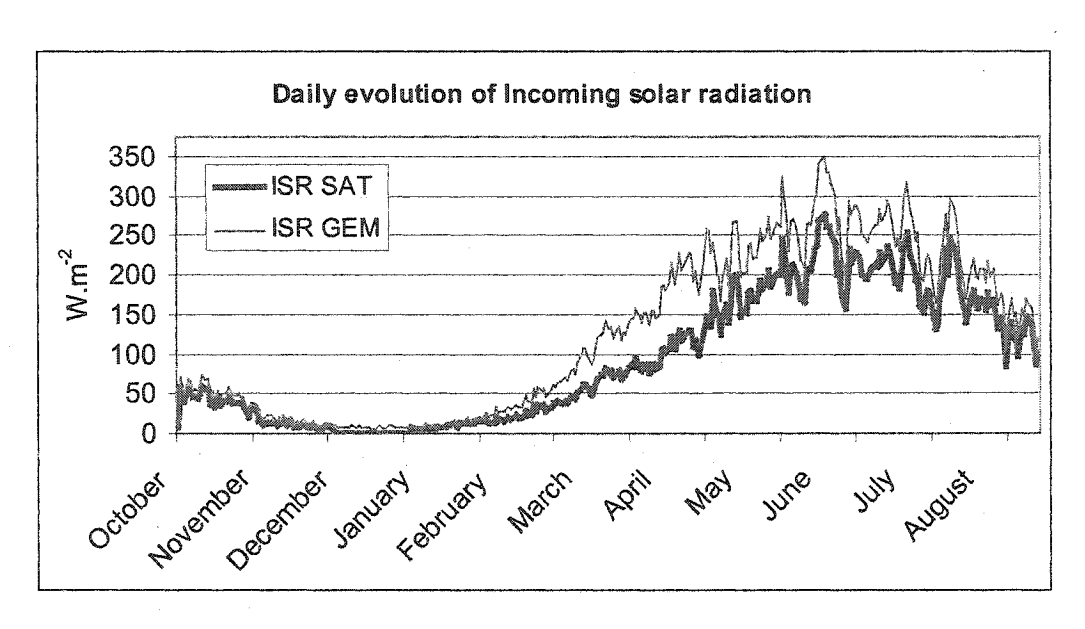


Figure 12: Daily basin average incoming solar radiation field.

Feng (2002) reports a GEM-CAGES rerun *net* solar radiation overestimation of the order of 30 %, relative to satellite observations of *net* solar radiation field for *summer months (June to August)*. The comparison was for co-located satellite and GEM-CAGES rerun data at about 40 sites in the Mackenzie River Basin. In the GEM simulation used here, the *basin average annual incoming* solar radiation was 36% greater than the corresponding satellite value, which is consistent with the result found by Feng (2002). Actually, in our GEM simulation, there is a 23% GEM overestimation for the summer months (July to October), 40% for spring months (April-June) and 72% in winter but with very low values (figure 13).

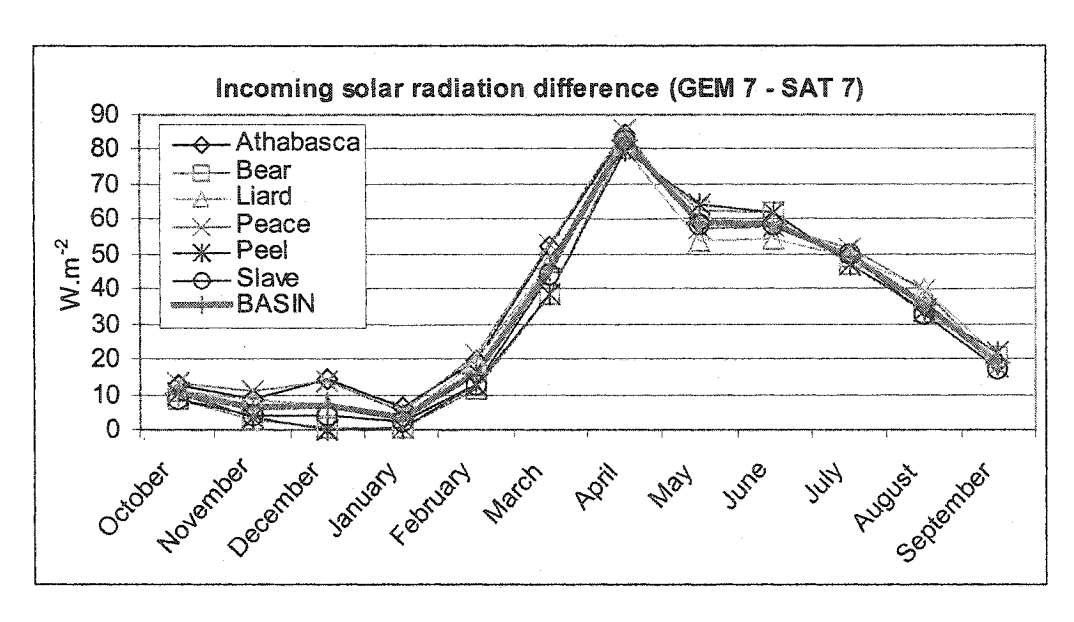


Figure 13: Monthly incoming solar radiation difference between GEM and SAT.

### 4. WATCLASS code modifications

#### A. 3-hour averages and albedo computation

The hourly values of incoming and net solar radiation fields ( $ISR_{GEM}$  and  $NSR_{GEM}$ ) were simply obtained from the three-hour average GEM fields by dividing the accumulated fields by three. Although this procedure does not change the total downward flux, it does generate errors in the flux absorbed at the surface because of the way surface albedo is stored in WATCLASS.

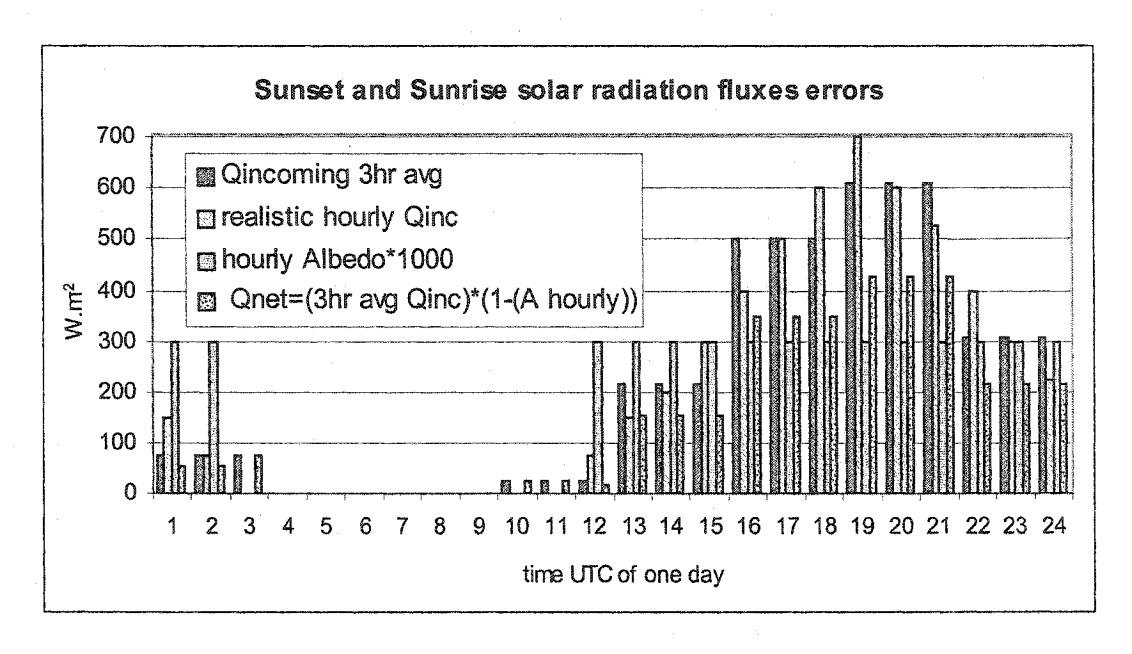


Figure 14: Albedo, 3-hour averaged and real hourly incoming solar radiation compared with the hourly net solar radiation for a typical day. Overestimation of the computed net solar radiation fluxes occurs at 3, 10 and 11 UTC.

At night, surface albedos are set to zero. The above procedure generates downward fluxes just before sunrise and after sunset. Because the surface albedo is set to zero at night, the flux absorbed at the surface is erroneously high. Figure 14 shows an example of the input to WATCLASS, the 3-hour average incoming solar radiation, the output from WATCLASS, the 30 minutes net solar radiation flux but here averaged to one hour for simplicity, and also the albedo. As seen in the figure 14, since the values at these times are not high, this error might not be significant but it may be expected to be present the whole year: in winter, albedo values are very high, but solar radiation is very low, and in summer, albedo values are low but solar radiation is high. In this study, we assumed this error not to be significant, and it should not have any impact on the sensitivity since the same error is simulated for all runs. However see Annexe A for some suggestion of modifications.

#### B. WATCLASS structure

WATCLASS was available to output a limited number of variables at up to three grid-boxes only, and for only one land class at the time, either every 30 minutes or accumulated / averaged over the day.

- For this study, we modified the code so that each variable of interest could be outputted at each grid-box of the basin. Furthermore, WATCLASS uses WATFLOOD indexes (figure 15), which are designed to route water masses and are based on the topography. Hence the first index is the most 'upstream' grid-box and the last one is at the delta. We changed the way to store and output variables of interest: topographical WATFLOOD index at each grid-box was changed to the CLASS index, which is the latitude/longitude grid.

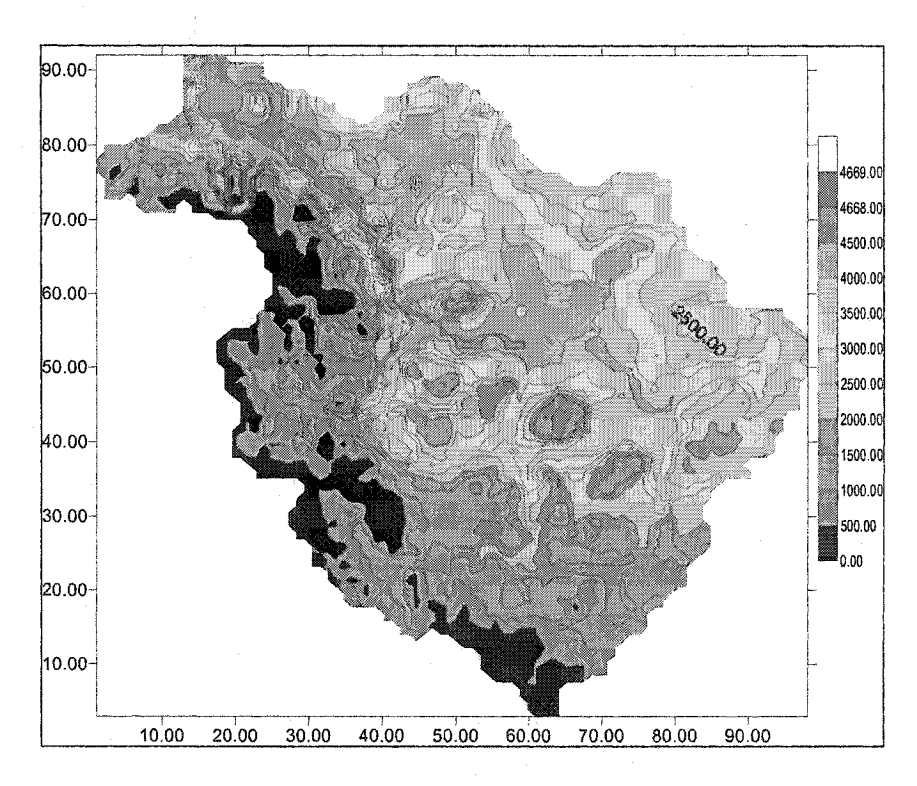


Figure 15: Water routing indices in WATFLOOD: a topographic index approach water routing goes from low to higher grid-box indexes, up to 4668 at the delta (in red).

- We also inserted several other variables not previously available. With these new variables and most importantly the output at each grid-box, we had then to face some

computer memory issues. The WATCLASS output time step is 30 minutes. Considering that our experiment runs for one year, 30-minute outputs are unnecessary and we therefore limited the output to only either a daily average or a daily accumulation, depending on the significance of the variable: hydrological variables such as runoff and precipitation are accumulated, while energy variables such as solar radiation or surface temperature are averaged over 24 hours.

- We finally added an accumulation procedure so as to be able to output variables, that are weighted averaged parameters with respect to the different land classes that make up each grid-box (see appendix A).

#### C. WATCLASS time

The atmospheric input file data are labeled in terms of UTC time, whereas WATCLASS uses local time and assumes local time in its input files. Hence a time inconsistency exists between the model and the input file. See appendix A.

WATCLASS computes the albedo at daylight hours only, and is set to zero at night. The time inconsistency, described above, if uncorrected (figure 16), results in large errors in flux absorbed at the surface as illustrated schematically in figure 17.

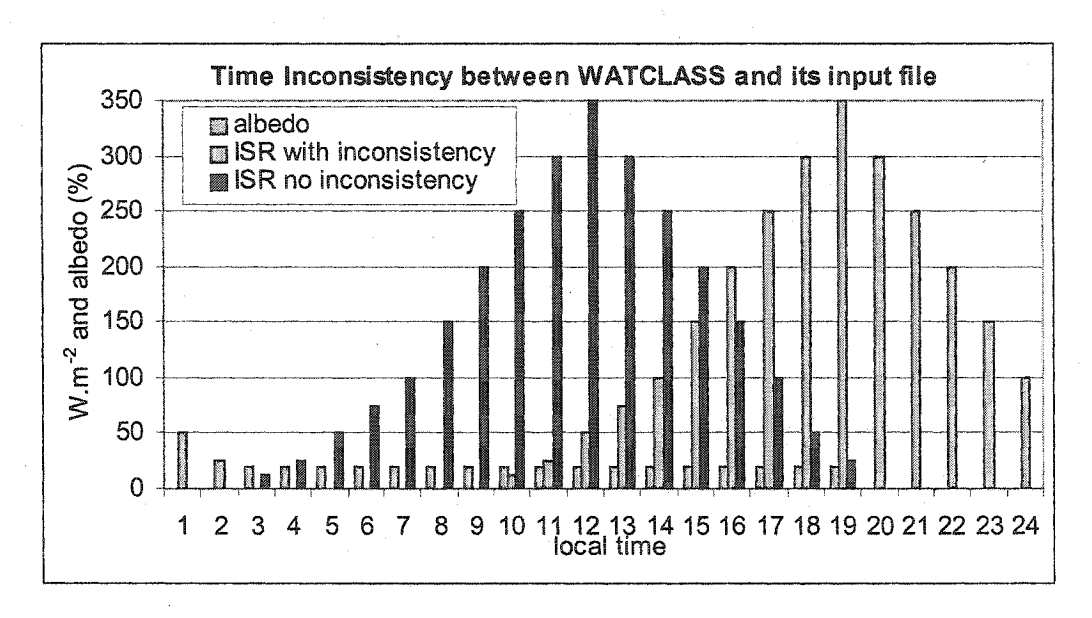


Figure 16: Incoming solar radiation (ISR) input with and without the time inconsistency, and non-zero albedo during local daylight hours for a typical day.

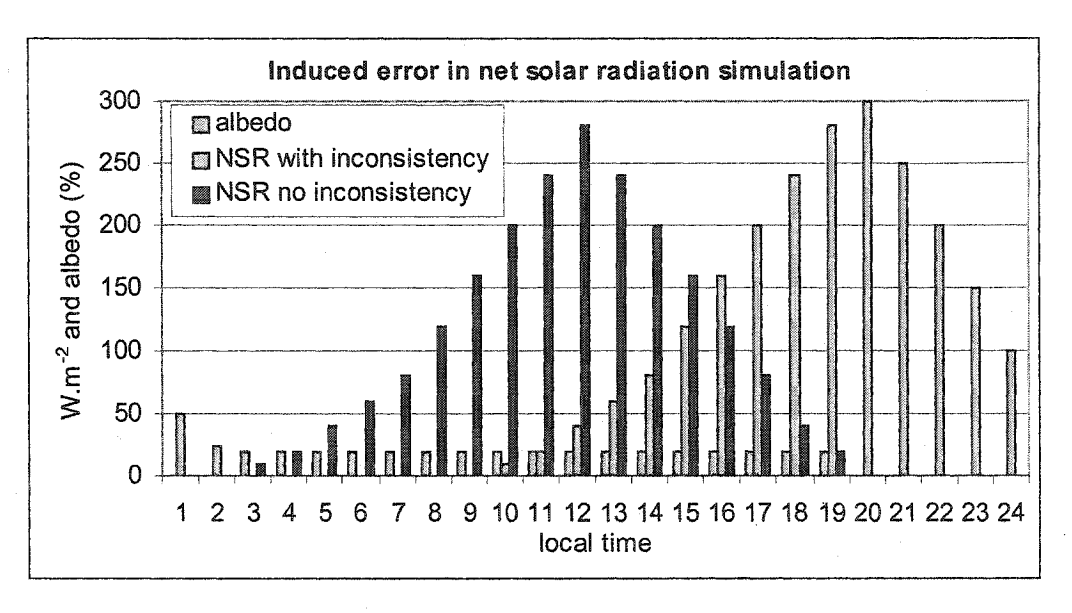


Figure 17: Non-zero albedo during daylight hours and net solar radiation (NSR) with and without the time inconsistency for a typical day: NSR overestimation if the inconsistency is not corrected.

We have quantified so far the uncertainties in the GEM simulated incoming solar radiation relatively to the equivalent field, retrieved from satellite measurements. These two ISR fields are then input to WATCLASS: those are the GEM and SAT runs. Next chapter presents and compares WATCLASS output variables.

# **Chapter IV**

# Results

Each WATCLASS run lasts for 343 days, starting October 1<sup>st</sup> 1998, to September 7<sup>th</sup> 1999. A minor technical issue forced the run to abort before completing a full year. In addition to our own code modifications, as described earlier in the WATCLASS code modifications section, the WATCLASS version used for these runs included University of Waterloo enhancements as of February 2002 for the single-land-class series of runs, and as of August 2002 for the seven-land-class series of runs.

In this section, GEM runs are compared relative to the SAT runs. Strictly speaking, since atmospheric input to WATCLASS are all provided by GEM, GEM runs should have been our references. However, since the incoming solar radiation input to SAT runs are more realistic, we refer to the SAT runs as being our reference runs and comparative statements are relative to them.

Several parameters have to be taken into account in the analysis of the different runs, since energy and moisture transports are interdependent: moisture transports such as condensation, snowmelt, evapotranspiration and sublimation (heat transport through stream flow is not yet simulated), are associated with an energy exchange. And each energy exchange has a direct or indirect feedback on moisture transport. In this results section, the sensitivity of different WATCLASS outputs are presented, separating energy fluxes from mass transports. However one should keep in mind that these fluxes are interconnected.

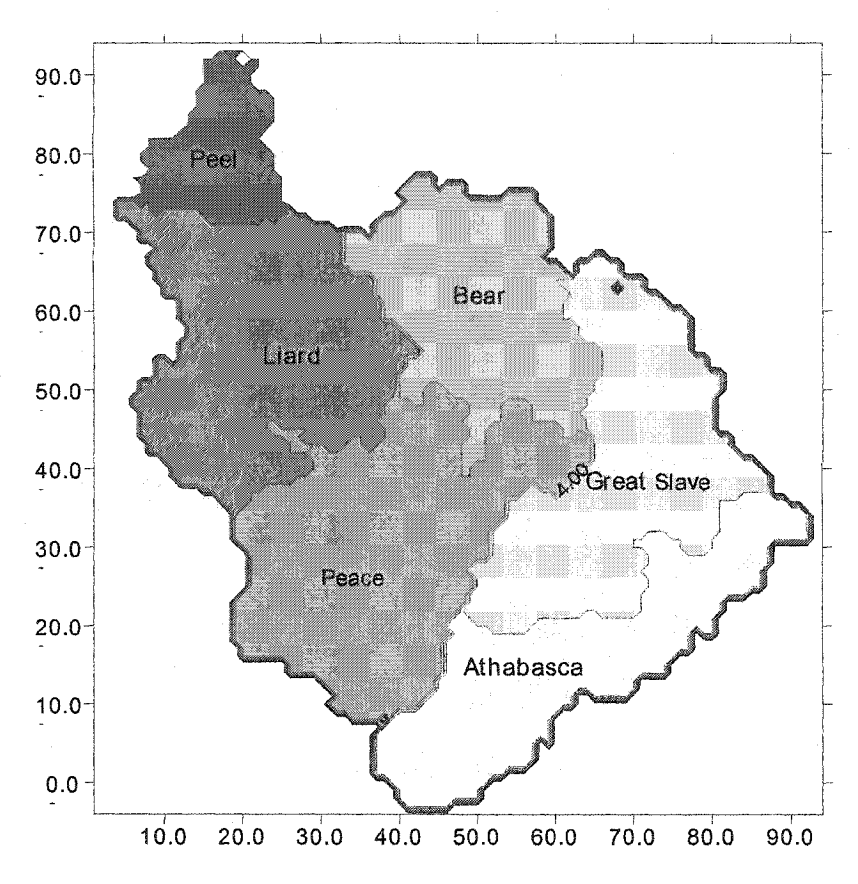


Figure 18: The sub-basins in the Mackenzie River Basin.

The first part will deal with energy variables while the second part will present the snowpack evolution, leading to the third part dealing with hydrological variables, i.e. mass transport. Furthermore, the discussion will be concentrated on the seasonal variability and especially on the snowmelt period: since the energy and the water balances endure important changes during or at the onset of snowmelt, we expect the largest sensitivity to be at that period. An equivalent analysis for the freeze-up period in fall would have required longer runs (1 year and a half runs) in order to be correctly

analyzed. Most of the analysis will be at the basin scale, but comparisons between sub-basins (figure 18) will provide information on regional variability (table 3 for the vegetation variability for example).

Fractional	Full	Athabasca	Bear	Liard	Peace	Peel	Slave
Land cover	Basin						
Canopy	0.51	0.6	0.43	0.61	0.6	0.18	0.46
Short Vegetation	0.49	0.4	0.57	0.39	0.4	0.82	0.54

Table 3: Fractional land cover for the seven land-class WATCLASS runs, distinguished as canopy or bare ground.

# 1. Energy budget

#### A. Net Solar Radiation and Albedo

Figure 19, showing the monthly basin average net solar radiation (NSR), has the same pattern as the ISR graph (figure 12). There is a yearlong GEM NSR overestimation, which is largest in absolute values in summer time but which is relatively the largest in winter. GEM runs overestimate annually the net solar radiation by 37% (30 W.m<sup>-2</sup>) for the single-land-class runs, and 36% (23 W.m<sup>-2</sup>) for the seven-land-class runs compared to the satellite retrievals. Also, it shows that NSR is larger for the single-land-class runs than for seven-land-class runs (22% on a basin annual average).

For the single-land-class runs, since the vegetation is 100% evergreen needle leaf, there is almost no sensitivity in the albedo to incoming solar radiation: therefore albedo differences between the two runs (GEM and SAT) are negligible throughout the basin over the whole year.

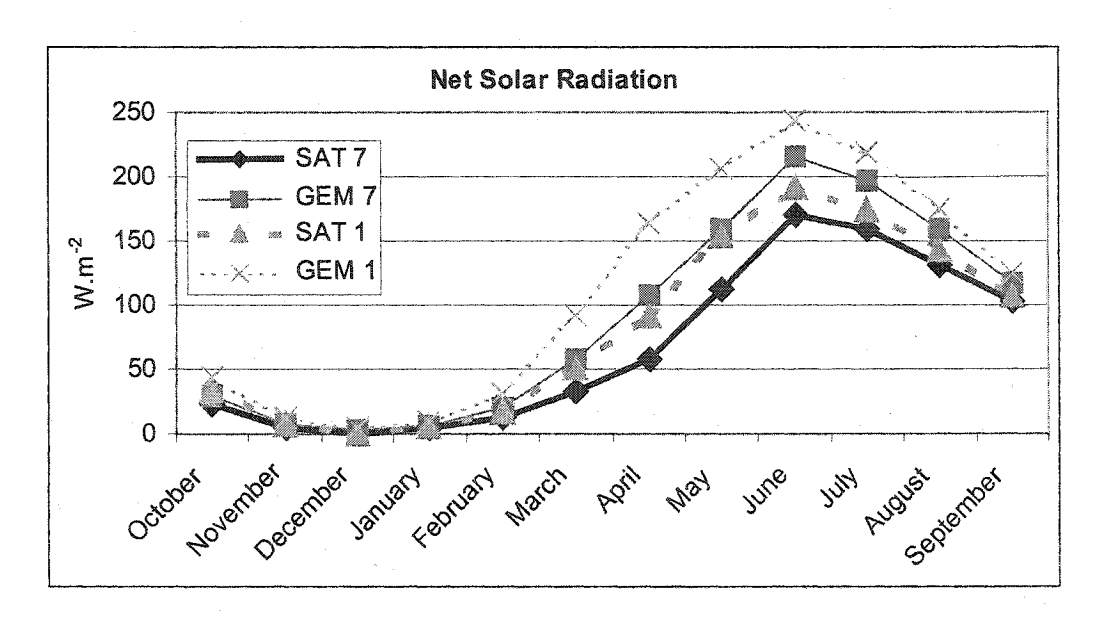


Figure 19: Monthly basin average NSR for the single and the seven-land-class runs.

For the seven-land-class runs, one should expect the surface albedo to respond to changes in ISR. In fact, the GEM 7 NSR induced basin average overestimation is also 36%. This implies that the albedo changes, which are most likely to be important during snowmelt and freeze-up, do not impact on the *annual* NSR. On a monthly scale however, we can see there that the GEM 7 NSR overestimation is larger in spring and early summer, and decreases right after.

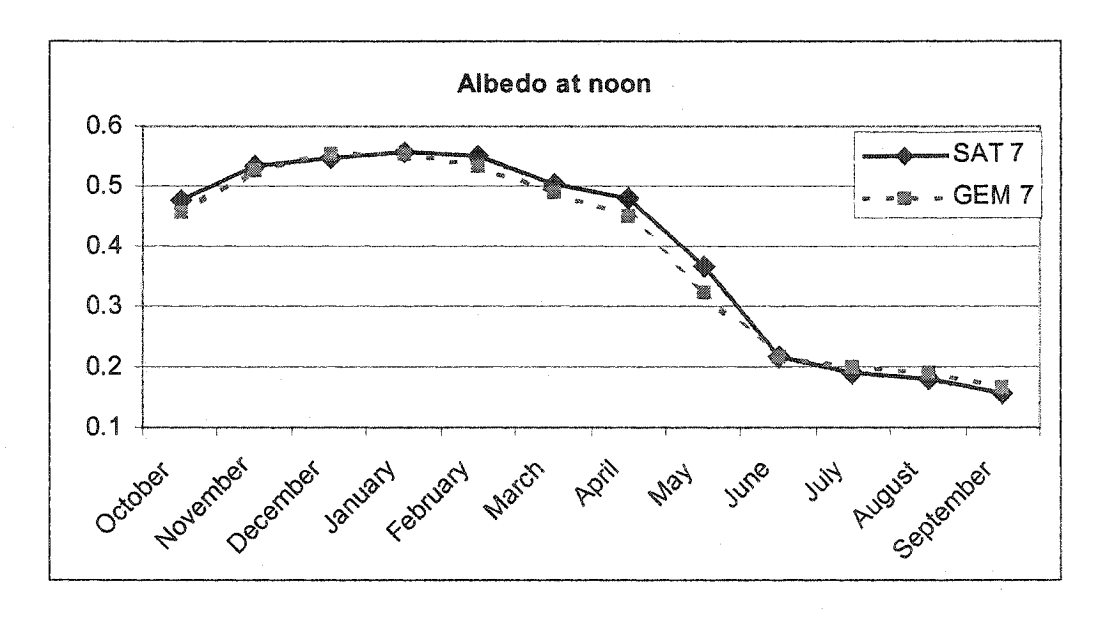


Figure 20: Monthly basin average albedo for the seven-land-class runs.

One notices in figure 20 the GEM 7 albedo underestimation from February to May: this makes the NSR GEM 7 overestimation larger in spring through:

where ISR<sup>+</sup> stands for the GEM incoming solar radiation overestimation, and NSR<sup>+</sup> for the net solar radiation overestimation. The number of '+' signs denotes the importance of the overestimation. 'A' stands for the induced WATCLASS albedo overestimation (A<sup>+</sup>) or underestimation (A<sup>-</sup>).

However, this larger overestimation is compensated by a GEM 7 albedo overestimation in summer, which lowers the GEM 7 NSR overestimation:

NSR fluxes (figure 21) in the sub-basins are generally quite similar, except from February to May. The February to May NSR dispersion is emphasized relatively to the dispersion in ISR (figure 13), especially in April. Likewise, the albedo monthly evolution (figure 20) shows the largest decrease between February and June, with the expected largest dispersion between sub-basins in April and May (figure 22). This results, we assume, from a different snowpack/snowmelt evolution between the different sub-basins at that time. As we will show later, the snowmelt in the different sub-basins starts at different times, which accounts for the range of albedo variations in spring. The surface albedos in spring are consistently larger in the SAT 7 run than the GEM 7 run, a result of earlier snowmelt in the GEM run. The differences in the onset of melting between the GEM and SAT runs in the different sub-basins further enhance the spread in NSR fluxes at that time.

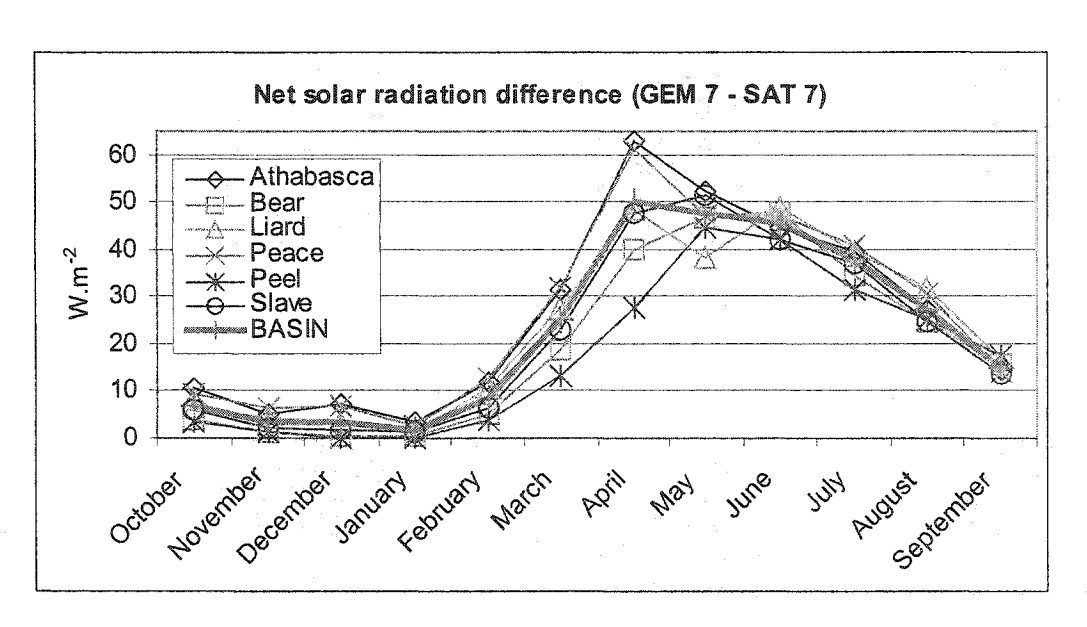


Figure 21: Monthly NSR absolute difference between GEM 7 and SAT 7 runs, in the different subbasins.

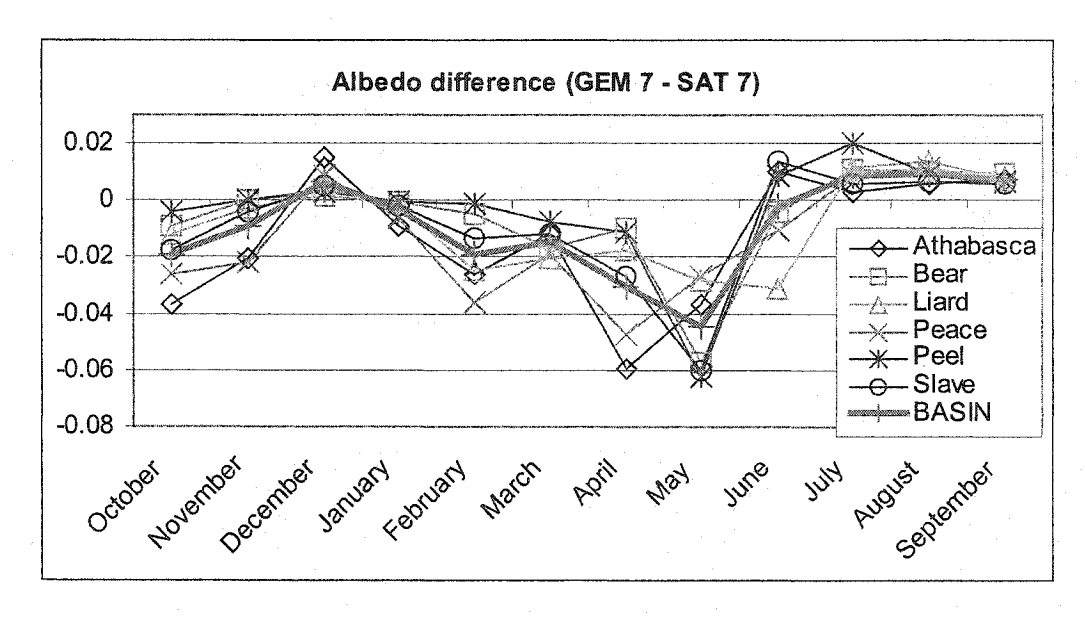


Figure 22: Monthly albedo absolute difference between GEM 7 and SAT 7 runs, for the different sub-basins.

#### B. Surface and canopy temperatures

The effective surface temperature is an average temperature of the ground, and the snow and the canopy, if present. The GEM basin annual average surface temperature overestimation is less for the single land-class (+0.55°C) than for the seven-land-class run

(+1.15°C) (figure 23): the 100% canopy cover damps changes in surface temperature. In summer, the short vegetation underlying canopy has cooler surface temperatures, but it has higher surface temperatures in winter.

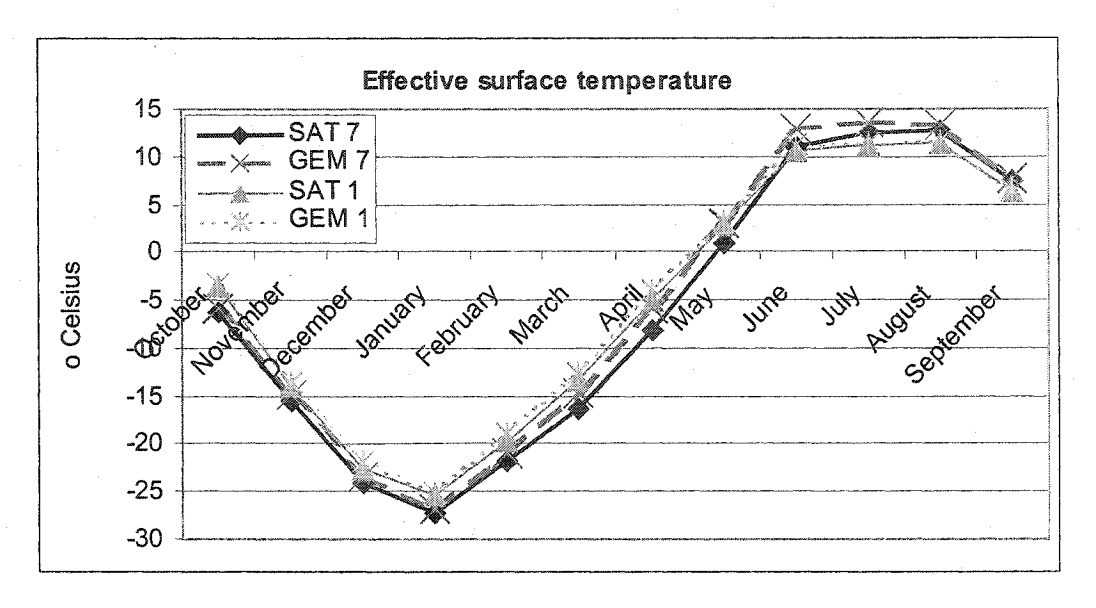


Figure 23: Monthly basin average surface temperature for the single and seven-land-class runs.

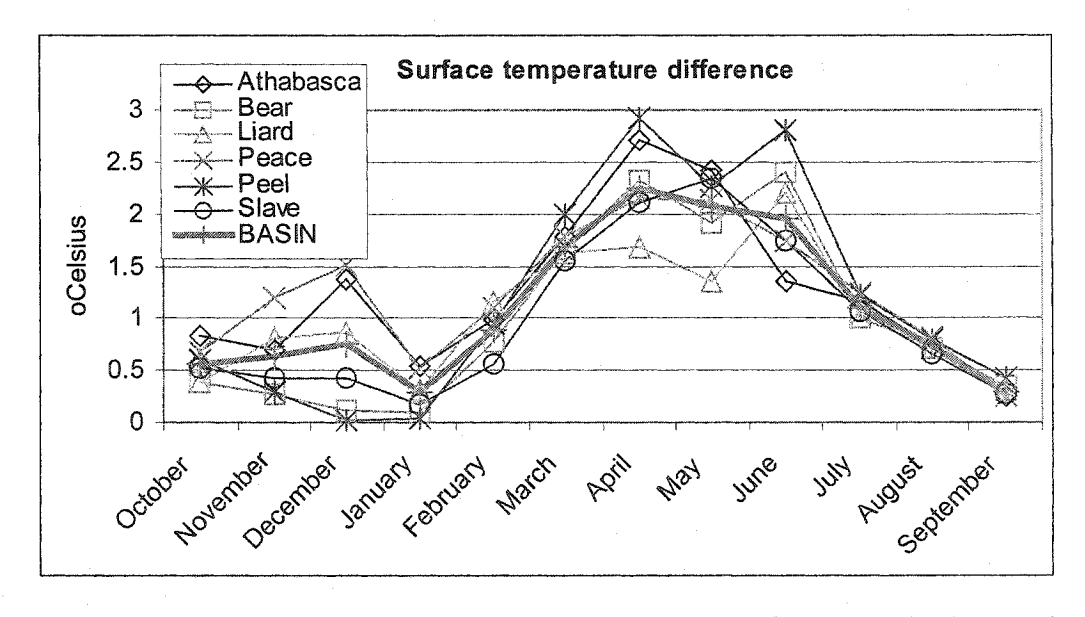


Figure 24: Monthly average surface temperature difference between GEM 7 and SAT 7 runs, in the different sub-basins.

Figure 24 shows the monthly average surface temperature difference for the subbasins: GEM surface temperature overestimation reaches up to 3.5°C in April in the Peel sub-basin, while the Peace and Athabasca sub-basins are the most sensitive in winter. The largest surface temperature overestimations are for the Athabasca, Peace and Peel sub-basins. The two southernmost watersheds, Athabasca and Peace, record the largest GEM NSR overestimations (~26 W.m<sup>-2</sup>) as seen in figure 21. However, the northernmost sub-basin, Peel, has the lowest NSR overestimation but has the largest short vegetation cover (table 3). GEM 7 surface temperature overestimations in March and April lead us to anticipate that snowmelt might occur there earlier and proceed faster.

The canopy temperature is less sensitive to the GEM NSR overestimation: the annual canopy temperature overestimation from GEM 7 is 0.35°C (figure 25) and on a monthly sub-basin scale barely reaches 1°C (figure 26), in the southernmost sub-basins with the largest canopy cover (Athabasca and Peace).

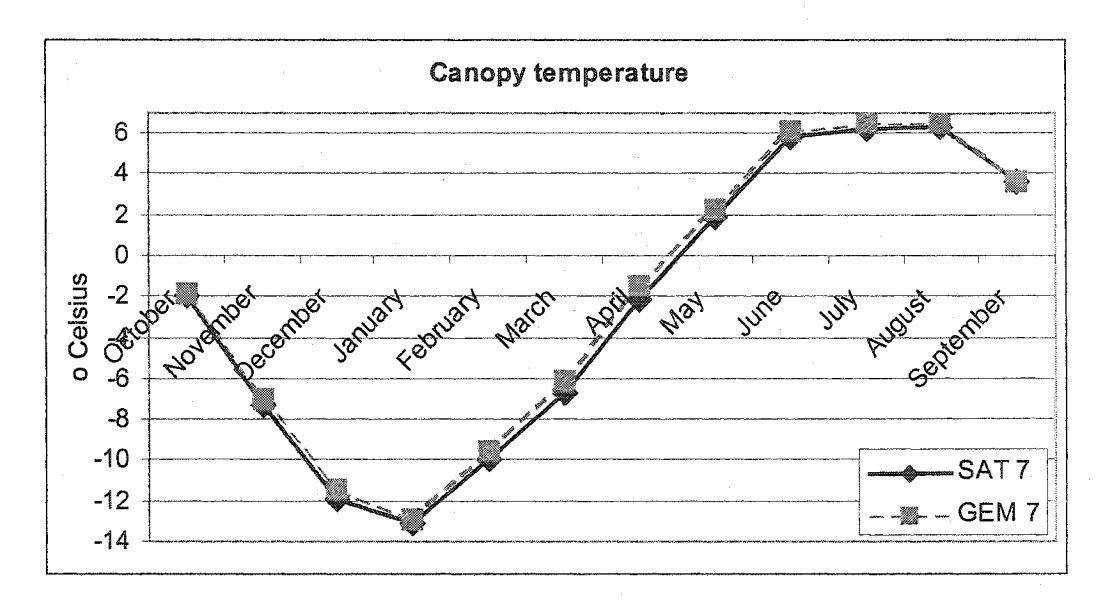


Figure 25: Monthly basin average canopy temperature for the seven-land-class runs.

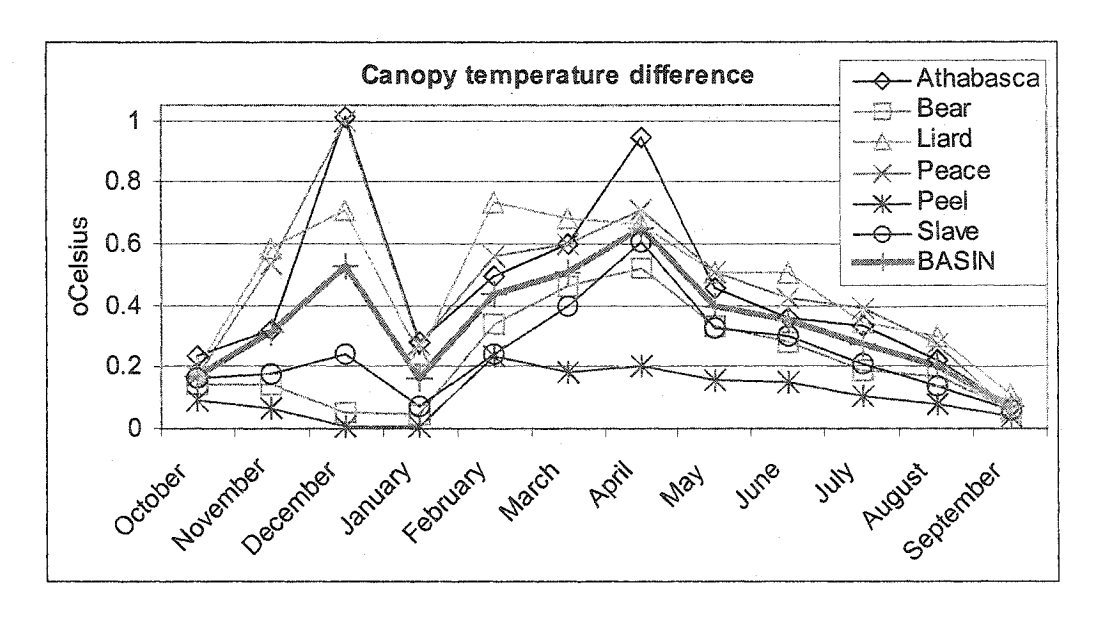


Figure 26: Monthly average canopy temperature difference between GEM 7 and SAT 7, for the different sub-basins.

#### C. Net Longwave radiation

Net longwave radiation (NLR) is negatively correlated to changes in surface, canopy and snow temperatures, with a basin annual average GEM 1 overestimation of 6% (2 W.m<sup>-2</sup>), and GEM 7 overestimation of 14% (5 W.m<sup>-2</sup>) (figure 27). The negative values of NLR throughout the year indicate the tendency for the basin to cool as a result of net loss of longwave radiation.

The warmer surface temperatures in the GEM runs enhance the net longwave cooling by up to 10 W. m<sup>-2</sup> (figure 28). The largest difference GEM 7-SAT 7 occurs from April to June: this results from the largest surface temperature difference (GEM 7 – SAT 7) at that time and from what we will show to be a different snow cover between the two runs at that period. The NLR flux difference GEM 1-SAT 1 would be less sensitive to snow cover differences because of the full canopy cover.

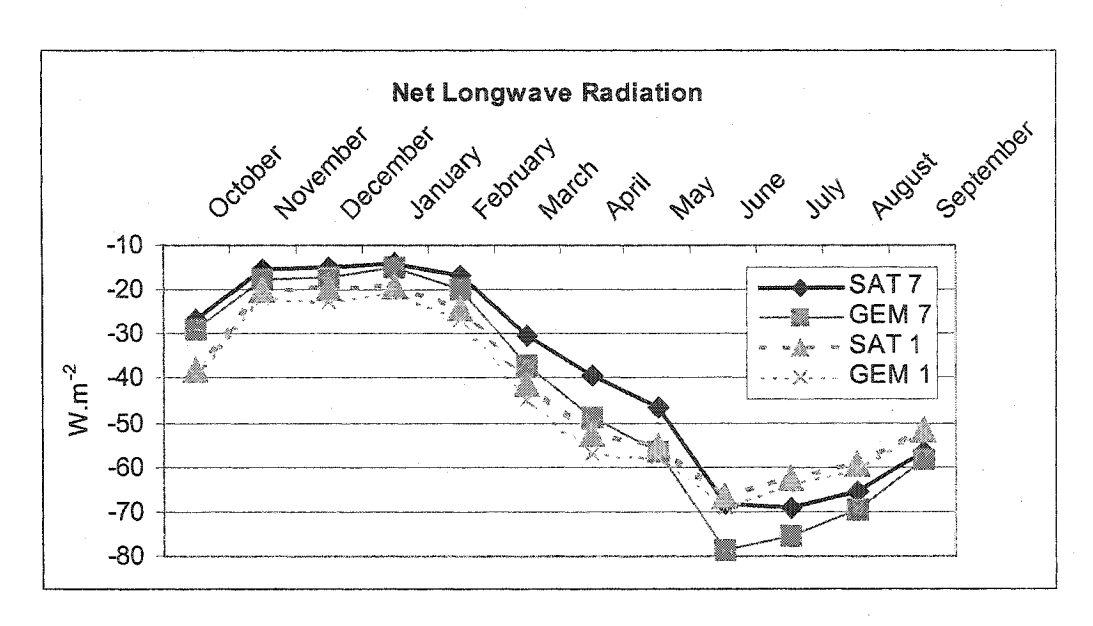


Figure 27: Monthly basin average NLR for the single and seven-land-class runs.

Figure 28 shows us that this large sensitivity difference between the GEM 7 and SAT 7 runs remains on a sub-basin scale, and reaches up to 15 W.m<sup>-2</sup> in June for Peel sub-basin. This figure also shows that largest differences in NLR fluxes between sub-basins occur during the freeze-up and snowmelt periods, resulting from the largest differences in NSR changes between sub-basins, and the related differences in the onset of the appearance snow-free surfaces in the spring.

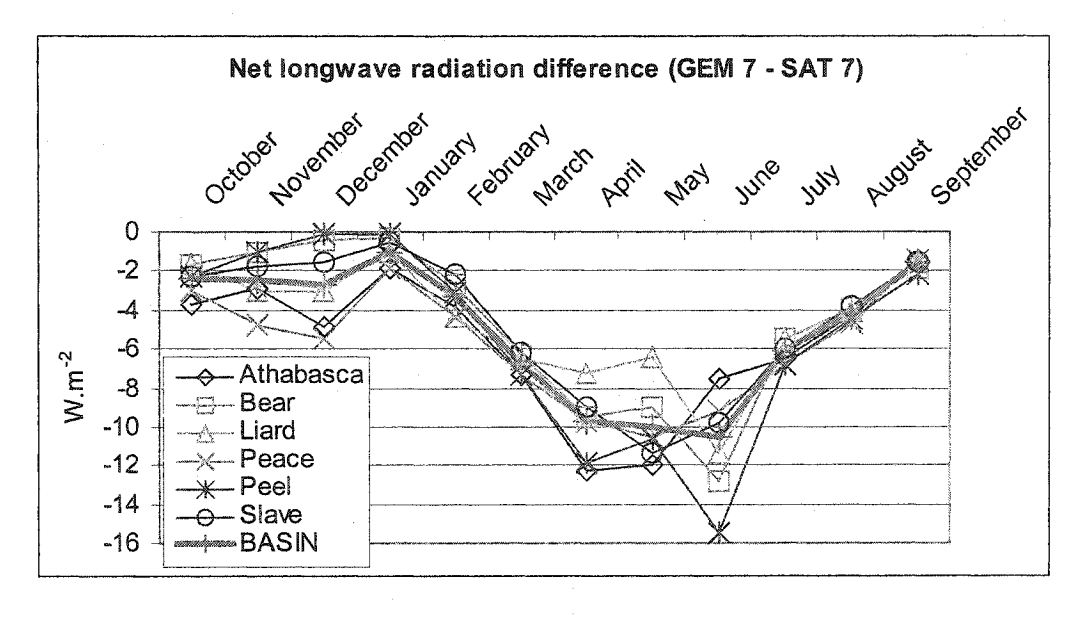


Figure 28: Monthly average NLR difference between GEM 7 and SAT 7 runs, for the different subbasins.

#### D. Latent Heat flux

The basin annual average induced GEM 1 latent heat (QE) overestimation is 18% (4 W.m<sup>-2</sup>), and the GEM 7 overestimation is 22% (4 W.m<sup>-2</sup>). The single-land-class run QE fluxes are larger in absolute values (figure 29) because of the larger NSR energy input discussed earlier, which drove the model to a warmer annual surface temperature (figure 19). Also the evaporation from the different surface types in the seven-land-class run will be different than from the coniferous forest in the single-land-class run. In particular, the smaller stomatal resistance of coniferous forest compared to mixed vegetation may contribute significantly. Similarly, the large basin-average latent heat flux difference (GEM 7 - SAT 7), reaching up to 15 W.m<sup>-2</sup> in May for the seven-land-class runs, indicates as we will show it more in detail later, an earlier GEM snowmelt.

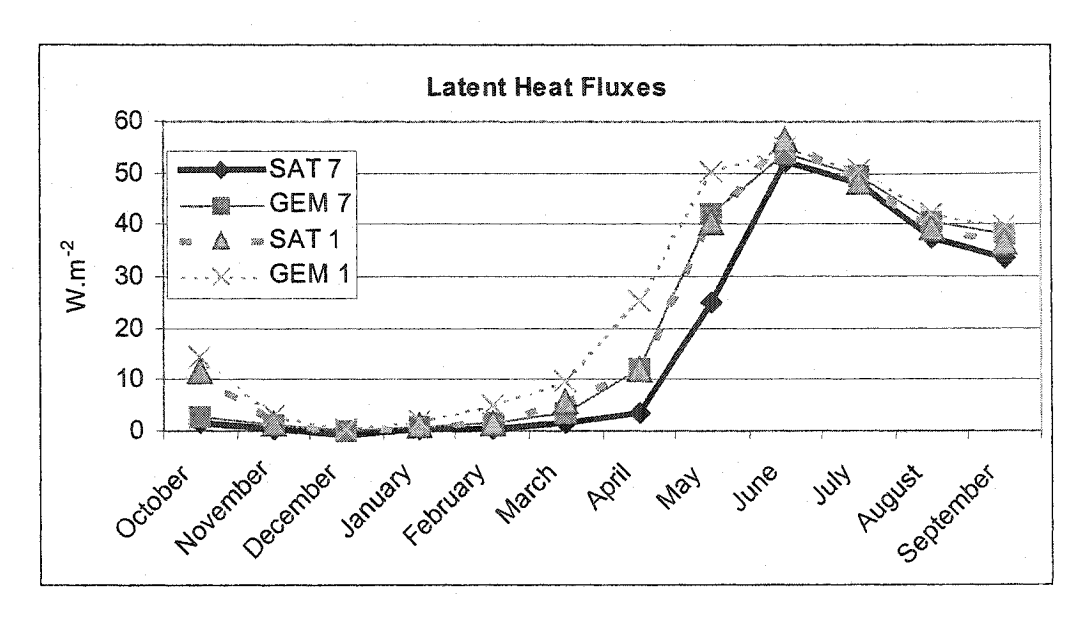


Figure 29: Monthly basin average latent heat flux for the single and seven-land-class runs.

Figure 30 shows that the differences between the sub-basins start in March-April and that the largest GEM 7 overestimation occurs in April-May. For the Athabasca, Peace and Slave sub basins, there is a SAT 7 overestimation in June and a decrease in the GEM 7 overestimation in the other sub-basins. This can be understood in terms of the delay of snowmelt in the SAT run and the corresponding increase in the importance of

sublimation relative to evaporation in this run. The GEM 7 overestimation in summer is the largest for the bare ground sub-basin Peel.

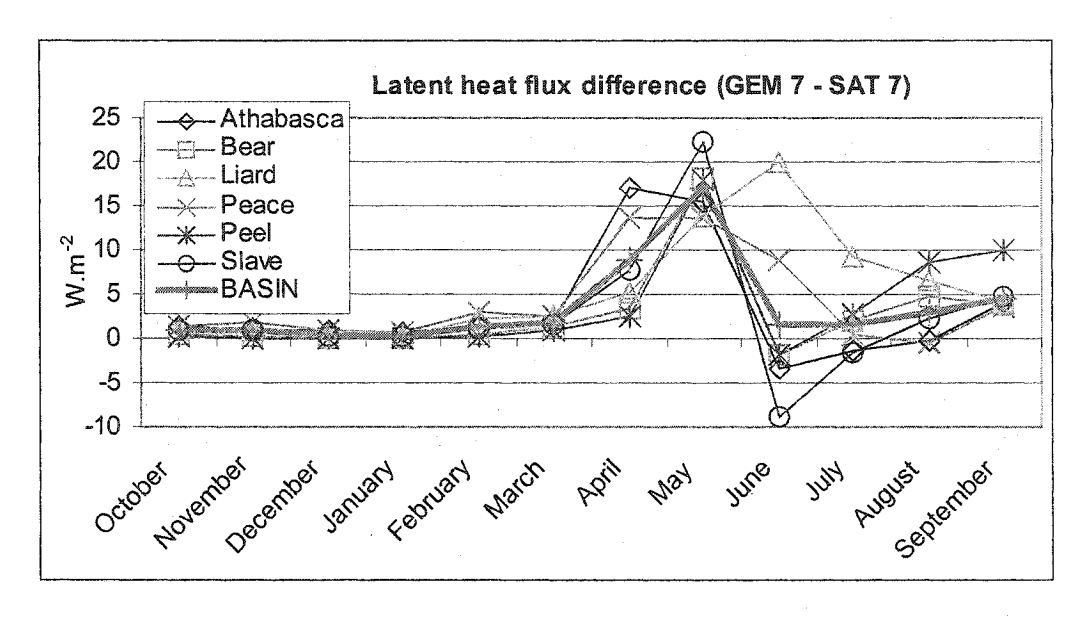


Figure 30: Monthly average QE difference between GEM 7 and SAT 7 runs, for the different subbasins.

#### E. Sensible Heat Flux

The basin annual average GEM 1 and GEM 7 overestimations approach 140%, i.e. annual absolute increases of 23 W.m<sup>-2</sup> and 14 W.m<sup>-2</sup> respectively. Figure 31 shows that the largest (GEM – SAT) difference occurs in June, with up to 40 W.m<sup>-2</sup> for the seven-land-class runs. The single-land-class run has a weaker surface temperature increase but a larger surface drag coefficient (100% coniferous versus a mixture of weaker drag coefficient vegetation types), leading to larger QH fluxes. Furthermore, the seven-land-class runs in the Athabasca and Peace sub-basins record highest sensible heat increases (figure 32), as they are mainly covered by canopy and have the largest surface temperature increases. And Peel, the sub-basin having the least canopy cover but a large surface temperature increase (figure 24), has the least sensible heat GEM-SAT difference (figure 32). Therefore, the vegetation is determinant in the sensible heat flux sensitivity.

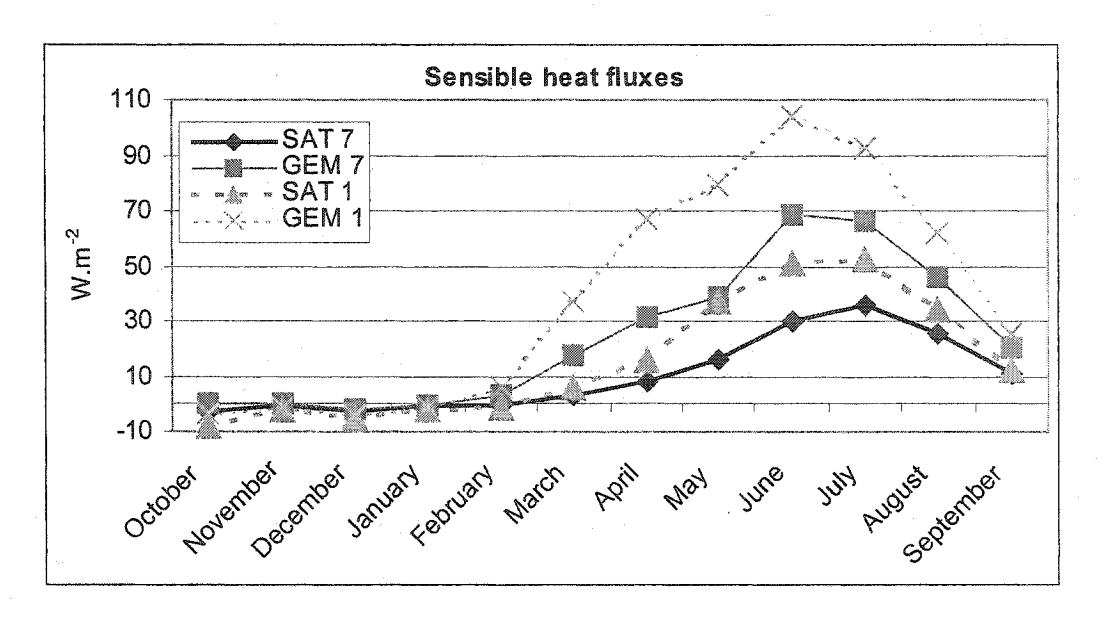


Figure 31: Monthly basin average QH for the single and seven-land-class runs.

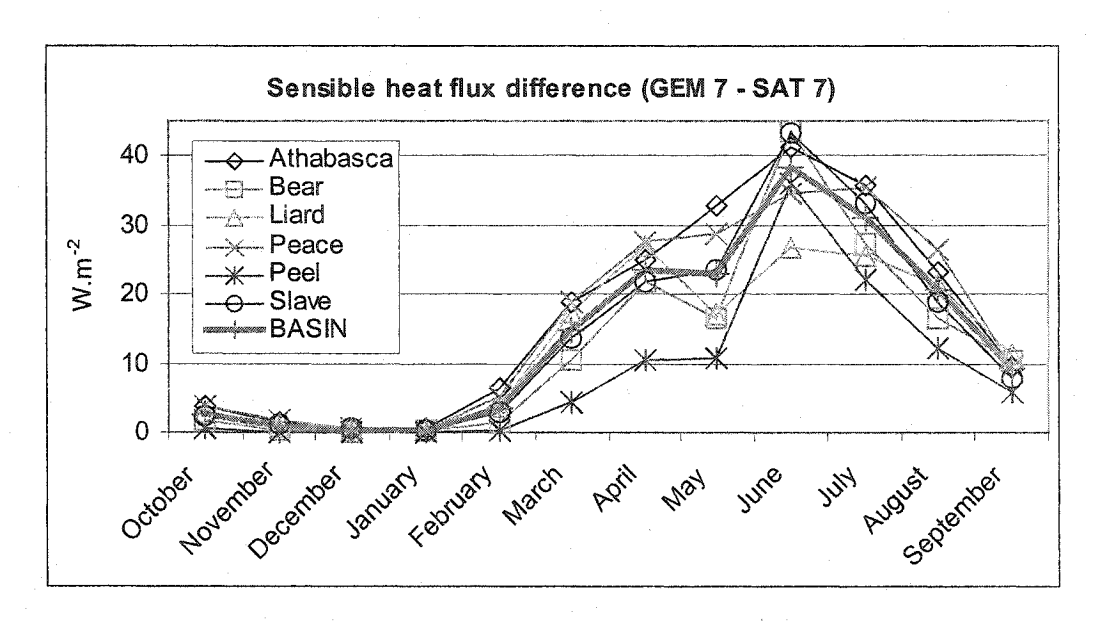


Figure 32: Monthly average QH differences between GEM 7 and SAT 7 runs, for the different subbasins.

With such sensitivity, QH is the most sensitive flux to an increase in ISR. This extra sensitivity is due to the fact that GEM drives WATCLASS offline: had there been feedbacks to the atmospheric model, the air temperature Ta would have increased, as would the temperature difference (Ta-T), and so:

 $(QH_{GEM}\text{-}QH_{SAT})\,/\,QH_{SAT}\text{=-}(T_{GEM}\text{-}T_{SAT})\,/\,(Ta\text{-}T_{SAT})\text{ would decrease}$  where T is either the bare ground or the canopy temperature.

#### F. Bowen Ratio QH/QE

Figure 33 shows the monthly basin average Bowen ratio for the seven-land-class runs. Ratios have meaningless values in spring and fall when sensible and latent heat fluxes reverse signs and reach near-zero values. From May to September, the Bowen ratios are of the order of 0.7 for the SAT 7 simulation and 1.1 for the GEM 7 simulation. This results from the larger GEM sensible heat overestimation (141%) compared to the GEM latent heat overestimation (22%).

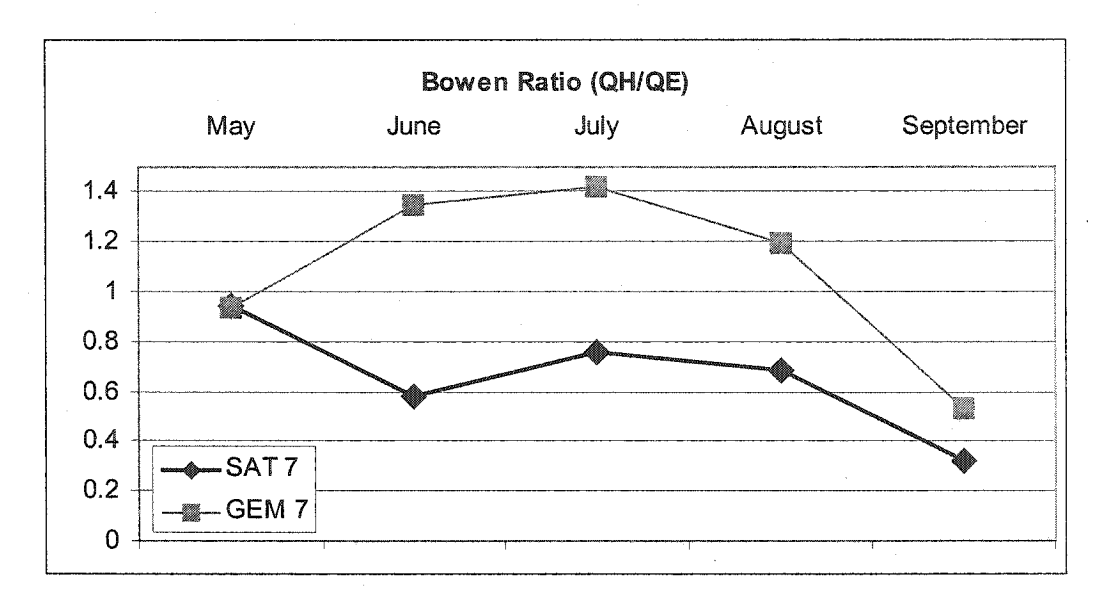


Figure 33: Monthly basin average Bowen ratio in summer, for the seven-land-class runs.

## G. Evaporative Fraction QE / (QH+QE)

The evaporative fraction is defined as the ratio of the latent heat flux to the sum of the latent and the sensible heat fluxes (Betts et al. 1999). It is, like the Bowen ratio, a measure of the repartition of the sensible and the latent heat fluxes, but it has the advantage of not having the denominator approaching zero-values when QH is small. Nevertheless, if QH and QE have opposite signs, as may happen in winter, this ratio may also become meaningless. Accordingly, we do not show values from October to February.

GEM 7 evaporative fraction is generally smaller, 0.12 less from March to September, as GEM 7 has a larger available energy but the moisture supply is similar for both runs. From March to May, GEM 7 and SAT 7 fractions increase, resulting from the snowmelt moisture supply and the increase in NSR. Furthermore, GEM 7 increase is larger, due to an earliest snowmelt and larger NSR. From May to June, SAT 7 still increases, due to the delayed snowmelt. However, GEM 7 starts decreasing, as the moisture supply decreases, as shown in a later section.

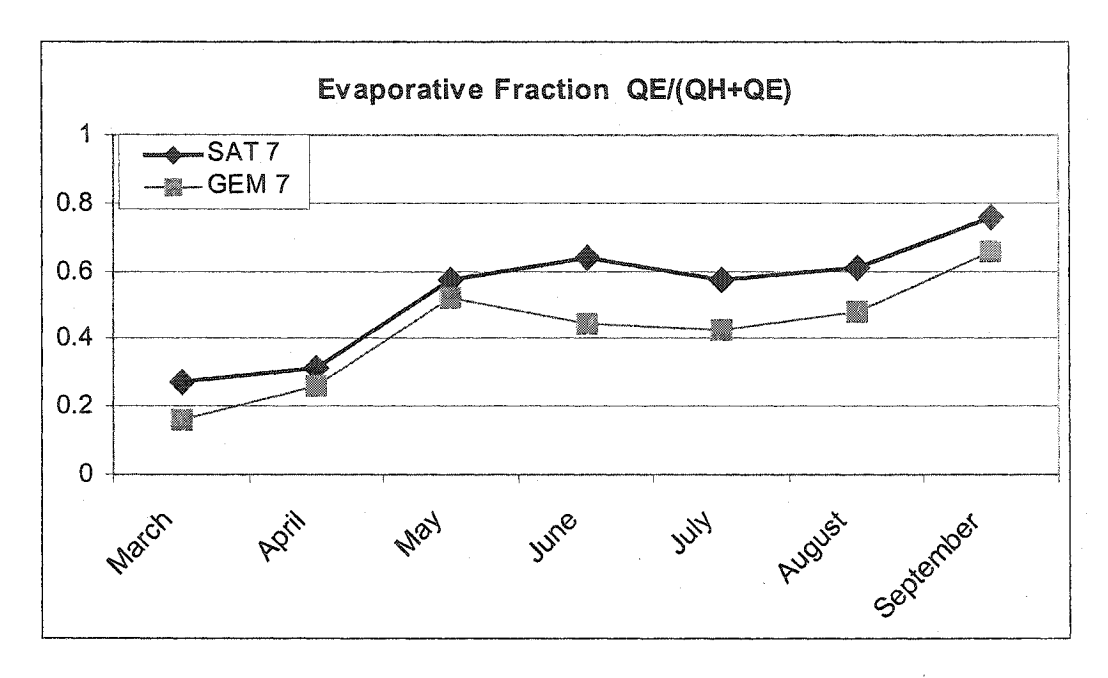


Figure 34: Monthly basin average evaporative fraction for the seven-land-class runs.

#### H. Ground heat conduction

Figure 35 shows good agreement between GEM 7 and SAT 7 fluxes, except from April to May, and one notices the GEM 7 sign change in April. This might be understood as a result of an earlier GEM 7 snowmelt and a greater heat flux into the snow-free surface. This is consistent with the GEM 7 surface temperature overestimation in March and April.

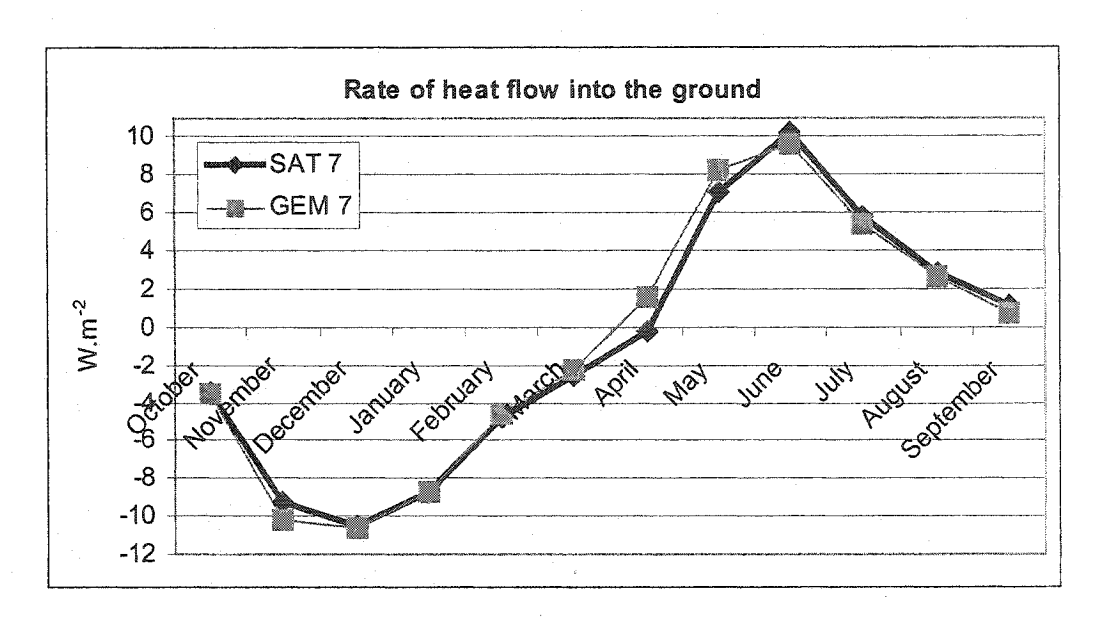


Figure 35: Monthly basin average heat flux into the ground, for the seven-land-class runs.

Figure 36 shows largest GEM 7 overestimation sensitivity between the sub-basins in April and May, while SAT 7 overestimation in June agrees with the idea of a SAT 7 delayed snowmelt. The SAT 7 overestimation in November suggests an earlier freeze-up for mountainous and northernmost sub basins.

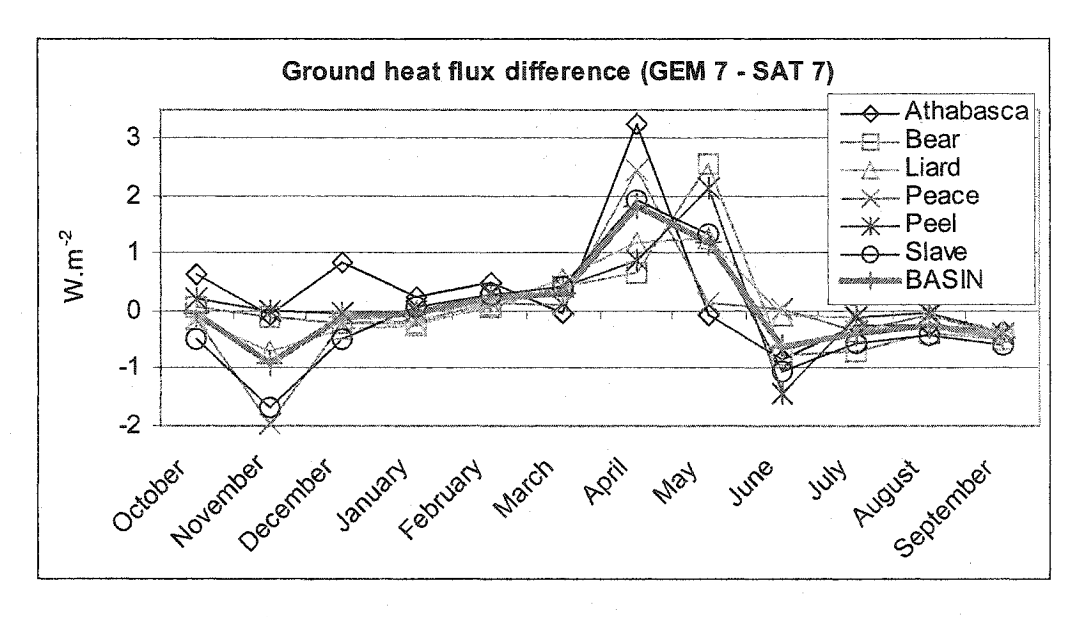


Figure 36: Monthly average heat flux into the ground difference between GEM 7 and SAT 7 runs, for the different sub-basins.

# 2. Snowpack

As seen in the previous section, the snowmelt period seems to be very sensitive to uncertainties in incoming solar radiation. This section will give further evidence from the energetic and mass transfers of an earlier GEM 7 snowmelt.

#### A. Snow temperature

When the surface is snow covered, the snow is the interface with the atmosphere. Figure 37 shows that GEM 7 overestimates snowpack temperature in spring, reaching up to 2°C on a monthly basin average, denoting a warmer snowpack, which might lead to an increased sublimation and an earlier surface melting, with less refreezing at the bottom of the snowpack.

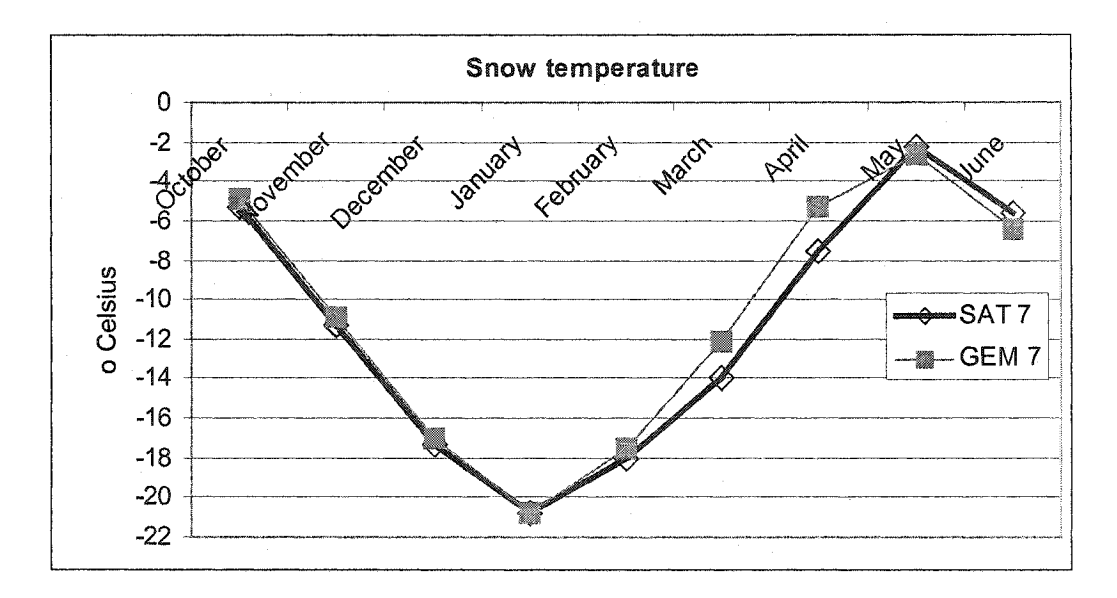


Figure 37: Monthly basin average snowpack temperature for the seven-land-class runs.

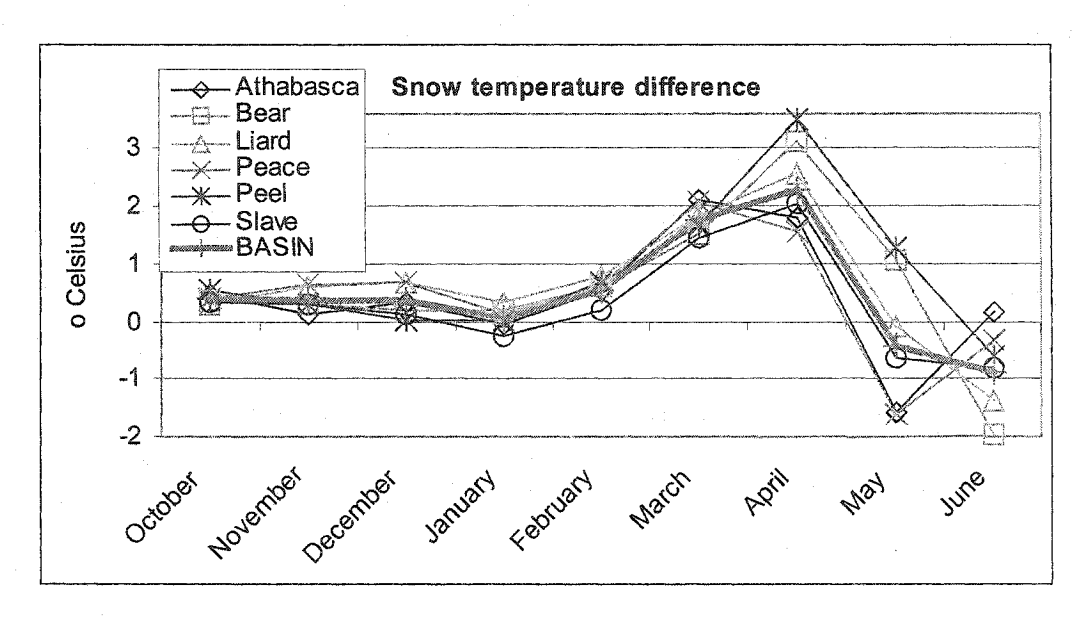


Figure 38: Monthly average snow temperature difference between GEM 7 and SAT 7 runs, for the different sub-basins.

Figure 38 shows us also a large spatial sensitivity of the snow temperature: each sub-basin responds differently, in response to different NSR overestimation, and also to different vegetation types. The Athabasca and Peace sub-basins have the smallest snow temperature GEM overestimation but largest NSR overestimation: their larger canopy cover absorbs the extra NSR and prevents the underlying snow from warming. Conversely, Peel and Bear have the lowest canopy cover and, despite the lowest NSR GEM 7 overestimation, the largest GEM 7 overestimation of snow surface temperature. The SAT 7 overestimation in June accounts for the SAT 7 snowmelt delay.

# B. Energy used for Snowmelt

The annual basin average snowmelt energy is larger in the seven-land-class runs than in the single-land-class (figure 39), as the two series of runs had a different snowpack initialization. In March, the snowmelt energy is larger in the single-land-class runs than in the seven-land-class runs: this might result from either an earlier snowmelt or from more sublimation in the single-land-class runs.

Monthly differences between GEM and SAT runs are largest in the seven-landclass runs: canopy cover tends to decrease the surface sensitivity. Comparing GEM 7 and SAT 7 simulations, snowmelts starts earlier for GEM 7, with a larger peak in April. The SAT 7 overestimation in May is consistent with the identical snow precipitation rate for the two runs. Furthermore, the annual basin average energy used for snowmelt is quite similar for SAT 7 and GEM 7 runs. This implies that there should not be any significant sublimation differences between GEM 7 and SAT 7 runs, as it will also be shown in the next section.

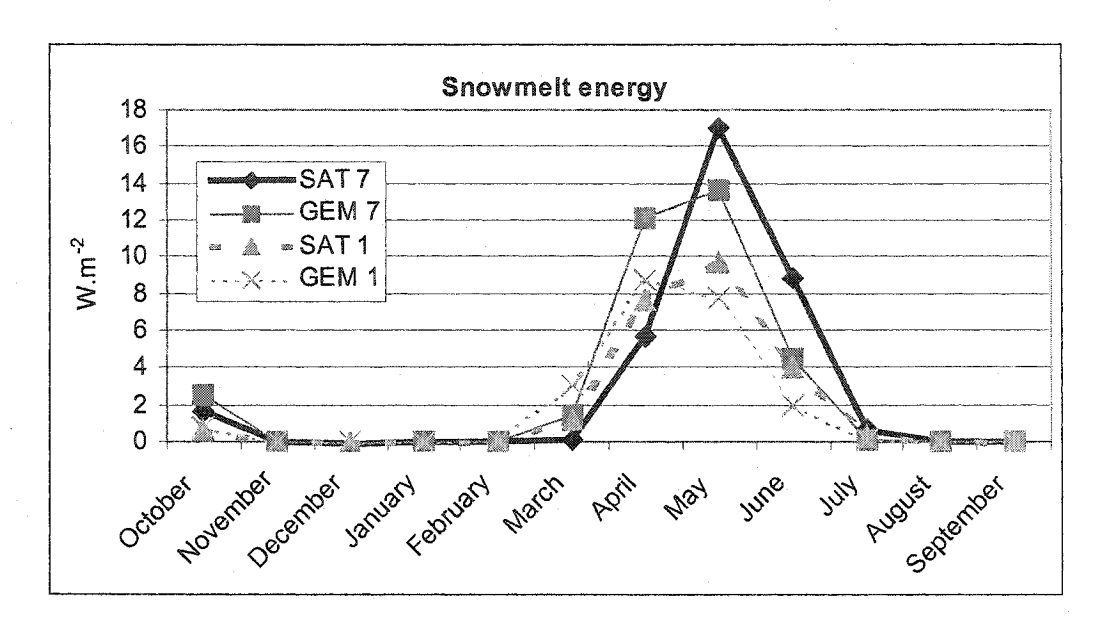


Figure 39: Monthly basin average snowmelt energy for the single and seven-land-class runs.

Figure 40 shows a GEM 7 overestimation starting in March for the southernmost sub-basins Athabasca, Slave and Peace, and which is largest in April. GEM 7 overestimation for northernmost sub-basins Peel and Bear starts later, but persists until May. These GEM 7 overestimations are followed by GEM 7 underestimations in May for southern sub-basins, and in June for northern sub-basins. This results from a delayed snowmelt between GEM 7 and SAT 7 runs. The Liard sub-basin large sensitivity may be interpreted as a larger snowmelt delay between GEM 7 and SAT 7 runs.

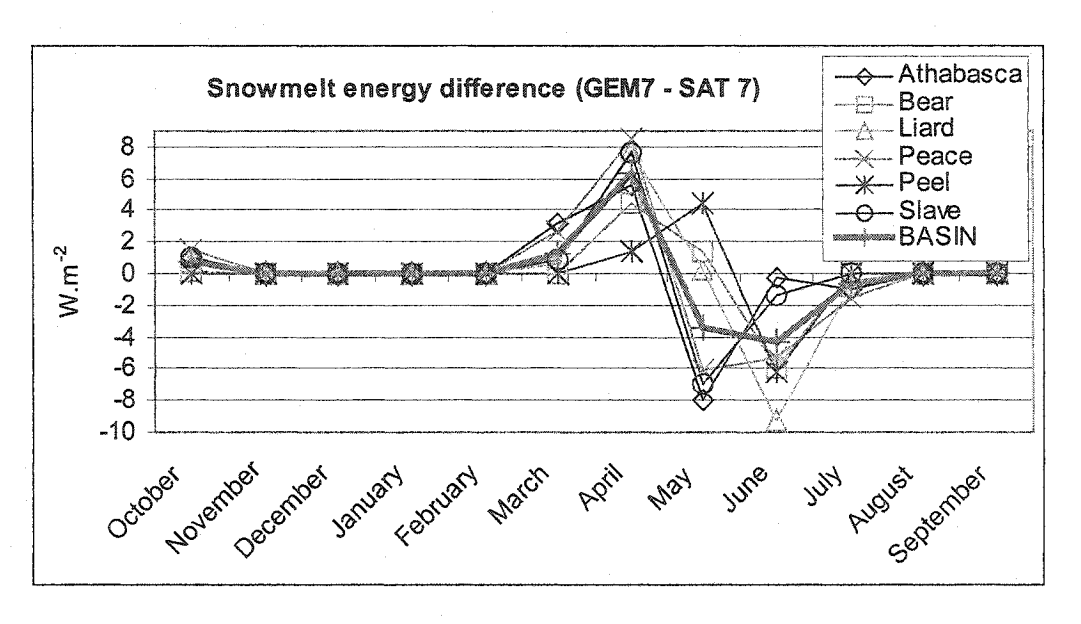


Figure 40: Monthly average snowmelt energy difference between GEM 7 and SAT 7 runs, for the different sub-basins.

### C. Precipitation

The different assumptions set up previously considering the analysis of energy fluxes are closely linked to mass transports through the water balance study.

The precipitation input to WATCLASS are GEM adjusted values (Louie et al., 2002), based on derived gridded observations from the climate network. The basin receives 454 mm of simulated precipitation per year. Mountainous sub-basins Liard and Peace receive most precipitation because of the orographic forcing (643 mm and 591 mm respectively) and are, with Peel sub-basins (426 mm) located on the west side. Athabasca sub-basin, which has also some mountains on its western part, receives 371 mm. Finally, the eastern plain sub-basins Bear and Slave receive about 350 mm (figure 41).

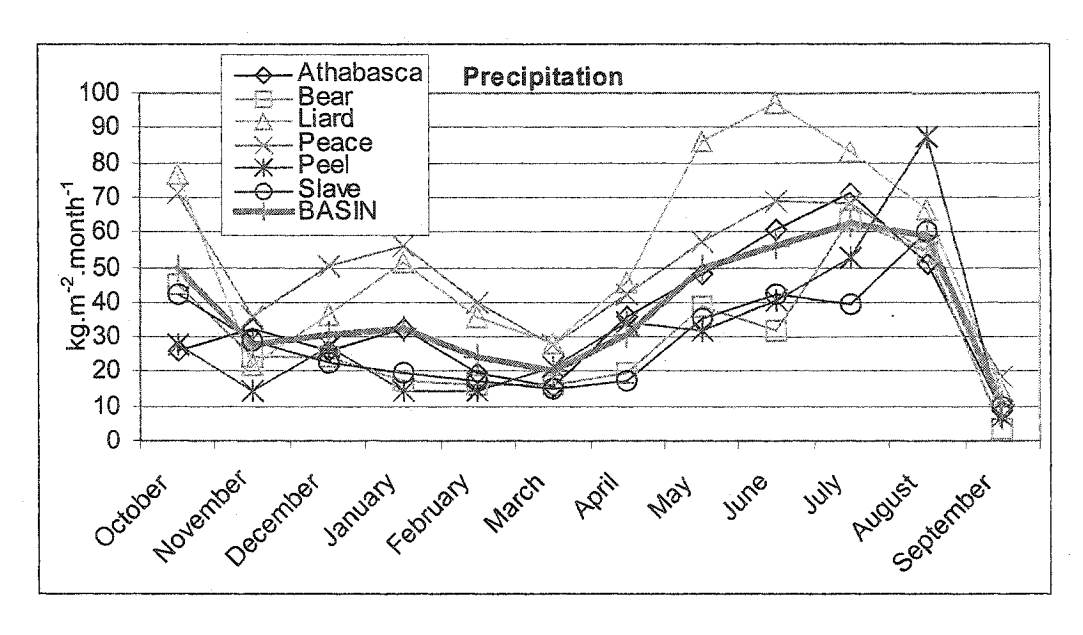


Figure 41: Monthly average accumulated precipitation in the different sub-basins.

## D. Snow Accumulation

GEM and SAT runs receive the same amount of precipitation, i.e. the same amount of snow or rain. However, snow accumulation responds differently to changes in energy fluxes in and at the surface of the snowpack (sublimation, ground heat conduction, sensible heat flux).

On an annual basis, the snowpack is 52 kg.m<sup>-2</sup> and 44 kg.m<sup>-2</sup> thick, in water equivalent, for respectively SAT 1 and GEM 1 runs. This is far less than 89 kg.m<sup>-2</sup> and 77 kg.m<sup>-2</sup> for respectively SAT 7 and GEM 7 simulations. However, this is partly due to a different snowpack initialization.

Figure 42 shows the daily basin average snow and precipitation accumulations. Accumulations start in November, when we are pretty sure that all precipitation is only snow. The spring first soft decrease in snow accumulation results from a mixture of snowmelt, late snowfalls and sublimation. Definitely, snowmelt starts earlier for GEM runs.

SAT 1 and GEM 1 lines are slowly diverging from the precipitation curve, and also from each other. Thus, sublimation is significant in full canopy cover area, accounting for a loss of moisture of up to 16 kg.m<sup>-2</sup> by the end of winter (mid-March) for GEM 1 run.

The sublimation rate is also sensitive to changes in net solar radiation with a loss of 10 kg.m<sup>-2</sup> between SAT 1 and GEM 1 runs by the end of winter.

GEM 7 line starts diverging in the beginning of February, and SAT 7 only in April. Sublimation is less significant for a mixture of short vegetation and mixed canopy areas and is also less sensitive to GEM 7 NSR overestimation. This is consistent with the similar snowmelt energy amount found in the earlier section for both GEM 7 and SAT 7 simulations.

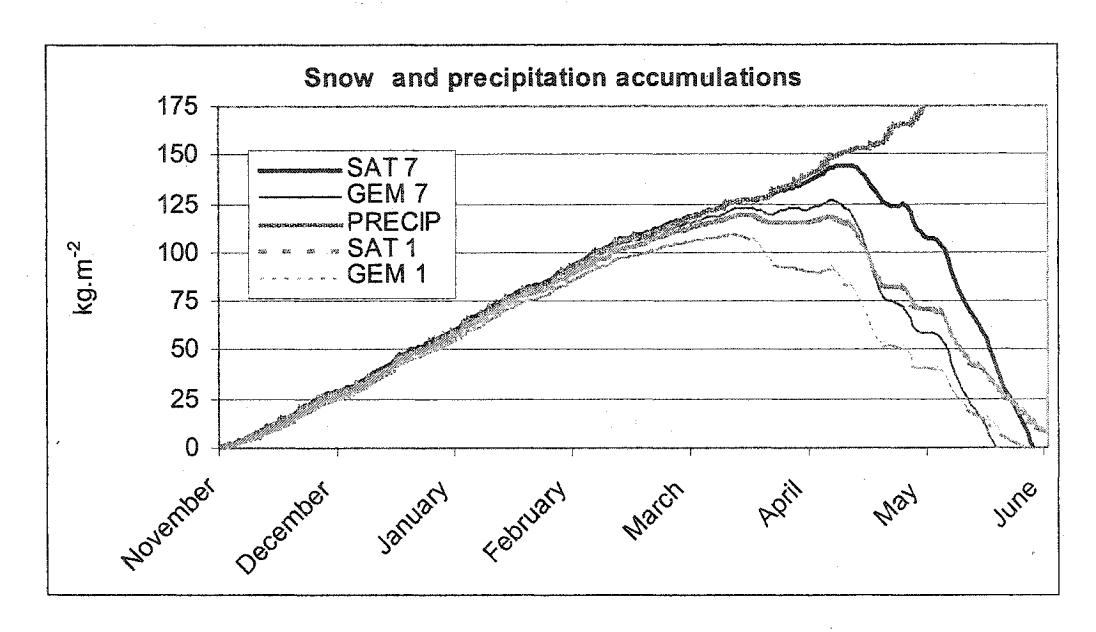


Figure 42: Daily snow and precipitation accumulations over the Mackenzie River Basin.

Figure 43 shows that GEM 7 snowpack starts decreasing in March-April for the southernmost sub-basins Peace and Athabasca, and in April for Bear, Liard and Slave sub-basins and end of April – May for Peel sub-basin. All SAT 7 snowpack start decreasing in April or April-May in Peel sub-basin. Peace and Liard record the heaviest snowpack, in concordance with the largest precipitation (figure 41).

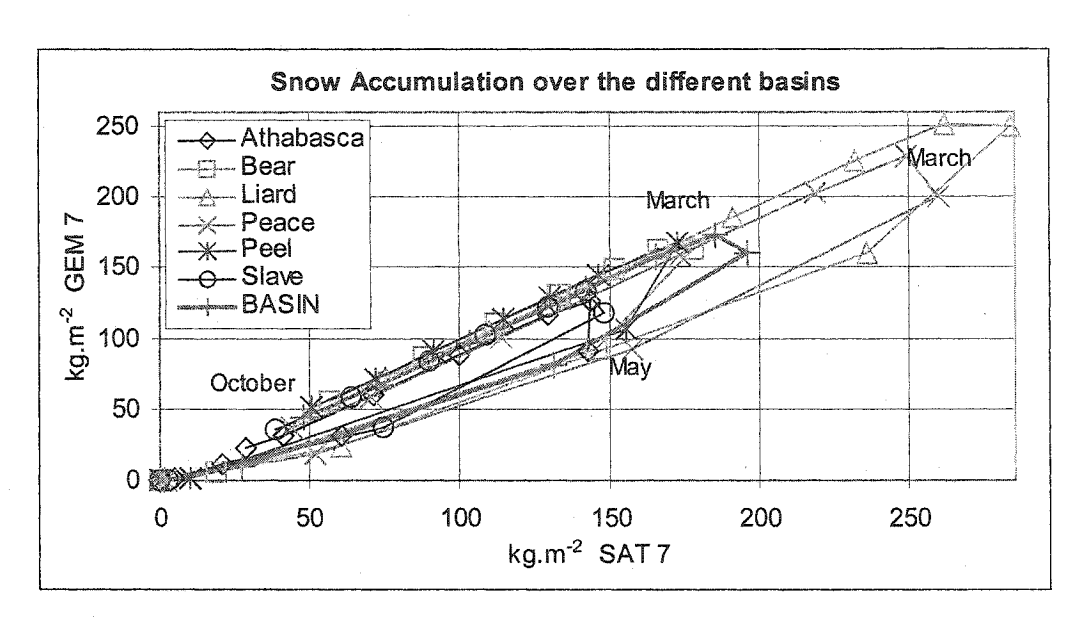


Figure 43: Correlation between the GEM 7 and SAT 7 runs accumulated snow accumulations, in the different sub-basins.

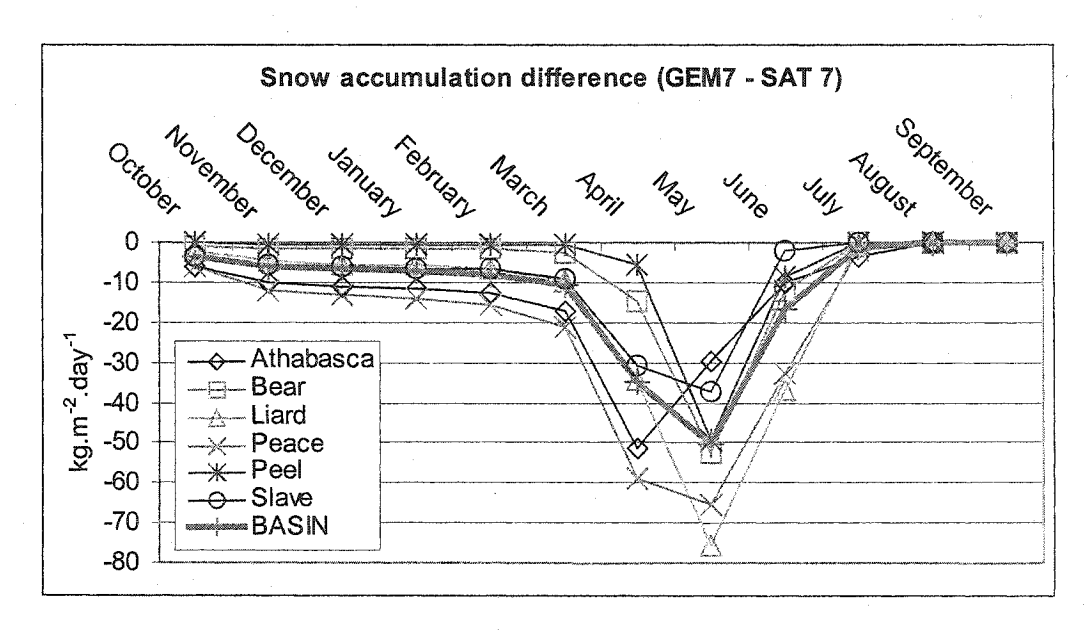


Figure 44: Monthly average snow accumulation differences between GEM 7 and SAT 7 runs, for the different sub-basins.

Figures 44 show that Athabasca and Peace have the largest GEM 7 snowpack underestimation in March-April: this results from their largest NSR overestimation and also from their largest canopy cover, which, as seen earlier, enhances sublimation. Consistently, Bear and Peel, the sub-basins having the lowest canopy cover and the

lowest NSR overestimation, record the smallest and shortest (GEM 7 - SAT 7) snow accumulation difference.

## E. Fractional snow cover

Snowmelt is sensitive to the land cover type (100% coniferous or several land classes), to the location of the sub-basin (latitude, eastern plains or western mountains) and to the NSR overestimation.

Fractional snow cover depletion can inform us on the snowmelt speed, i.e. when snowmelt has started for long enough that underlying ground is visible. The criterion we artificially chose to quantify the snowmelt speed sensitivity is when the fractional snow cover has depleted by 10% of its maximal value.

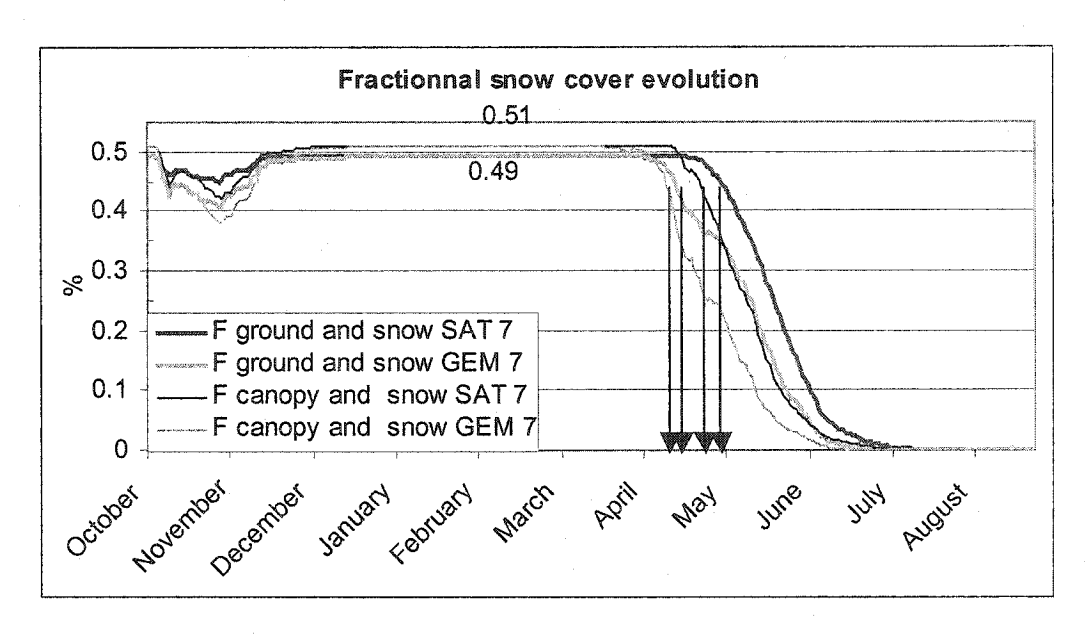


Figure 45: Daily fractional snow cover, averaged over bare ground or canopy areas, for GEM 7 and SAT 7 runs.

Figure 45 shows the basin average fractional snow cover evolution for bare ground and for canopy covered areas. There is 18 days delay between GEM 7 and SAT 7 simulations for bare ground areas and 13 days for canopy areas. Since canopy prevents the ground surface to heat up rapidly, the shortest delay in response to the NSR overestimation was expected for bare ground areas. Actually, a large portion of the

canopy-covered area is in the south, sustaining the largest NSR overestimations, whereas short vegetation areas are located in the north (figure 5). Therefore we should look at the different sub-basin fractional snow cover depletion.

Figure 46 shows the daily differences in the sub-basin average fractional snow cover between GEM 7 and SAT 7 runs. Clearly, the southernmost sub-basins (Athabasca and Peace) have the earliest snowmelt, with a difference in cover of 0.5 in April, in response to the largest uncertainty in solar radiation input (see figure 21). The northernmost sub-basin (Peel) has the latest snowmelt, with also a very large response to the smaller differences in solar radiation input. Since the Peel basin is characterized by the largest short vegetation fractional area, this suggests that this large sensitivity may be due to the short vegetation cover. Slave and Bear, the eastern plains sub-basins, have an intermediate sensitivity, in response to an intermediate uncertainty in solar radiation input. The Liard sub-basin has the smallest sensitivity but the differences in snow-cover last longer: this results from an intermediate difference in solar radiation input, but might also be influenced by a mainly canopy covered area. It thus seems that the fractional snow cover response lasts longer in regions with a larger canopy cover area.

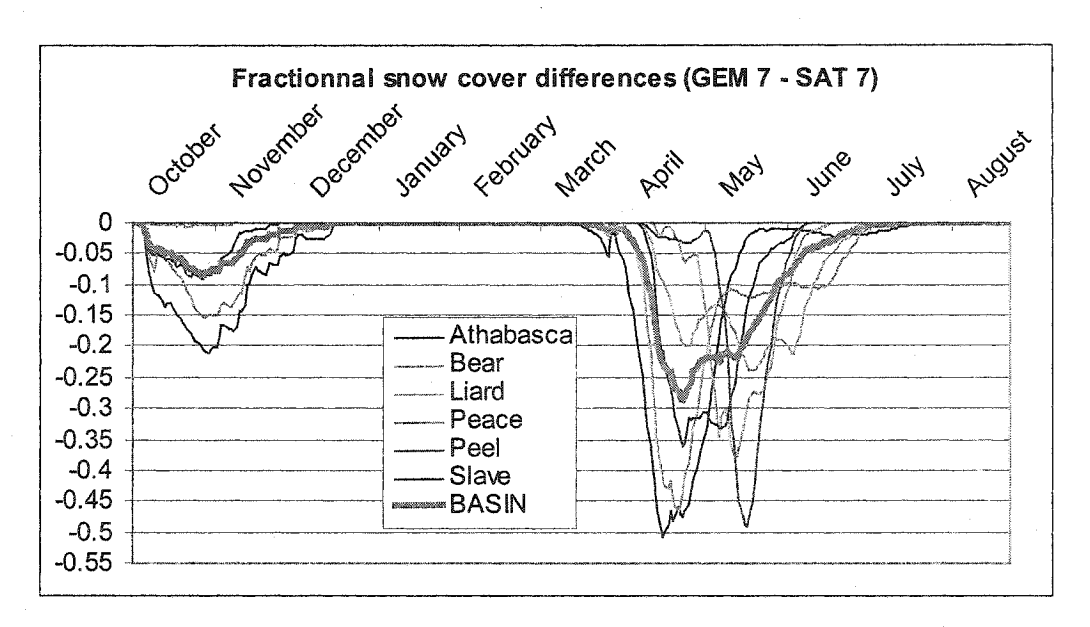


Figure 46: Daily fractional snow-cover differences between GEM 7 and SAT 7 runs, for the different sub-basins.

In summary, the fractional snow cover response is sensitive to both uncertainties in incoming solar radiation and vegetation type, with the fraction of short vegetation being most important.

## 3. Water Balance

# A. Evapotranspiration

Water loss through evapotranspiration and sublimation is associated with the latent heat fluxes. The basin annual average sublimation-evapotranspiration rates for the single-land-class runs are significantly larger than for the seven-land-class runs (figure 47), by 27% and 22%, for respectively the SAT and GEM simulations. This results from the full canopy cover in the single-land-class but also might partly result from the more active sublimation process in these simulations. Differences between GEM 7 and SAT 7, however, are due mainly to snowmelt differences because sublimation is not significant, as explained earlier. The largest differences between GEM and SAT runs occur again from March to May.

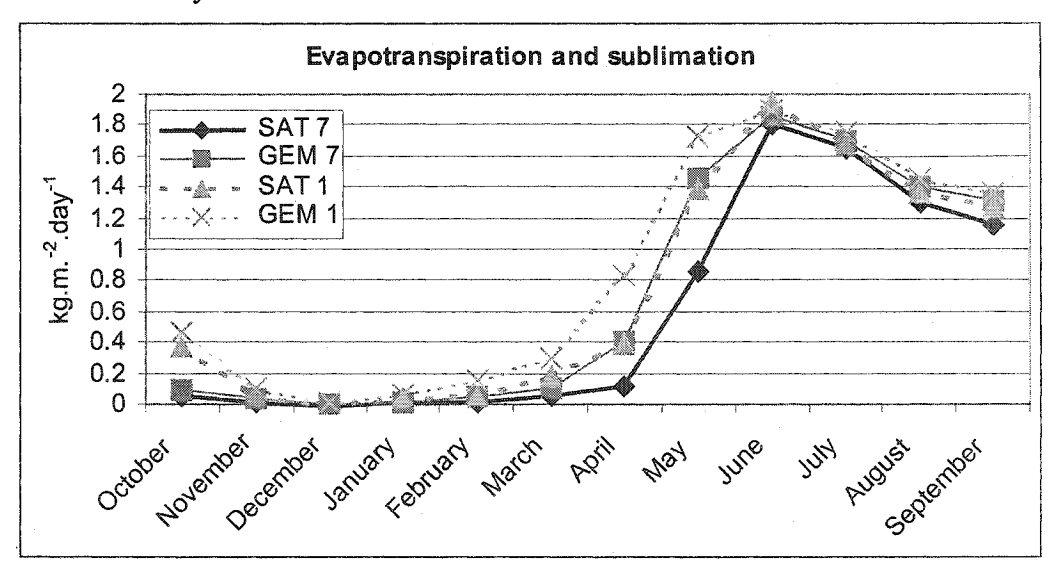


Figure 47: Monthly basin average evapotranspiration rate for the single and seven-land-class runs.

Figure 48 shows the variability on the sub-basin scale of the seven-land-class runs. In April, when snowmelt starts in the southernmost sub-basins, these basins record the largest differences between GEM and SAT in evapotranspiration. This corresponds to the period and locations of largest differences in incoming solar radiation. These graphs are similar to the latent heat flux graphs and show, again, the delayed SAT 7 snowmelt relatively to the GEM 7 one. The sub-basin vegetation, location and respective net solar radiation overestimation determine the delay.

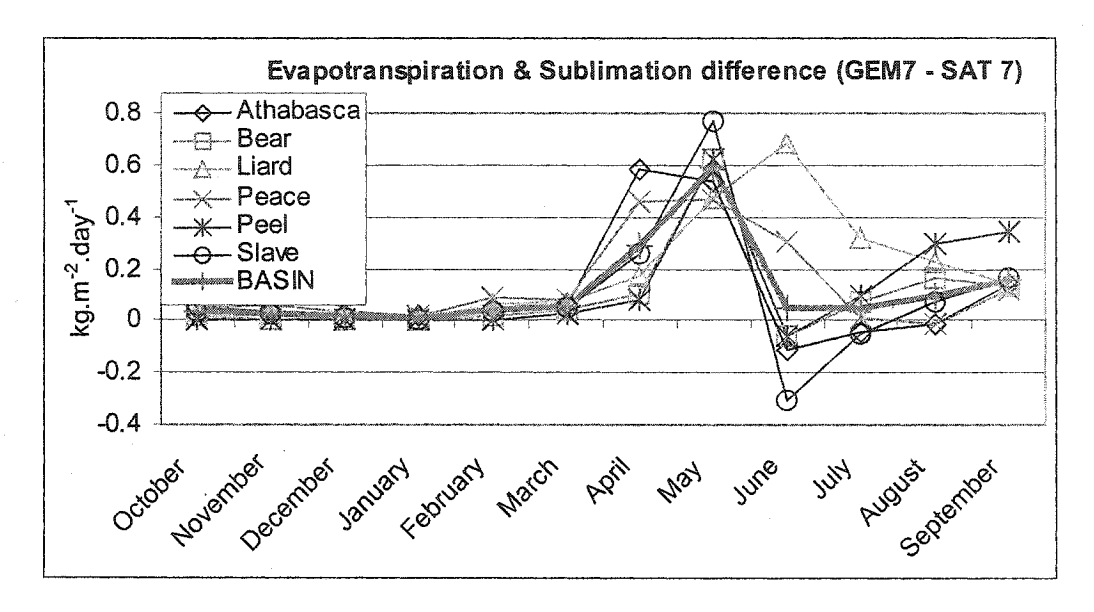


Figure 48: Monthly average differences in the evapotranspiration and sublimation rate between GEM 7 and SAT 7 runs, for the different sub-basins.

# B. Moisture Storage

Changes in moisture storage are due to changes in evapotranspiration and snowmelt. Figure 49 shows the basin average monthly accumulation of liquid, frozen, and total moisture contents in the three soil layers for the seven-land-class runs. GEM 7 and SAT 7 simulations agree quite well the whole winter and differences start in April. The total moisture content is at the highest level in May, at the end of the snowmelt period, and is larger for the SAT 7 simulation by almost 2 mm. This coincides with the highest GEM 7 overestimation of moisture loss via evapotranspiration. Furthermore, the

basin GEM evapotranspiration overestimation for summer months results in a GEM moisture storage daily underestimation of about 20 kg.m<sup>-2</sup>.

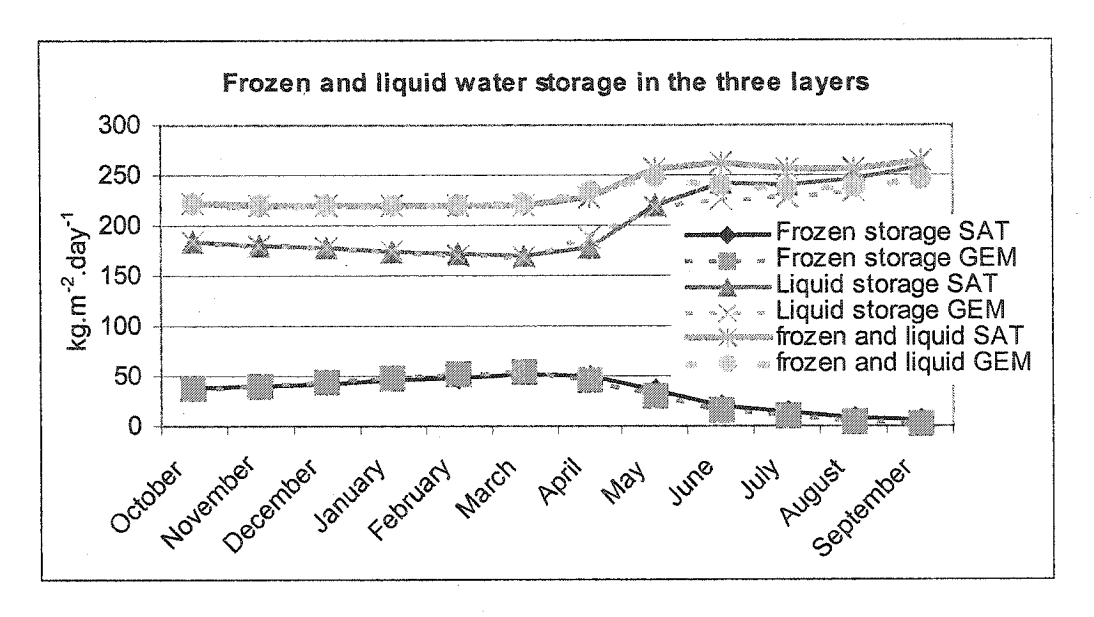


Figure 49: Monthly basin average frozen and liquid moisture contents of the 3 layers for the sevenland-class runs.

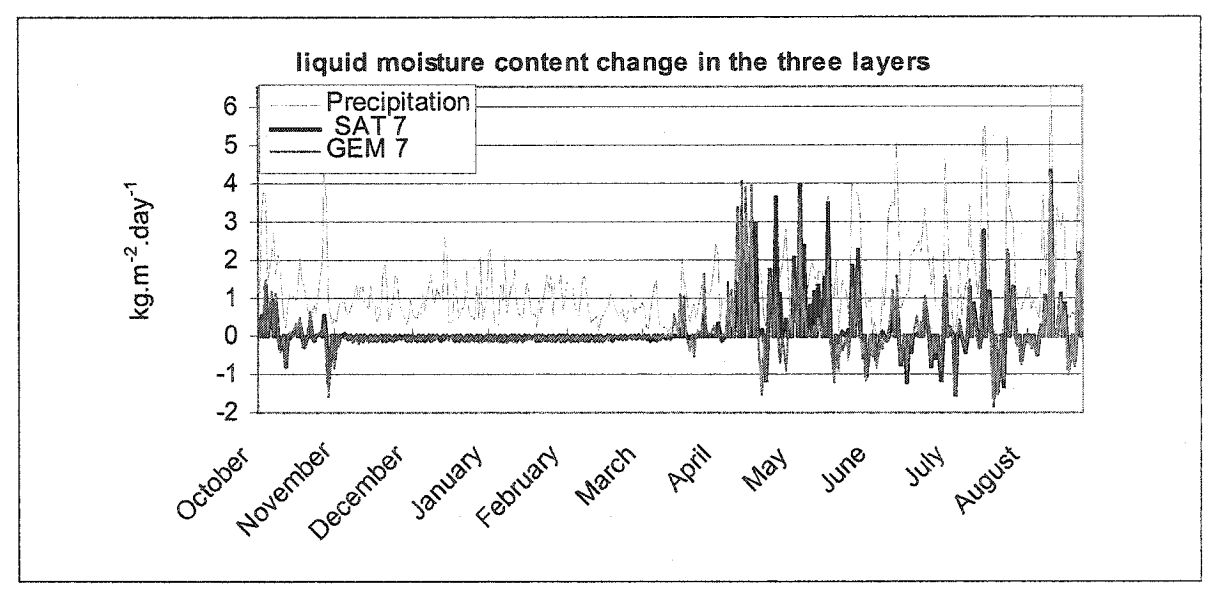


Figure 50: Daily basin average liquid moisture content change in the three soil layers for GEM 7 and SAT 7 runs.

Figure 50 shows the basin average daily changes in the liquid moisture content. GEM 7 and SAT 7 simulations agree during winter, but GEM 7 snowmelt starts by the

end of March, while only in mid-April for SAT 7 simulation. In both SAT 7 and GEM 7 simulations, liquid moisture changes have about the same fluctuation pattern after June.

The following figure 51 shows earlier GEM 7 frozen moisture content changes compared to SAT 7, with larger amplitudes from March to the end of April. SAT 7 changes tend to be larger after April, indicating again the delayed SAT 7 snowmelt.

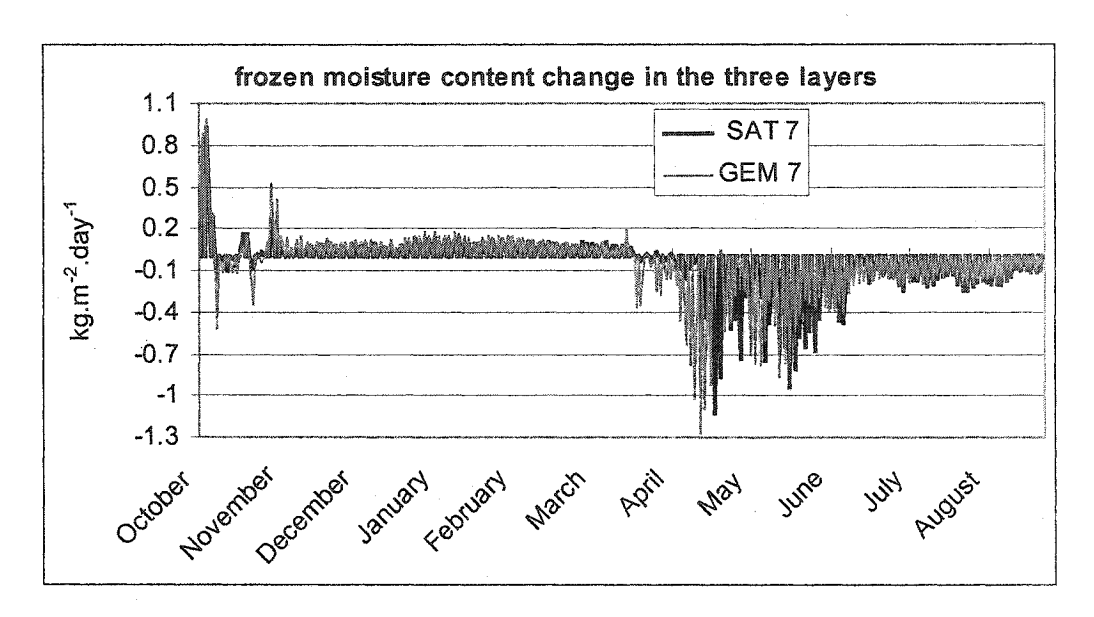


Figure 51: Daily basin average frozen moisture content in the three soil layers for the seven-landclass runs.

Figure 52 shows the different moisture storage sub-basin sensitivities: mountainous basins are the most sensitive, with the Liard sub-basin being especially responsive. This might partly results from the largest snowmelt delay between GEM 7 and SAT 7 runs in the Liard sub-basin.

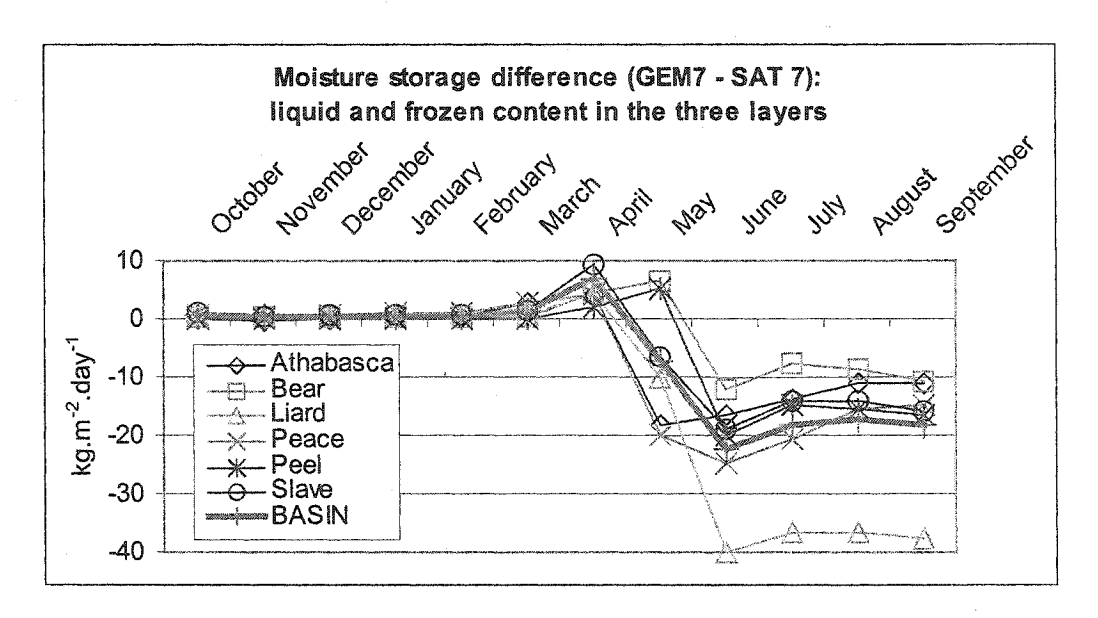


Figure 52: Monthly average liquid and frozen moisture content differences between GEM 7 and SAT 7 runs, in the three soil layers and for the different sub-basins.

# C. Runoff

Changes in runoff are due to changes in evapotranspiration and moisture storage. Figure 53 shows the basin daily accumulated runoff: there is a delay in runoff peaks with the largest runoff difference (GEM 7-SAT 7) reaching 2 mm per day in April. There is a basin annual average GEM runoff underestimation of 16% and 10% for, respectively, the single and seven-land-class runs, which is due to GEM runs evapotranspiration overestimations and which is consistent with the GEM runs moisture storage underestimations.

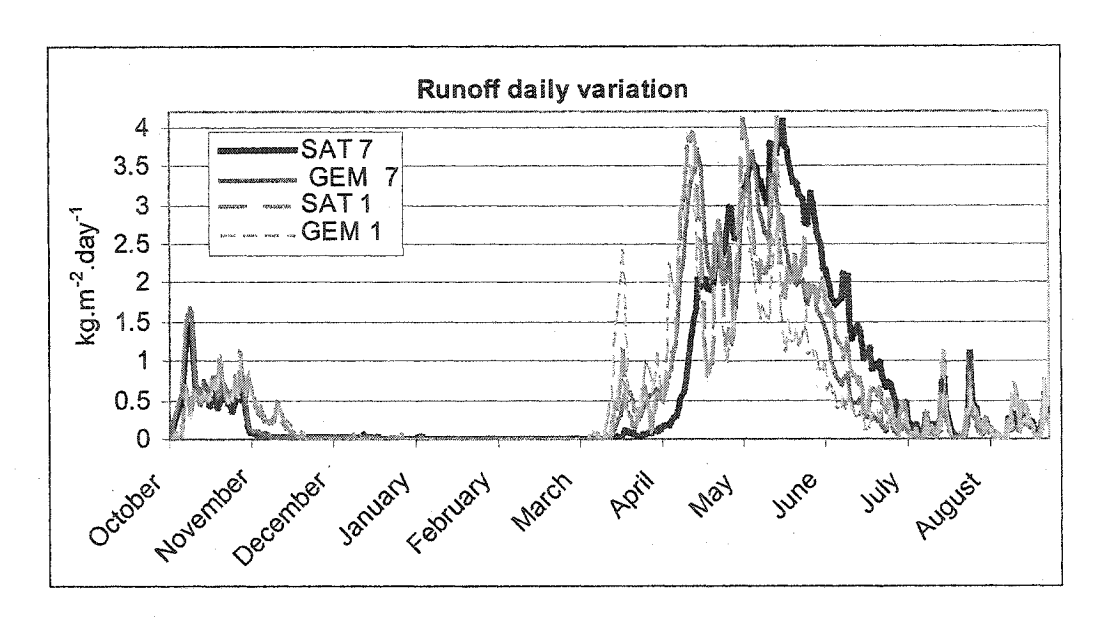


Figure 53: Daily basin average runoff for the single and seven-land-class runs.

Figure 54 shows that mountainous Peace and Liard sub-basins have the largest runoff differences in April. The GEM 7 runoff overestimation in April, due to a GEM 7 earlier snowmelt, is followed by a GEM 7 runoff underestimation in May related to the delayed SAT 7 snowmelt.

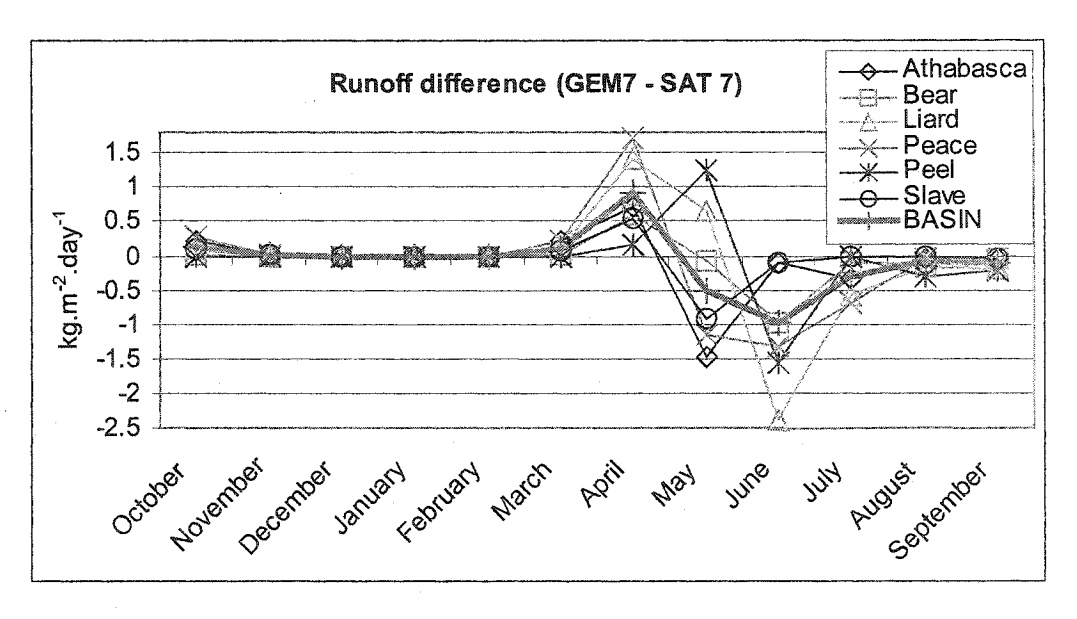


Figure 54: Monthly average runoff differences between GEM 7 and SAT 7 runs for the different subbasins.

In summary, uncertainties in incoming solar radiation generate a GEM 7 overestimation of 40 mm in evapotranspiration and sublimation, a GEM 7 underestimation of 20 mm in moisture storage by the end of the simulations and 21 mm in runoff. Both, GEM 7 and SAT 7 simulations, have an annual positive water balance, with a residual of 5 and 21 mm respectively (figure 55), with the largest differences in April and May. The water balance in March is opposite in sign in SAT 7 and GEM 7 runs. This results from GEM 7 early snowmelt, which also accounts for the GEM 7 water balance overestimation in April and underestimation in June.

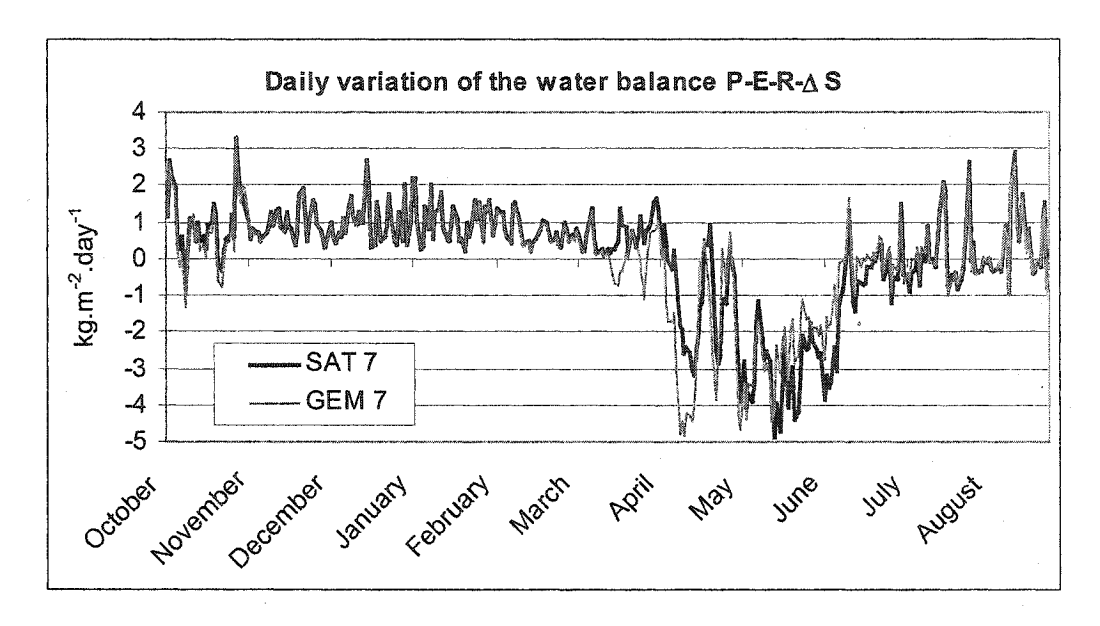


Figure 55: Daily basin average water balance for the seven-land-class runs.

# D. Stream flow

Before interpreting the results of the stream flow sensitivity to uncertainties in incoming solar radiation, one has to point out a routing issue. Figure 56 gives the location of the different gauge stations, where observed streamflows were available.

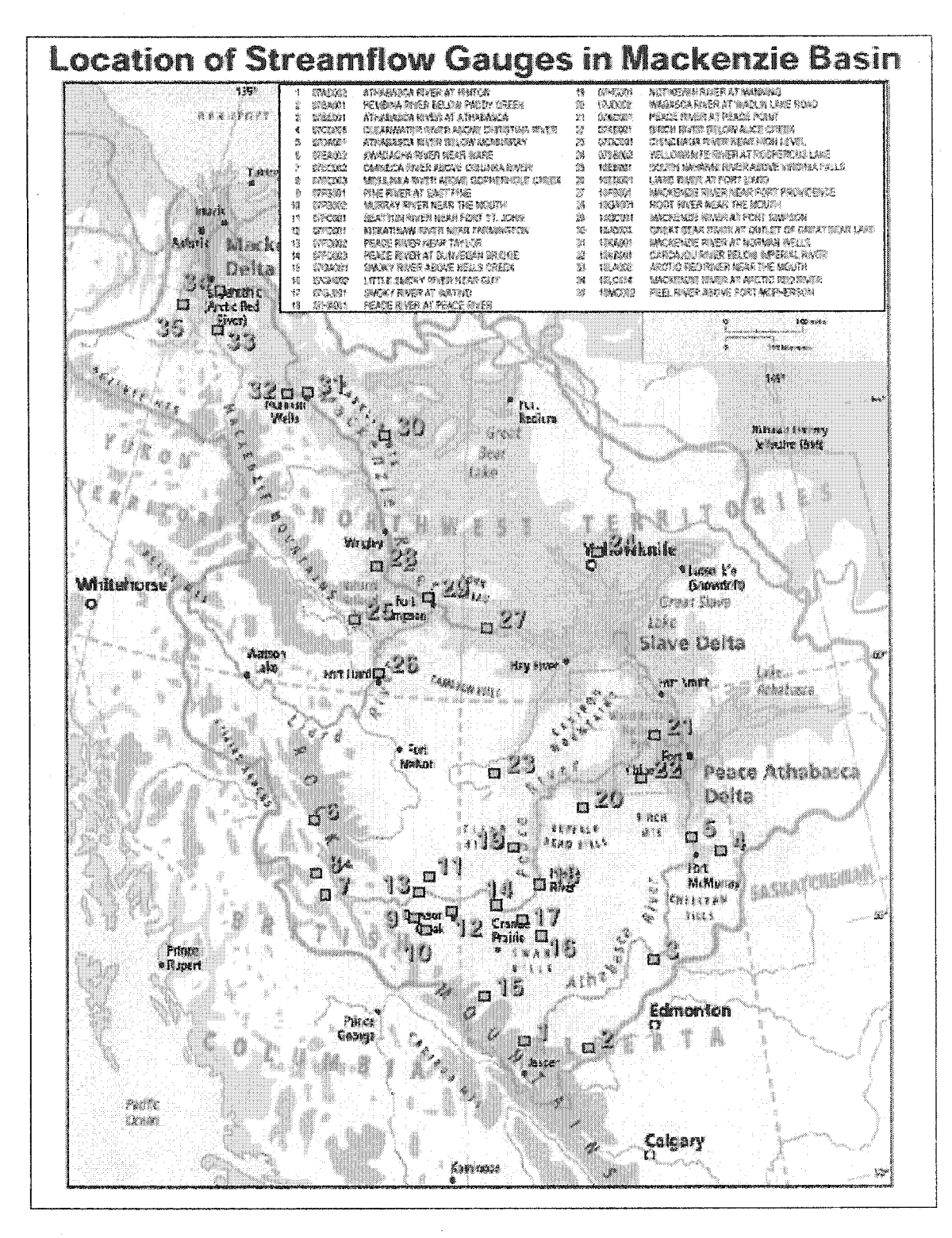


Figure 56: Location of gauge stations in the Mackenzie River Basin.

Figure 57 shows the first discharge peaks of the Mackenzie River at Arctic Red River (#34), near the delta, in spring, as simulated by WATCLASS: GEM 7 and SAT 7 simulation peaks are significantly delayed and smaller compared to the observed peak.

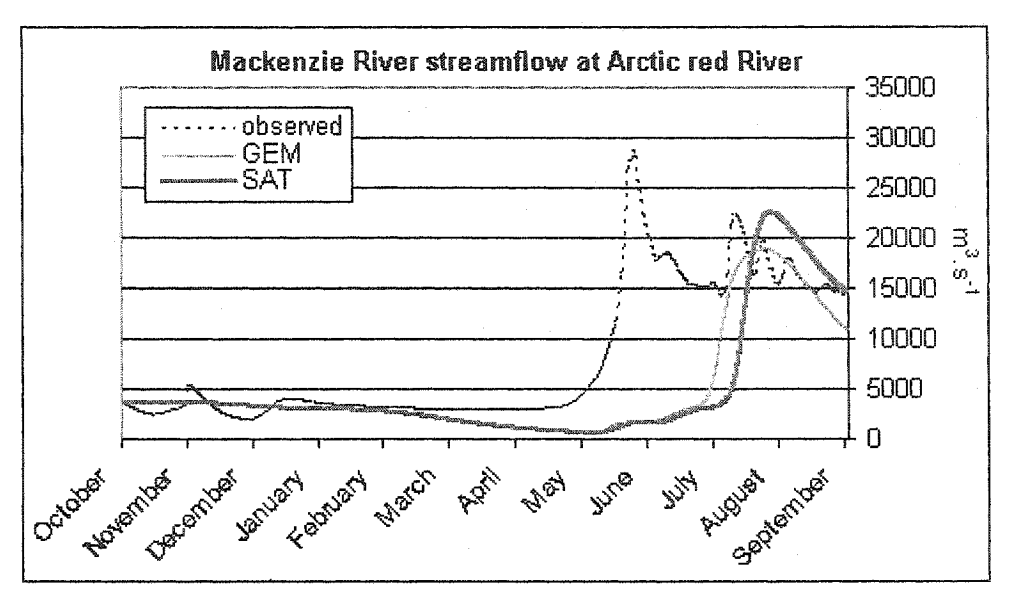


Figure 57: GEM 7, SAT 7 and observed stream flows at Mackenzie River at Arctic Red River.

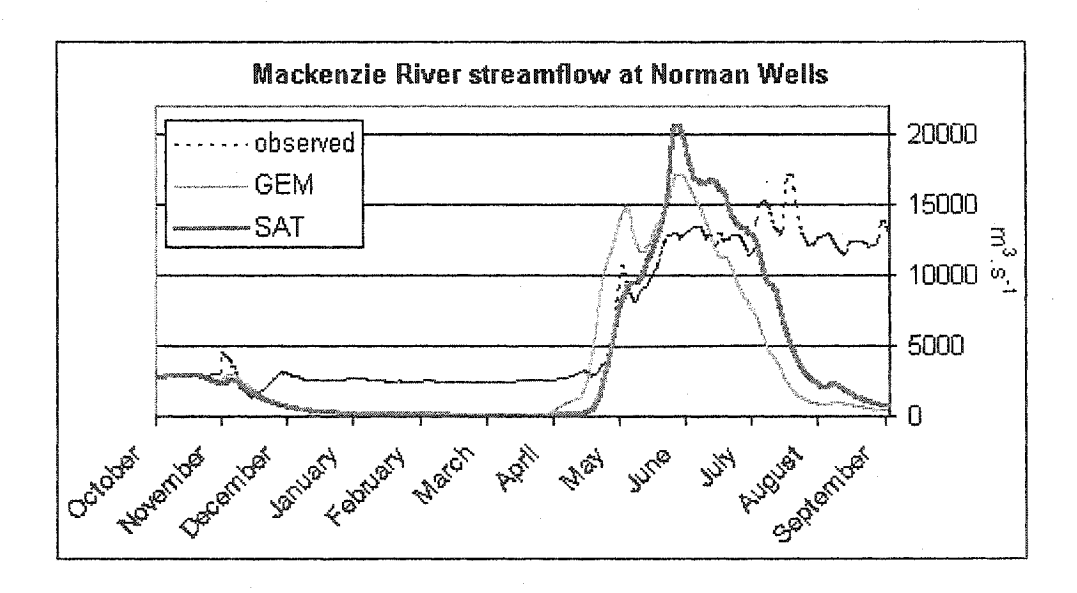


Figure 58: GEM 7, SAT 7 and observed stream flows at Mackenzie River at Norman Wells.

However upstream at Norman Wells (#31), the hydrographs for both the GEM 7 and SAT 7 simulations are now larger than the observed flow and their timing agrees with observations (figure 58). At most of the other gauge stations we obtained similar

agreement as at Norman Wells. The simulated streamflows are initialized with the observed streamflows but some parameters such as the soil moisture content are not initialized. This might explain why simulated streamflows reach extremely low values just before snowmelt (figures 57 and 58).

Within this sensitivity study, we are mainly concerned by the induced changes in the simulated hydrographs. However, this routing issue should be considered when interpreting the results on a basin scale, as this limit of WATCLASS might interfere with the sensitivity study.

The four following figures show the hydrographs at different gauge stations along the Athabasca, Peace, Liard and Mackenzie Rivers. In the Athabasca river hydrograph (figure 59), we note that in both GEM 7 and SAT 7 simulations, at the most upstream station (#1, at Hinton), the peak flow is delayed compared to the downstream stations at Athabasca (#3) and below McMurray (#5). We notice the differences in the timing of the first spring freshet in the GEM 7 and SAT 7 simulations, where SAT 7 first peak is about 10-days later, and has a significantly larger flow rate, especially and as expected at the most downstream station #5.

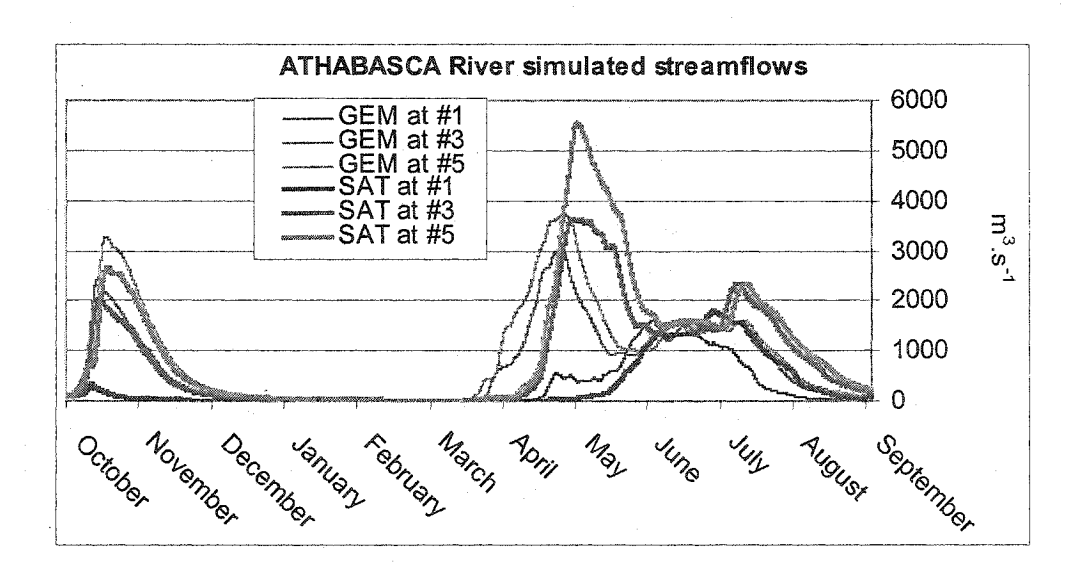


Figure 59: Athabasca River streamflows at Hinton (#1), Athabasca (#3) and below McMurray (#5), obtained through GEM 7 and SAT 7 runs.

The Peace River hydrograph below (figure 60) has the same pattern as above, with an even larger GEM 7 underestimation of the magnitude of the first discharge peak at the most downstream station at Peace Point (#21).

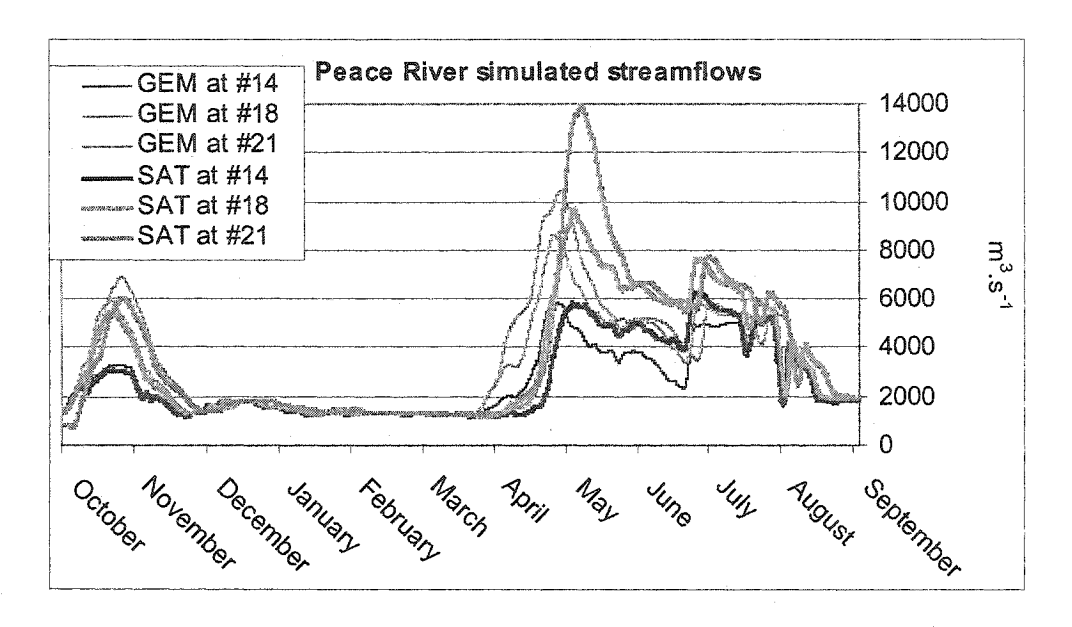


Figure 60: Peace River streamflows at Dunvegan Bridge (#14), at Peace River (#18) and at Peace Point (#21), obtained through GEM 7 and SAT 7 runs.

The Liard River hydrograph below (figure 61) shows also earlier but weaker GEM 7 spring freshets, followed by smaller streamflows during the recession period.

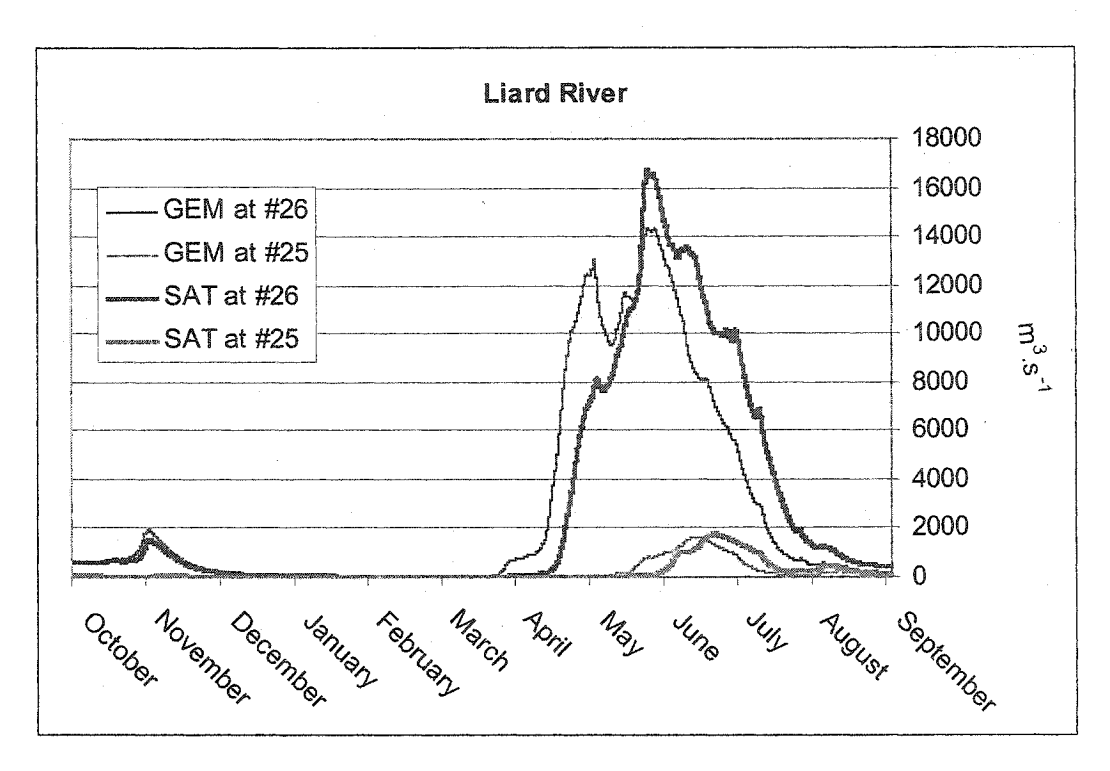


Figure 61: Liard River stream flow at Fort Liard (#26) and South Nahanni River streamflow above

Virginia Falls (#25), as simulated by GEM 7 and SAT 7 runs.

The results for the Mackenzie River hydrographs (figure 62) show similar agreement with the previous hydrographs, in which GEM 7 simulation has an earlier and weaker spring freshet and whose stream flow is lower during the recession period. However, there are some characteristic differences in the Mackenzie River hydrographs compared to the previous ones: the spring freshets occur in summer, they look like domes and the most downstream station at Arctic Red River (#34) has a lower magnitude than the upstream station at Norman Wells (#31). This might be a consequence of the routing issue exposed earlier.

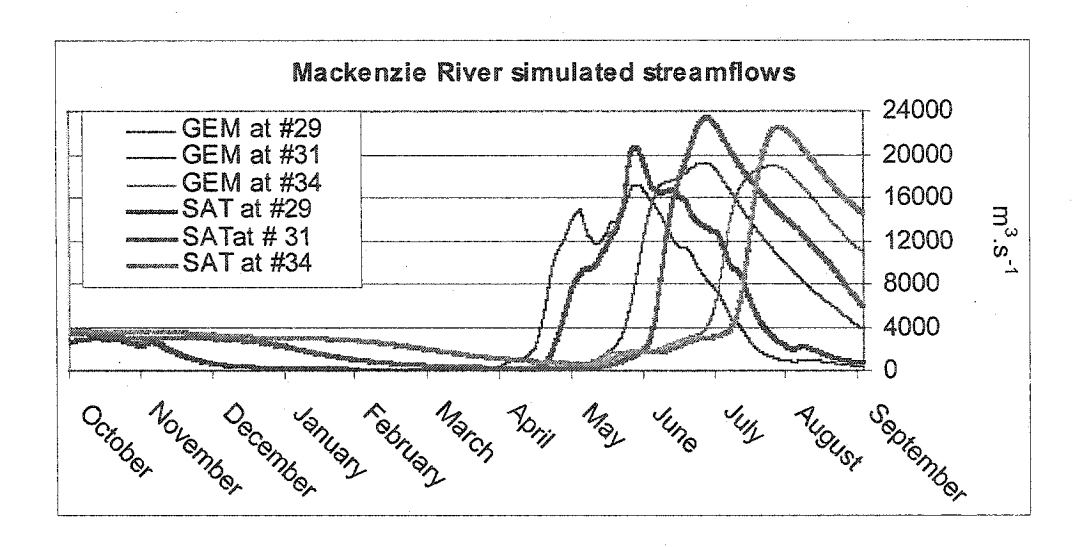


Figure 62: Mackenzie River streamflows at Fort Simpson (#29), at Norman Wells (#31) and at Arctic Red River (#34), obtained through GEM 7 and SAT 7 runs.

## E. Discharge

Mean annual discharge differs also, as indicated in table 4. All annual GEM discharges are underestimated, except at Mackenzie River at Arctic Red River for the seven-land-class simulation. The single-land-class simulations were processed with an early version of the WATFLOOD runoff routing subroutine, while the seven-land-class simulations used a newer version (Snelgrove et al. 2002): hence the larger discharges sensitivity of the single-land-class simulations might result either from the vegetation variability (16% runoff underestimation compared to 10% only for the seven-land-class simulations), or from the change in the routing subroutine.

On a sub-basin scale, for example the Athabasca and the Peace sub-basins, the sensitivity increases, as the station is more downstream. This results from the input of highly sensitive smaller scale rivers (the Watino river for example, see table 4).

Mean annual discharge (343 days) relative	(GEM 7-SAT 7)	(GEM 1 – SAT 1)
error in %	/ SAT 7	/ SAT 1
Mackenzie River at Arctic Red River (#34)	+1	- Pand
Mackenzie River at Normal Wells (#31)	-5	-9
(+ Bear sub-basin contribution)		
Mackenzie River at Fort Simpson (#29)	-7	-13
(+ Liard sub-basin contribution)		
Mackenzie River near Fort Providence (#27)	-11	-4
(Athabasca , Peace and Slave sub-basins		. '
contributions)		
Bear sub-basin		
Great Bear River at outlet of Great Bear Lake	-9	-4
(#30)		
Liard sub-basin		
Liard River at Fort Liard (#26)	-6	-15
Slave sub-basin		
Yellowknife River at outlet from Prosperous	-4	<b>-7</b>
Lake (#24)		
Peace sub-basin		
Peace River at Peace Point (#21)	-6	-10
Peace River at Peace River (#18)	-5	-8
Smoky river at Watino (#17)	(-10)	(-16)
Peace River at Dunvegan Bridge (#14)	-3	-6
Peace River near Taylor (#13)	-2	-4
Athabasca sub-basin		
Athabasca River below McMurray (#5)	-14	-22
Athabasca River at Athabasca (#3)	-15	-21
Athabasca River at Hinton (#1)	-8	-12.5

Table 4: Discharge relative errors between GEM and SAT runs for the single and the seven-landclass simulations. Arrows indicates the flow direction, from the most upstream to the most downstream gauge station.

As one might expect, simulations are less sensitive on a basin scale, i.e. at Arctic Red River for the Mackenzie River, for very large discharges. Because the main large flow contributions (the Athabasca and Peace Rivers) have joined the Mackenzie River before Fort Providence (through the Athabasca lake), the Mackenzie River sensitivity decreases as the station is more downstream (from Mackenzie River near Fort Providence to Mackenzie River at Arctic Red River). However the very low sensitivity of the basin scale and even the positive value for the seven-land-class simulation of the Mackenzie River stream flow at Arctic Red River are inconsistent with the results at the upstream stations: how can the GEM 7 discharge underestimation at each station in the basin drive to the GEM 7 discharge overestimation of the Mackenzie River near the delta at Arctic Red River? Actually, the late timing of the Mackenzie River freshet (figure 62), which occurs only at the end of July, that is much later than the observations, might be a consequence of the WATFLOOD routing issue discussed at the beginning of this section. This late freshet causes the recession period of the Mackenzie River at Arctic Red River not to be completed by the end of the simulation. The basin scale discharge sensitivity is therefore unreliable.

In summary, the impact of an overestimation of incoming solar radiation on the hydrograph are an earlier spring freshet of lower magnitude, with a lower stream flow during the recession period and an annual discharge underestimation. Induced annual and seasonal changes in the discharge are significant on the sub-basin scale and expected to be lower on the basin scale, although this last point has not been accurately quantified.

# **Chapter V**

# **Discussion – Conclusion**

# 1. Summary

Our objective was to assess the sensitivity of the hydrology of the Mackenzie River Basin, as simulated by WATCLASS, to uncertainties that may arise in the simulation of incoming solar radiation fluxes. Feng (2002) reports a GEM *net* solar radiation overestimation of the order of 30 %, relative to satellite observations of *net* solar radiation field for *summer months*. The comparison was for co-located satellite and GEM data at about 40 sites in the Mackenzie River Basin. In the GEM simulation used here, the *basin average annual* incoming solar radiation was 36% greater than the corresponding satellite value, which is consistent with the result found by Feng (2002).

We carried out four WATCLASS one-water-year period simulations. Runs were different in either their land cover (100% canopy or mix of forest and short vegetation) or in the incoming solar radiation inputs (from the GEM output, or renormalized GEM

output to conform to the average satellite value denoted by satellite observations), and the sensitivity of the energy balance, the water balance and snowpack were assessed.

Since all variables are interdependent, a scheme interconnecting variables might be drawn (see figure 63): GEM incoming solar radiation overestimation generated a net solar radiation overestimation of the same order of magnitude, i.e. 36%. Through the CLASS energy balance computation, the surface temperature was raised by up to 0.6 °C and 1.2°C, as a basin annual average, for the single and seven-land-class runs, respectively. This resulted in the net longwave radiation fluxes being underestimated by 14% for the seven-land-class simulation, and 6% for the single-land-class WATCLASS runs. The surface temperature overestimation produced sensible and latent heat overestimations of 141% and 22% respectively, for the seven-land-class simulation, and 142% and 18% for the single-land-class simulations. Finally, associated to the surface temperature increase, the heat conduction into the ground in spring is also enhanced. The presence of short vegetation increases the sensitivity of the surface temperature, the latent heat fluxes and the net longwave radiation fluxes. However, it decreases the sensible heat flux sensitivity.

The snowpack is sensitive to energy variations: the surface temperature increase drives an overestimation of snow ablation through sublimation, which is more or less important depending on the vegetation type. Thus, the snowpack erodes faster and disappears earlier where, again, vegetation is a determinant parameter for changes in snowmelt intensity.

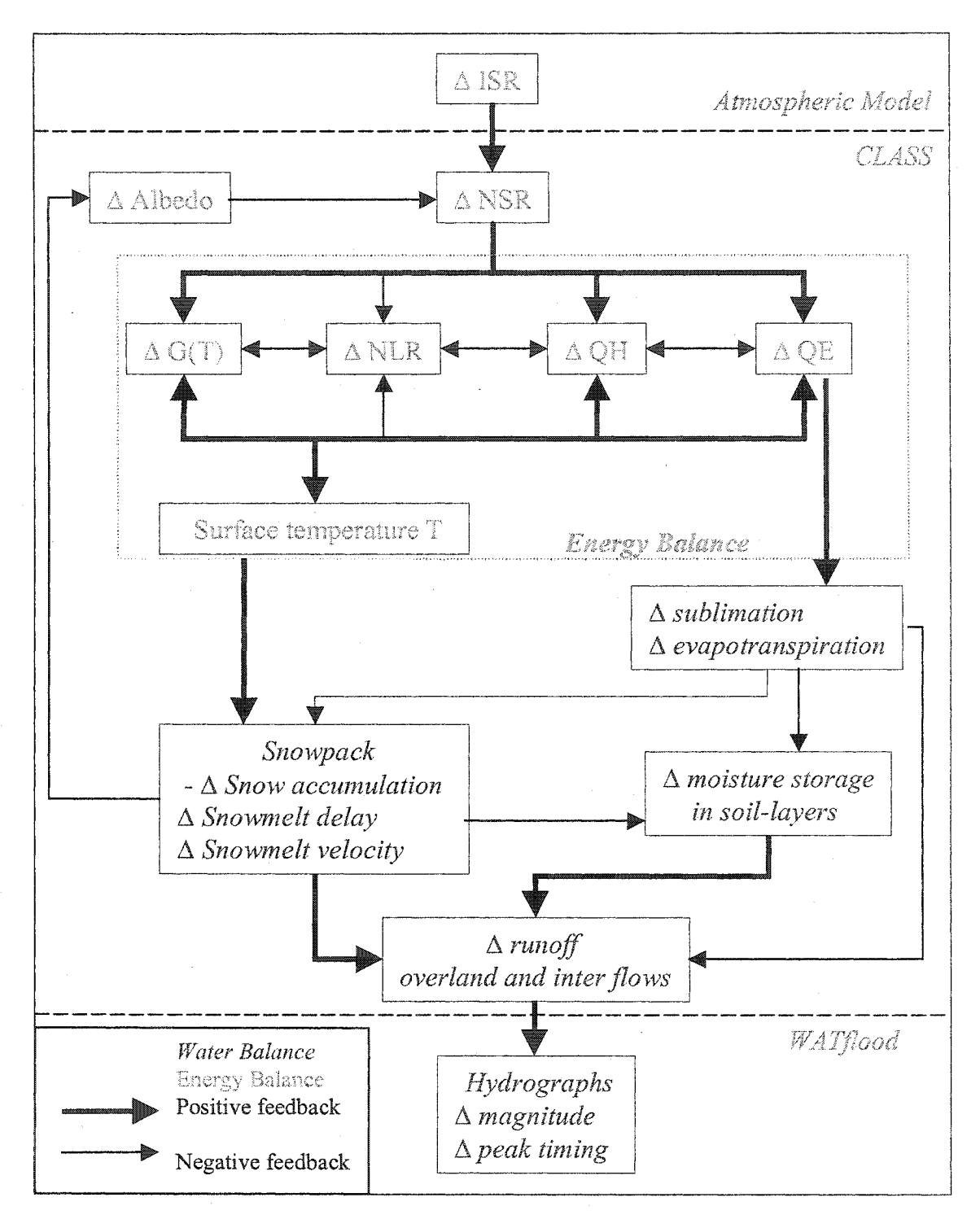


Figure 63: Scheme presenting the relationships between components of the energy budget and the water balance. ISR is incoming solar radiation, NSR net solar radiation, NLW net long wave radiation, QE latent heat, QH sensible heat and G(T) the heat conduction into the ground.

The water balance is also sensitive to uncertainties in incoming solar radiation. The surface temperature increase drives an overestimation of 17% or 21% of the loss of water through evapotranspiration, for the single and seven-land-class runs, respectively. This impacts on the moisture storage (-6% for the seven-land-class runs), and both, changes in moisture content and in evapotranspiration rate, are responsible for a runoff underestimation of 16 and 10% for the single and seven-land-class runs respectively. When considering stream flow at different gauge stations, hydrographs show an earlier freshet, however with a smaller magnitude and a lower stream flow during the recession period. Annual discharges are also underestimated. However, it is known that the hydrological parameters of the Mackenzie Basin, for these simulations, have not been totally optimized (Soulis – private communication) so the sensitivity of the characteristics of the freshet might vary.

We can conclude from these results that the basin is significantly sensitive to uncertainties in incoming solar radiation and one should consider the accuracy of incoming solar radiation when interpreting the hydrographs. Although the single-land-class simulations were carried out initially as a test, these simulations proved to be very useful in understanding the seven-land-class simulations. Furthermore, the results show that a realistic vegetation distribution is essential to obtain reasonable simulations of the energy and water budgets.

# 2. Comparison with similar studies

In this study, WATCLASS was driven offline by the atmospheric model. In reality, we expect some feedbacks from the hydrology back into the atmosphere. For example, through the huge increase in the sensible heat flux (140%), one could have expected an increase in the air temperature: sensible and latent heat fluxes would have been affected, as well as the form of precipitation as rain or snow. Also, the increase in the evapotranspiration rate could, perhaps, have been expected to modify precipitation locally, changing, amongst other processes, the spring freshet timing and magnitude.

## A. WATCLASS sensitivity to incoming longwave

## radiation

Fassnacht et al (2001) assessed the sensitivity of the snowmelt hydrology of the Upper Grand River basin in central southwestern Ontario, as simulated by WATCLASS, to changes in the cloud cover. More specifically, they looked at the impact of the changes in incoming longwave radiation (ILR) resulting from imposed changes in cloud cover from the initial default value of 0.5. Four seven-land-class WATCLASS runs were processed, each driven with same input fields except for the incoming long-wave radiation ILR. Incoming longwave radiation fields were generated through the equation:

ILR = 
$$\varepsilon_{at}(C_{Cloud})$$
.  $\sigma . T_a^4$ ,

where  $\epsilon_{at}$  is the integrated effective emissivity of the atmosphere and canopy, and is function of the cloud cover  $C_{Cloud}$ .  $T_a$  is the near-surface air temperature and ILR is the incoming longwave radiation flux.

The cloud cover was either set to a default value of 0.5, which is the annual average, variable within a narrow range about 0.5 (maximum of  $\pm 0.1$ ), full cover or clear sky. The cloud cover variation from 0 to 1 resulted in a 40% ILR increase. Incoming solar radiation inputs field were identical for all runs. Hydrographs for the Grand River at Galt from the period of March 24 to April 9 show differences in timing and magnitude of the spring freshet: the WATCLASS simulation with the ILR input field computed through for a permanently overcast sky had the earliest but weakest freshet, and the clear sky simulation had the latest freshet, with the same low magnitude as the overcast simulation but with greater discharge afterwards. The variable cloud cover and 0.5 cloud cover simulations agree well with each other, with a larger freshet than the previous runs, and timing being intermediate between the two extreme cases. That is, the WATCLASS response to an underestimation of incoming longwave radiation is a lower but earlier freshet followed by a decrease in stream flow, relative to the default 0.5 cloud cover simulation. However, fluctuations in incoming longwave radiation, such as from the 0.5 to variable cloud cover, do not lead to any significant changes in the hydrographs.

For a significant cloud cover decrease (such as from 1 to 0), resulting in a significant decrease in incoming *longwave* radiation, the WATCLASS simulations by Fassnacht et al. show a delay in the first spring freshet with a similar magnitude, a smaller magnitude for the following stream flow peaks and less discharge during the recession period. The present results show that, for a decrease in the cloud thickness, which generates an increase in incoming solar radiation, WATCLASS simulates freshet and stream flow characteristics similar to our results. However, since unfortunately Fassnacht did not specify the change in *net* longwave radiation and did not discuss the energy budget, relating his results to ours is not justified. Nevertheless, the two sets of results do show interesting parallels.

## B. CRCM/CLASS - WATFLOOD: ISR decrease

Mackay et al (2002) carried out a simulation for the same period as ours with the Canadian Regional Climate Model CRCM (Caya and Laprise, 1999), coupled to the land surface scheme CLASS. The CRCM has been shown to underestimate *net* solar radiation by about 10% in summer time because it overestimates the cloud cover by 20% (Feng et al, 2002). Outputs from the CRCM/CLASS simulation were used to drive WATFLOOD offline and results from CRCM/CLASS and WATFLOOD were compared to measurements. Results were consistent with ours: the simulated basin annual average surface temperature was 2°C cooler than measured. This generated an overestimation of the snow accumulation and a longer snow-covered season. Hydrographs were compared at Athabasca River at Athabasca, Smoky River at Watino, Liard River at Fort Liard and Mackenzie River at Red Arctic River. The CRCM/CLASS-WATFLOOD spring freshet was delayed compared to observations at all four gauge sites, with similar or larger magnitudes. This is consistent with our previous conclusion on the sensitivity of WATCLASS to uncertainties in solar radiation.

The Mackay et al. run included hydrological feedbacks on the atmosphere: the CRCM/CLASS snow accumulation overestimation was due to an earlier onset of below-freezing temperatures in fall, meaning that precipitation fell as snow rather than rain.

Furthermore, Mackay et al. argue that they obtained a plausible P-E compared to observations. Since our simulations did not include feedbacks into the atmospheric model GEM, our precipitation amount remained constant whereas the Mackay et al. precipitation rate increases slightly: our P-E changes are therefore not comparable with Mackay et al. results. Hence, although our results seem to agree for the hydrographs, not surprisingly, individual processes might differ. Finally, our studies agree with a very large sensitivity of runoff and moisture storage in the mountainous regions, especially in the Liard sub-basin. Mackay et al. suggested that it was the result of unstable moisture content after a saturated soil initialization, even after a long spin up. Our study reveals, however, that the mountainous regions are particularly sensitive to errors in incoming solar radiation, which might have contributed to the excessively large values of P-E obtained by Mackay et al in the Liard sub-basin.

We cannot determine what aspect of the Mackay et al. simulation is responsible for the similarity with the hydrographs in our results. It might result from the induced incoming solar radiation underestimation, a possible incoming longwave overestimation (longwave underestimation at the top of atmosphere has been demonstrated by Feng 2002), or from uncertainties in the simulation of other processes such as precipitation. Again, the similar hydrographs between our study and from Mackay et al. simulation are very encouraging but comparative statements would not be appropriate.

# References

- Aagard, K., and E. C. Carmack, 1989: The role of sea ice and other fresh water in the Arctic circulation. J. Geophys. Res., 94.
- Betts, A.K., M. Goulden, S. Wofsy, 1999: Controls on Evaporation in a Boreal Spruce Forest. *Journal of Climate* 12, no. 6 (June 1999): 1601.
- Cao, Z., Stewart R.E., Hogg W.D., 2001: Extreme Winter Warming Events over the Mackenzie Basin: Dynamic and Thermodynamic Contributions. *J. Meteor. Soc.* Japan, Vol. 79, No. 3, pp. 785-804, 2001
- Côté, J., S. Gravel, A. Méthot, A. Patoine, M. Roch, and A. Staniforth, 1998: The operational CMC-MRB Global Environmental Multiscale (GEM) model: Part I Design considerations and formulation, *Mon. Wea. Rev.* 126, 1373-1395.
- Côté, J., J.-G. Desmarais, S. Gravel, A. Méthot, A. Patoine, M. Roch, and A. Staniforth, 1998: The operational CMC-MRB Global Environmental Multiscale (GEM) model: Part II Results, *Mon. Wea. Rev.* 126, 1397-1418.
- **Deardoff, J.W., 1978**: Efficient Prediction of ground surface temperature and moisture, with inclusion of a layer of vegetation. *J. Geophys.* Res. 83:1989-1903.
- **Fassnacht, S.R., K.R. Snelgrove and E.D. Soulis, 2001**: Daytime long-wave approximation for physical hydrological modeling of snowmelt: a case study of southwestern Ontario. Soil-Vegetation-Atmosphere Transfer Schemes and Large-Scale Hydrological Models (Proceedings of a symposium held during the Sixth IAHS Scientific Assembly at Maastricht, The Netherlands, July 2001). *IAHS Publ. No. 270*, 2001.
- Feng, J., 2001: Solar Radiation in the Mackenzie River Basin: retrieval from satellite measurements and evaluation of atmospherics models. Ph.D. Thesis, Dept. of Atm. and Oc. Sc., McGill Univ. Montreal, Quebec, 194 pp.
- Feng, J., H.G. Leighton, M.D. Mackay, N. Bussieres, R. Hollman and R. Stuhlmann, 2002: A comparison of solar radiation budgets in the Mackenzie River Basin from satellite measurements and a regional climate model, Atmosphere-Ocean, 40, 221-232, 2002.
- Feng, J., H.G. Leighton, M.D. Mackay, 2003: Radiation budget in the Mackenzie River Basin. *CAGES Special Issue of J. of Hydrometeorology*.
- Hall, F.G., 1999: Introduction to special section: BOREAS in 1999: Experiment and science overview. J. Geophys. Res. BOREAS Special Issue II, 104(D22), pp. 27627-27640.
- Kouwen, N., E.D. Soulis, A. Pietroniro, J. Donald and R.A. Harrington, 1993: Grouping Response Units for Distributed Hydrologic Modelling. ASCE J. of Water Resources Management and Planning, 119(3), May/June, 289-305.

- Li, Z., H.G. Leighton, K. Masuda, and T. Takashima 1993: Estimation of SW Flux Absorbed at the surface from TOA Reflected Flux. *Journal of Climate*, 6, 317-330.
- Li, Z., Leighton H.G., 1992: Narrowband to Broadband conversion with spatially autocorrelated reflectance measurements. J. Appl. Meteor, 31, 653-670.
- Louie, P.Y.T., W.D. Hogg, M.D. Mackay, X. Zhang, R.F. Hopkinson 2002: The Water Balance Climatology of the Mackenzie Basin with Reference to the 1994/95 Water Year. *Atmosphere-Ocean*, 40(2): 159-180.
- Mackay, M.D., K. Szeto, D. Verseghy, F. Seglenieks, E.D. Soulis, K.R. Snelgrove, A. Walker, 2003: Modeling Mackenzie Basin Surface Water Balance During CAGES with the Canadian Regional Climate Model. CAGES Special Issue of J. of Hydrometeorology. Accepted for publication.
- Rouse, W.R., E.M. Blyth, R.W. Crawford, J. R. Gyakum, J.R. Janowicz, B. Kochtubajda, H.G. Leighton, P. Marsh, L. Martz, A. Pietroniro, H. Ritchie, W.M. Schertzer, E.D. Soulis, R.E. Stewart, G.S. Strong, and M.K. Woo 2002: Energy and Water Cycles in a High Latitude, North-Flowing River System: Summary of Results from the Mackenzie GEWEX Study Phase 1. Accepted for publication in BAMS, 2002.
- Soulis, E.D., Snelgrove K.R., Kouwen N., Seglenieks F., Verseghy D.L., 2000: Towards Closing the Vertical Water Balance in Canadian Atmospheric Models: Coupling of the Land Surface Scheme CLASS with the Distributed Hydrological Model WATFLOOD. *Atmosphere-Ocean* 38(1) 2000, pp. 251-269.
- Snelgrove, K., E.D.Soulis, N. Kouwen, F. Seglenieks, A.Pietroniro, 2002: A Framework for Hydrological Modelling in MAGS. *CAGES Special Issue of J. of Hydrometeorology*.
- Stewart, R.E., Leighton H.G., Marsh P., Moore G.W.K., Ritchie H., Rouse W.R., Soulis E.D., Strong G.S., Crawford R.W., Kochtubajda B. 1998: The Mackenzie GEWEX Study: The Water and Energy Cycles of a Major North American River Basin. Bull. Am. Met. Soc., 79, 2665-2683.
- Suttles, J.T, R.N. Green, P. Minnis, G.L. Smith, W.F. Taylor, B.A. Wielicki, I.J. Walker, V.R. Taylor and L.L. Stowe, 1988: Angluar Radiation Models for Earth-Atmosphere System. Volume I Shortwave Radiation. NASA reference publication 1184.
- Verseghy, D. L., 1991: CLASS A Canadian Land Surface Scheme for GCMs, I. Soil Model. Int. J. of Climatology, 11, 111-133.
- Verseghy, D. L., N. A. McFarlane and M. Lazarre, 1993: CLASS A Canadian Land Surface Scheme for GCMs, II. Vegetation Model and Coupled Runs. *Int. J. of Climatology*, 13, 347-370.
- Woods, J. D., 1984: The upper ocean and air-sea interaction in global climate. *The Global Climate*, J. T. Houghton, Ed., Cam-bridge University Press

# Appendix A

# **WATCLASS CODE Modifications**

#### a) Albedos and transmissivities at sunrise and sunset

To improve the zero albedo values at sunset and sunrise times, we expand the albedo calculation from only daytime to every time step (days and nights). These changes have not been fully tested, so this would be our suggestion of improvement. Changes might not be significant and interesting, as regards the implied additional computation time.

#### SUBROUTINE CANALB(...)

- C \* 1. 1 ALBEDO CALCULATIONS FOR CANOPY OVER BARE SOIL.
- C \* NEEDLELEAF AND BROADLEAF TREES.
- c 2002, May 3rd N. Voisin test to improve albedo values at sunrise/sunset
- c IF(FC(I).GT.0. .AND. COSZS(I).GT.0.) THEN ! replaced by IF(FC(I).GT.0.) THEN

[...]

and similarly for the other albedo and transmissivities computations, we remove the constraint "COSZS(I).GT.0.":

- \* CROPS AND GRASS.
- \* TOTAL ALBEDOS.

- \* NEEDLELEAF AND BROADLEAF TREES.
- \* CROPS AND GRASS.
- \* TOTAL ALBEDOS.

- \* NEEDLELEAF TREES.
- \* BROADLEAF TREES.

<sup>\* 1.2</sup> ALBEDO CALCULATIONS FOR CANOPY OVER SNOW.

<sup>\*2.1</sup> TRANSMISSIVITY CALCULATIONS FOR CANOPY OVER BARE SOIL.

- \* CROPS AND GRASS.
- \* TOTAL TRANSMISSIVITIES.

- \* NEEDLELEAF TREES.
- \* BROADLEAF TREES.
- \* CROPS AND GRASS.
- \* TOTAL TRANSMISSIVITIES AND CONSISTENCY CHECKS.

## b) WATCLASS code changes to output requested variables:

Outputs were available at up to three grid-boxes, and for one land class at the time only. We store the requested variables for every grid-box with CLASS index instead of WATFLOOD index, and we accumulate them so as to output them as weighted averaged with respect to the different land classes that make up each grid-box.

```
do I=1, NLAND

if( mosaic_aclass(n,ii).gt.0.0 ) then

[...]

l=wf_yy(n) ! North-South grid index

j=wf_xx(n) ! East-West grid index

[...]

FSSTAR_DAY(1,j)=FSSTAR_DAY(1,j)+mosaic_aclass(n,ii)*FSSTAR(I)

[...]

endif
enddo
```

where NLAND is the number of grid-boxes to simulate and equals the number of grid-boxes in the basin (4668 indices), times the number of land classes (7), I is the WATFLOOD index for a specified land class, 1 and j are the corresponding CLASS North-South and East-West indices respectively, independent of the land class, and FSSTAR\_DAY(l,j) is the daily averaged net solar radiation flux, for seven land classes whereas FSSTAR(I) is the net solar radiation flux for one land class only, and 'mosaic\_aclass' is the fractional cover of the land class 'ii' in the grid-box with WATFLOOD index 'n'.

<sup>\*2.2</sup> TRANSMISSIVITY CALCULATIONS FOR CANOPY OVER SNOW.

#### c) Time inconsistency between input file and WATCLASS

The atmospheric input file data are labeled in terms of UTC time, whereas WATCLASS uses local time and assumes local time in its input files. Hence there is a time inconsistency between the model and the input file WATCLASS.BIN. Therefore WATCLASS had to be made reading UTC time. We implemented a DEGLON\*180/12 delay, where DEGLON is the basin average longitude, in the time initialization file, CLASS.INI, so that WATCLASS knows that input files are in time UTC. Hence, with one-hour delay per 15° of longitude, an 8-hour delay for the Mackenzie basin has been included in the file. Basically, only two lines have been modified:

for a February WATCLASS run in time UTC. The WATCLASS.BIN input file starts on the 32<sup>nd</sup> Julian day at 1 UTC and ends on the 59<sup>th</sup> at 24 UTC. Hence we told WATCLASS through the time initialization file, that the input file starts at 16PM, local time, on the 31<sup>st</sup> Julian Day, until the 58<sup>th</sup> Julian Day same time, i.e. a 31-day run, which does not change.

# Appendix B WATCLASS Code Structure

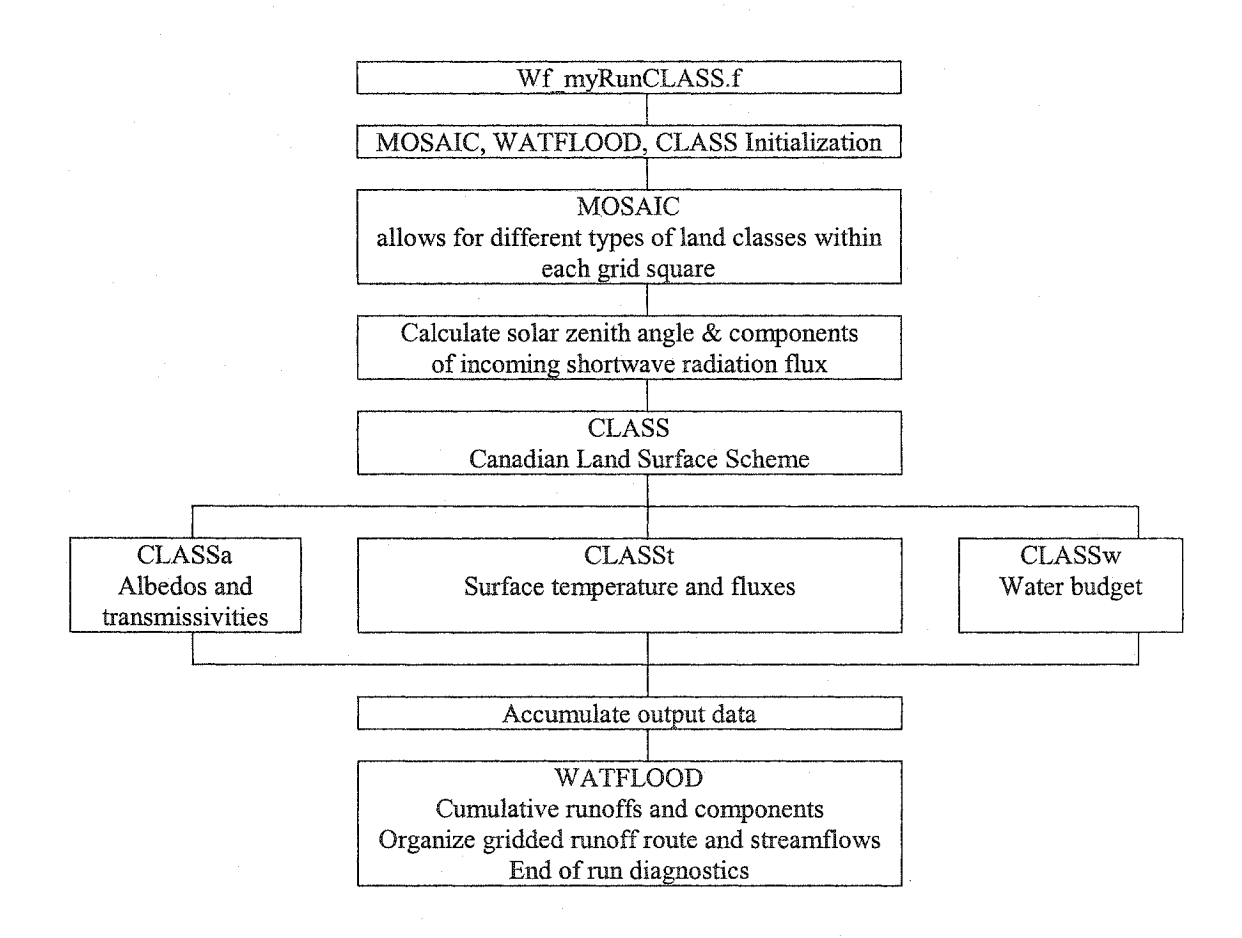
WATCLASS was a new model with scarce information about the code. In order to figure out all the variables that WATCLASS was simulating, and how it outputted them, I had to go into the code and I first did a synthesis of the different subroutines. The following document is the original code synthesis just mentioned.

A second part, not presented here, was to track variables of interest through the code.

# WATCLASS STRUCTURE

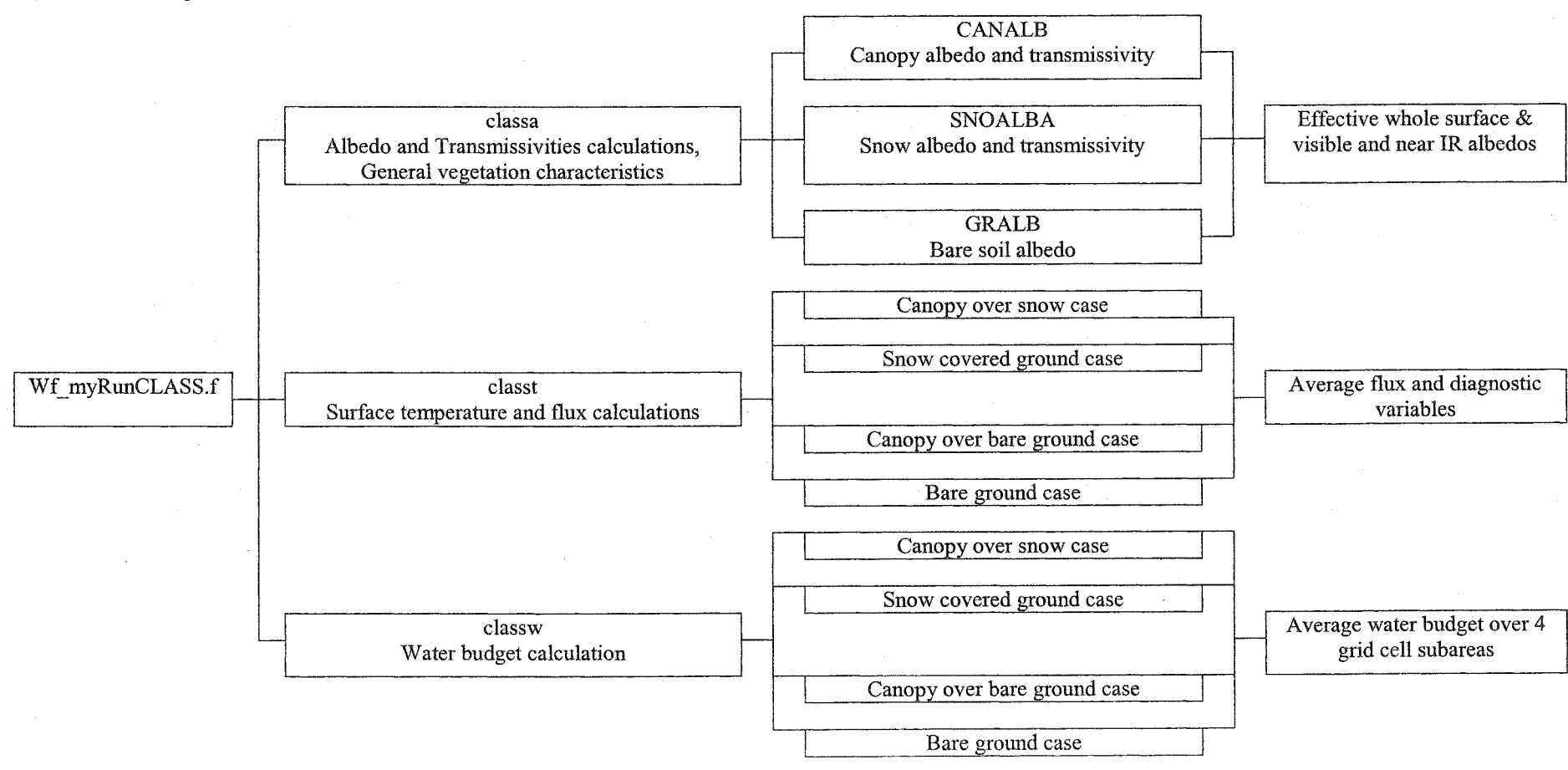
## 09/07/2001 Version 1.0 By Nathalie Voisin Nathalie.voisin@mail.mcgill.ca

## 1. WATCLASS code structure

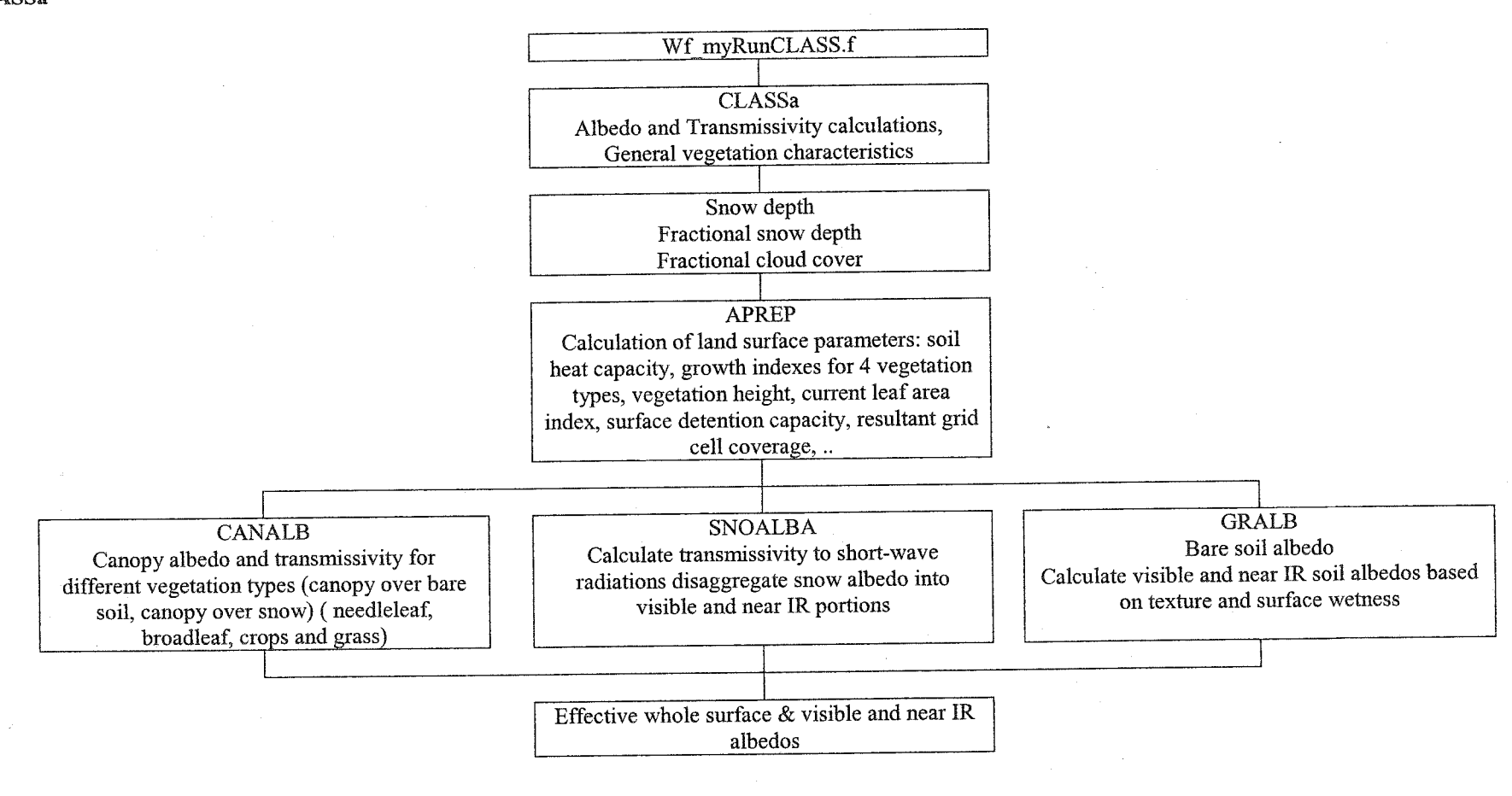


## 2. CLASS code structure

## 1) Overview of CLASS



## 2) CLASS code CLASSa



#### APREP

Calculate soil heat capacity

Determine growth index for crops, needleleaf trees, broadleaf trees and grass

Calculate vegetation height, corrected for growth stage for crops and for snow cover for crops and grass

Calculate current leaf area index for the four vegetation types (needleleaf, broadleaf, crops, grass)

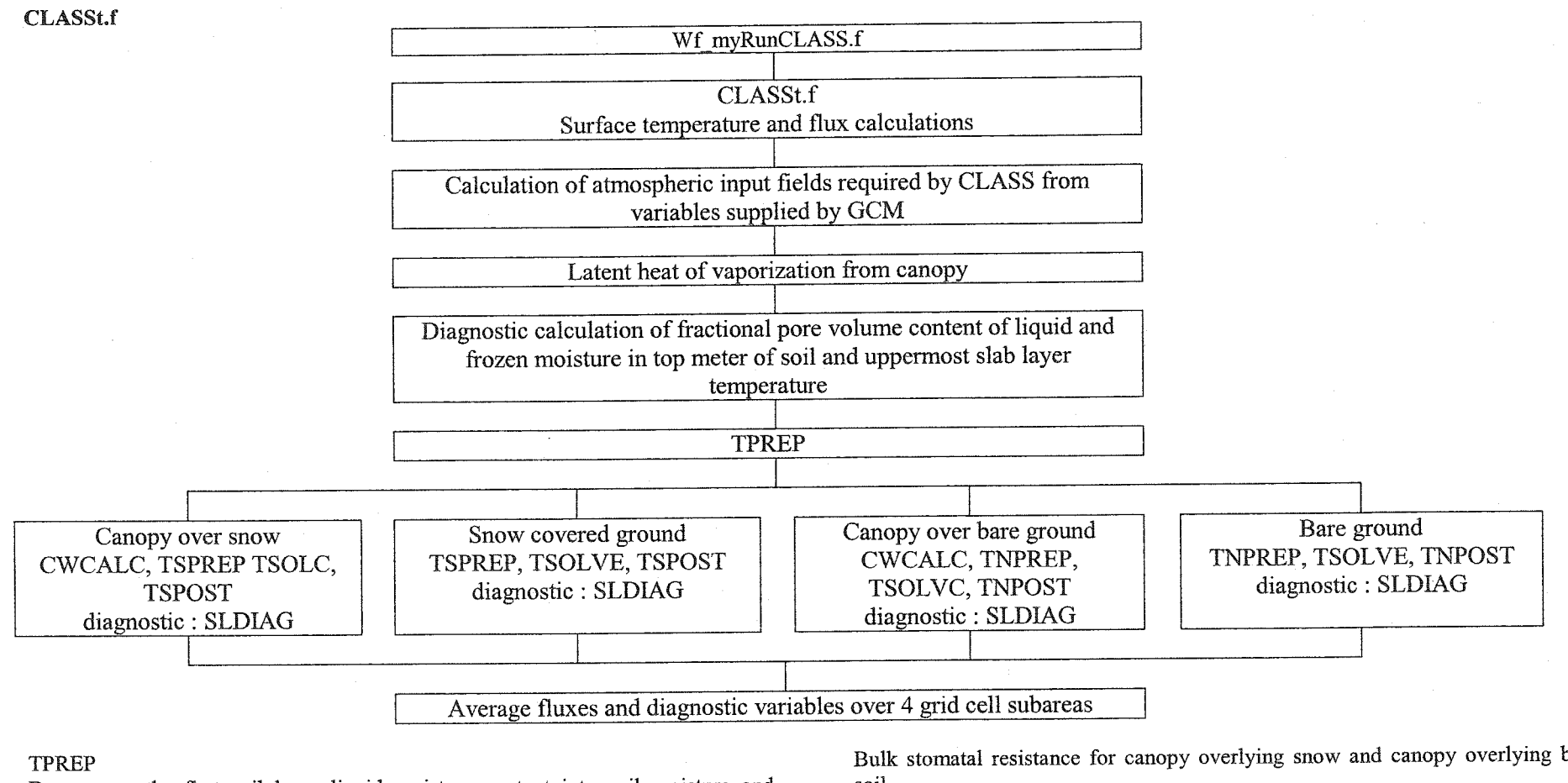
Partition intercepted liquid and frozen moisture between canopy overlying bare ground and canopy overlying snow: add residual to soil moisture or snow (if present). Calculate relative fractions of liquid and frozen intercepted moisture on canopy

#### **CANALB**

Albedo calculation for canopy over bare soil (needleleaf and broadleaf trees, crops and grass, total albedo)

Albedo calculation for canopy over snow (needleleaf and broadleaf trees, crops and grass, total albedo) Transmissivity calculation for canopy over bare soil (needleleaf trees, broadleaf trees, crops and grass, total)

Transmissivity calculation for canopy over snow (needleleaf trees, broadleaf trees, crops and grass, total)



Decompose the first soil layer liquid moisture content into soil moisture and ponded water

Surface moisture variables for bare soil energy balance calculation

Bulk soil moisture suction for stomatal resistance

Fractional transpiration extracted from soil layers

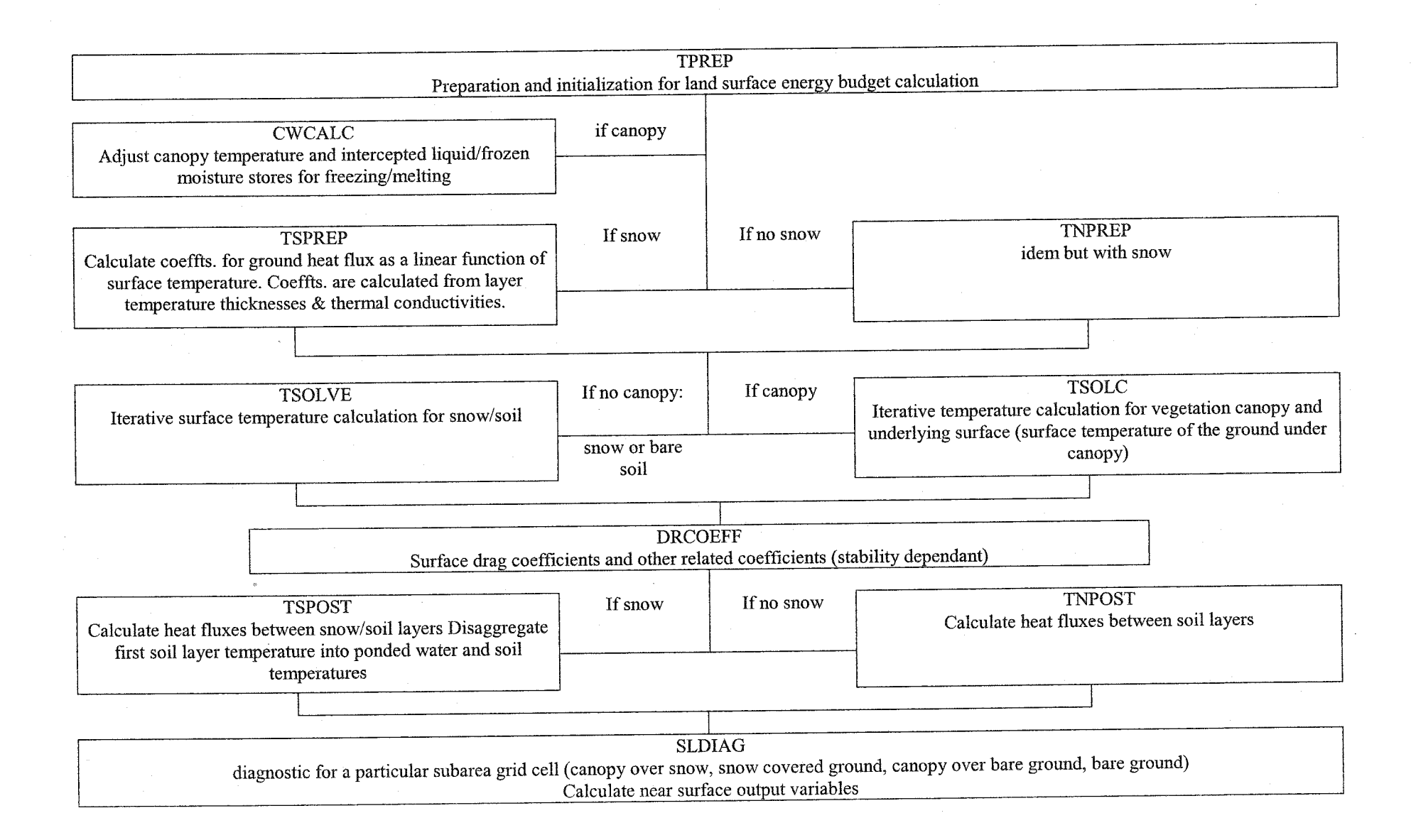
Bulk stomatal resistance for canopy overlying snow and canopy overlying bare

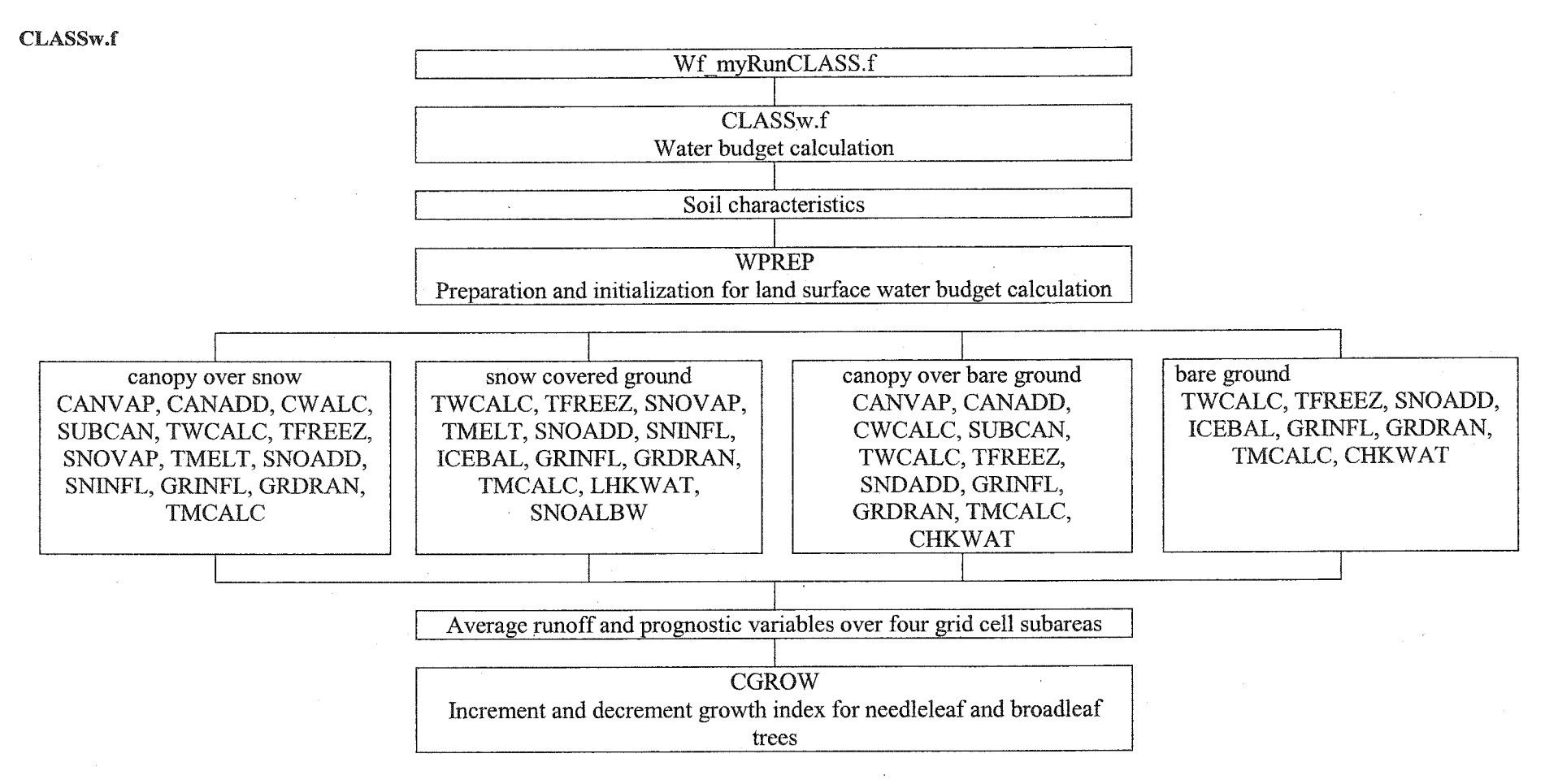
Volumetric heat capacity of soil layers

Thermal properties of snow

Thermal conductivities of soil layers

Note the four different cases: canopy over snow, snow-covered ground, canopy over bare ground, bare ground.

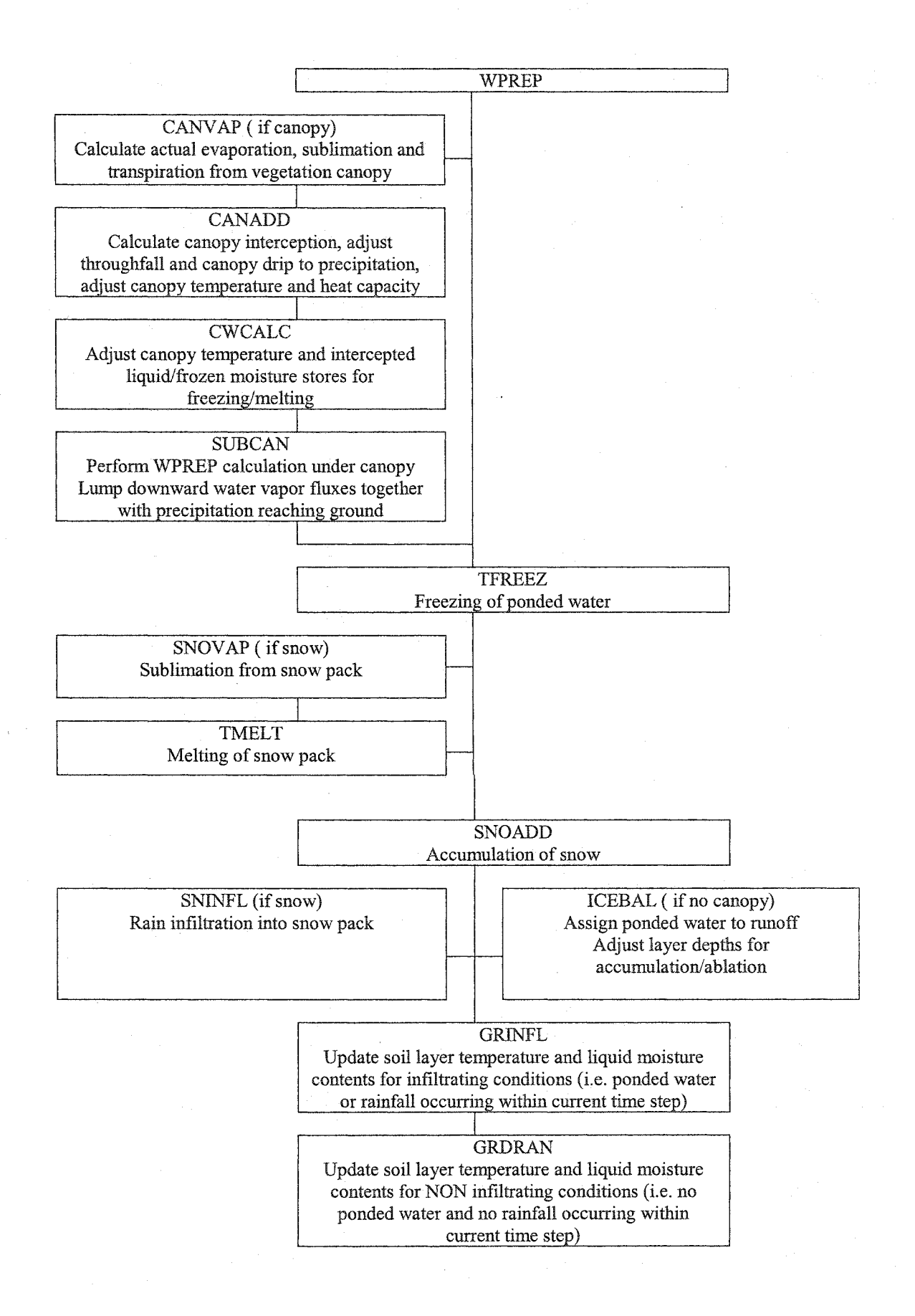


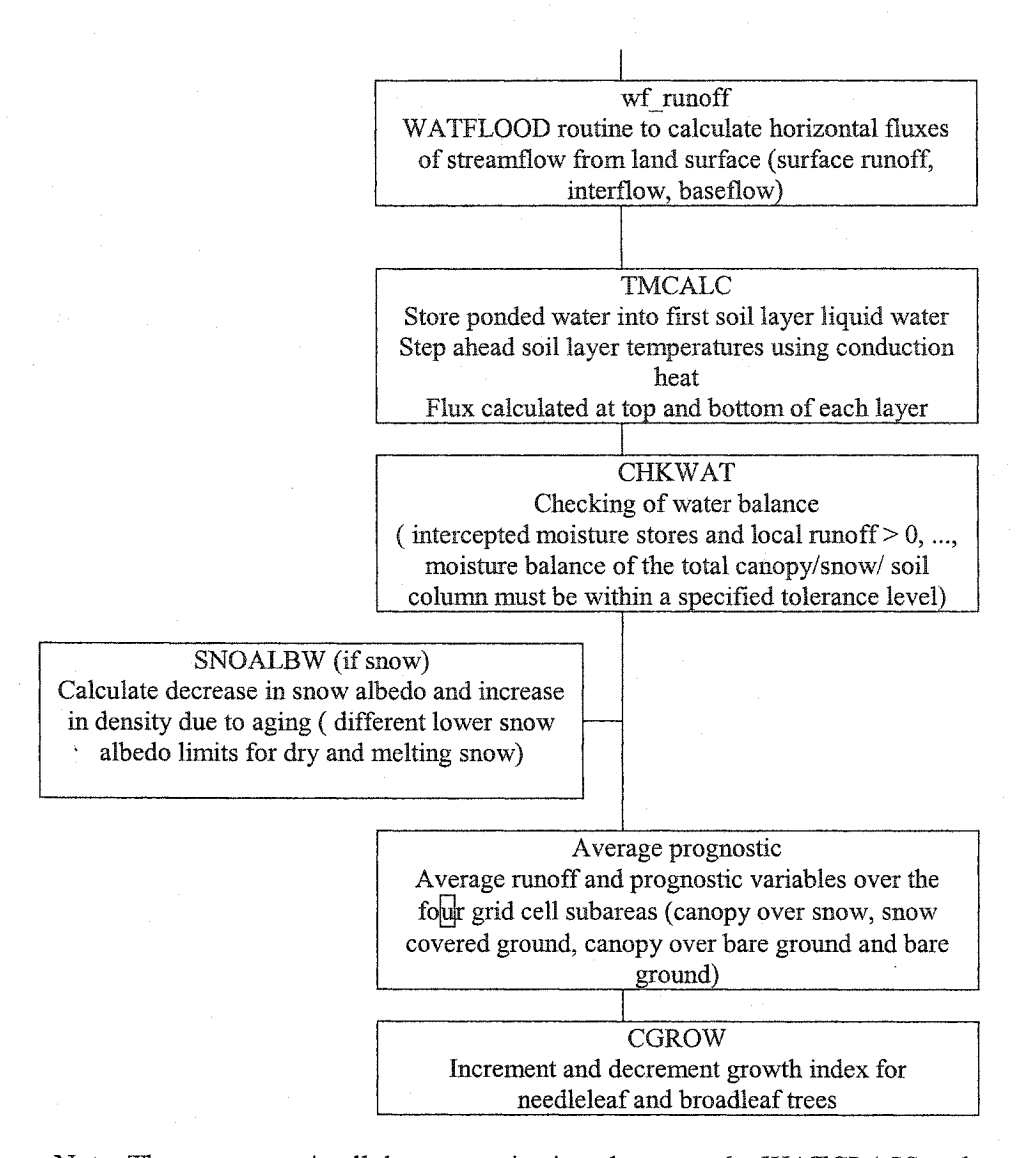


#### WPREP

Diagnose precipitation as rain or snow

Downward water vapor fluxes are lumped together with snowfall/rainfall for the four different grid cell subareas (canopy over snow, snow-covered ground, canopy over bare ground and bare ground).





Note: The comments in all these organization charts are the WATCLASS code comments.